Physics Reports 1043 (2023) 1–35

Contents lists available at ScienceDirect

Physics Reports

journal homepage: www.elsevier.com/locate/physrep

Iron oxide nanoparticles (Fe_3O_4, γ-Fe_2O_3 and FeO) as photothermal heat mediators in the first, second and third biological windows

A.G. Roca [a], J.F. Lopez-Barbera [a], A. Lafuente [a], F. Özel [a,b], E. Fantechi [a,c], J. Muro-Cruces [a], M. Hémadi [d], B. Sepulveda [e,*], J. Nogues [a,f]

[a] Catalan Institute of Nanoscience and Nanotechnology (ICN2), CSIC and BIST, Campus UAB, Bellaterra, 08193 Barcelona, Spain
[b] Department of Physics, Gebze Technical University, 41400 Gebze, Kocaeli, Turkey
[c] Centro di Cristallografia Strutturale (CRIST), Università degli Studi di Firenze, Sesto Fiorentino 50019 Firenze, Italy
[d] Université Paris Cité, CNRS-UMR 7086, Interfaces, Traitements, Organization et Dynamique des Systèmes (ITODYS), Paris, France
[e] Instituto de Microelectrónica de Barcelona (IMB-CNM, CSIC), Campus UAB, Bellaterra, 08193 Barcelona, Spain
[f] ICREA, Pg. Lluís Companys 23, 08010 Barcelona, Spain

ARTICLE INFO

Article history:
Received 6 August 2023
Accepted 6 October 2023
Available online 4 November 2023
Editor: Gerrit E.W. Bauer

Keywords:
Iron oxides
Photothermal mediators
Photothermia
Fe_3O_4, FeO
Wüstite
γ-Fe_2O_3
First biological window
Second biological window
Absorption
Photothermal efficiency
NIR-I, NIR-II
NIR-III
Nanotherapies
Photothermal applications

ABSTRACT

Nanotherapies are gaining increased interest for the treatment diverse diseases, particularly cancer, since they target the affected area directly, presenting higher efficacy and reduced side effects than traditional therapies. A promising nanotherapy approach is hyperthermia, where the nanoparticle can induce a local temperature increase by an external stimulus in the sick tissue to selectively kill the malignant cells. Among the diverse hyperthermia methods, photothermia is based on the absorption of light by the nanoparticles and further conversion into heat. Within the very wide range of nanostructured photothermal agents, iron oxides offer remarkable features since they are already approved by the FDA/EMA for various biomedical applications, they are biodegradable, easily manipulated using magnetic fields and can be imaged by diverse techniques. Here, we summarize the advantages of using the second biological window, both from the perspective of the skin and the optical properties of iron oxides. Further, we review the photothermal performance of iron oxide nanoparticles in the first, second and third biological windows. Overall, the results show that, for different types of iron oxide nanoparticles (Fe_3O_4, γ-Fe_2O_3, wüstite-FeO), both the heating capacity (i.e., induced temperature increase) and the photothermal conversion efficiency, η, vary in a complex way with the light wavelength, depending critically on the measurement conditions and physiochemical properties of the materials. Despite the spread in the reported photothermal properties of iron oxides, Fe_3O_4 particles tend to perform better than their γ-Fe_2O_3 counterparts, particularly in the second biological window. Interestingly, FeO, which has not been exploited so far from a photothermal perspective, shows very appealing absorption properties. Our preliminary studies using FeO/Fe_3O_4 core/shell nanoparticles evidence that they have excellent photothermal properties, outperforming Fe_3O_4 in both first and second biological windows. Finally, some applications beyond cancer treatment of iron oxide nanoparticles, exploiting the enhanced properties in the second spectral window, are discussed.

Contents

* Corresponding author.
E-mail addresses: alejandro.gomez@icn2.cat (A.G. Roca), borja.sepulveda@csic.es (B. Sepulveda), josep.nogues@icn2.cat (J. Nogues).

https://doi.org/10.1016/j.physrep.2023.10.003

1. Introduction

Hyperthermal nanotherapies (e.g., magnetic hyperthermia and photothermia, among others) [1–4] mediated by nanometric thermal agents are gaining increasing interest as local therapies with minimal systemic side effects for cancer treatment [5–31]. The principle of the hyperthermal nanotherapies is to induce a local temperature increase by an external stimulus (e.g., light, magnetic field, ultrasounds, among others) only at the site of action (e.g., the tumor) to produce a controlled death of the malignant cells. The local character of the treatment is a result of the presence of heat-mediator nanostructures only inside the sick tissues, which heat up as a response to the external stimulus and the focused irradiation, only in the area of interest (see Fig. 1). The local character of the effect generates minimal effects in healthy neighbouring tissues, thus resulting in minimal side effects. The particular interest of hyperthermal therapies for cancer treatment is based on the fact that cancerous cells are more sensitive to heat than healthy cells [2]. In addition, the heat dissipation in tumors is less effective than in healthy tissues, making them more prone to heat-induced cell death [2]. In the case of photothermal therapies (PTT) in the near infrared (NIR) many different types of nanostructured mediators have been proposed, such as plasmonic nanoparticles (e.g., Au nanoparticles), carbon-based materials, organic dyes, transition metal oxide nanoparticles or chalcogenide nanostructured materials [5–23]. Interestingly, ferrimagnetic iron oxide nanoparticles (e.g., magnetite — Fe_3O_4 and maghemite — γ-Fe_2O_3) often form part of composite nanostructures accompanying classical photothermal mediators (e.g., Au plasmonic nanoparticles, carbon-based materials, organic materials or chalcogenides) [32,33]. However, their role is not related to their potential photothermal properties, but to their magnetic properties. In fact, iron oxide nanoparticles have very appealing features, since their magnetic character allows them to be easily guided to and concentrated in tumors using magnetic field gradients [34,35], which can be appealing not only for hyperthermal treatments but also to deliver drugs to sick tissues [36]. Moreover, iron oxide nanoparticles can be tracked *in vivo* by different imaging techniques (e.g., magnetic resonance imaging, MRI – both in T_2 and T_1 modes – [37,38], magnetic particle imaging, MPI [39–41], magneto-acoustic imaging [42] and photo-acoustic imaging [43]) or they can be used as heat mediators for magnetic hyperthermia [44,45]. Although from the hyperthermia point of view iron oxide nanoparticles have been traditionally studied mainly as mediators for magnetic hyperthermia [44,45], in recent years, the importance of Fe_3O_4 and γ-Fe_2O_3 nanoparticles as stand-alone photothermal agents (i.e., without the presence of other photothermal mediators) has been put forward, thereby continuously increasing the interest in iron oxides (particularly Fe_3O_4) for biomedical photothermia [46] (and other photothermal-related applications). Most of the photothermal applications of Fe_3O_4 nanoparticles have been carried out in the so-called first biological window (wavelength λ between 650 nm and 950 nm; NIR-I; typically using $\lambda = 808$ nm, although other wavelengths have been used, such as 650, 660, 665, 671, 680, 690, 694, 730, 750, 785, 800, 810, 850, 885, 900 nm and even 980 nm)

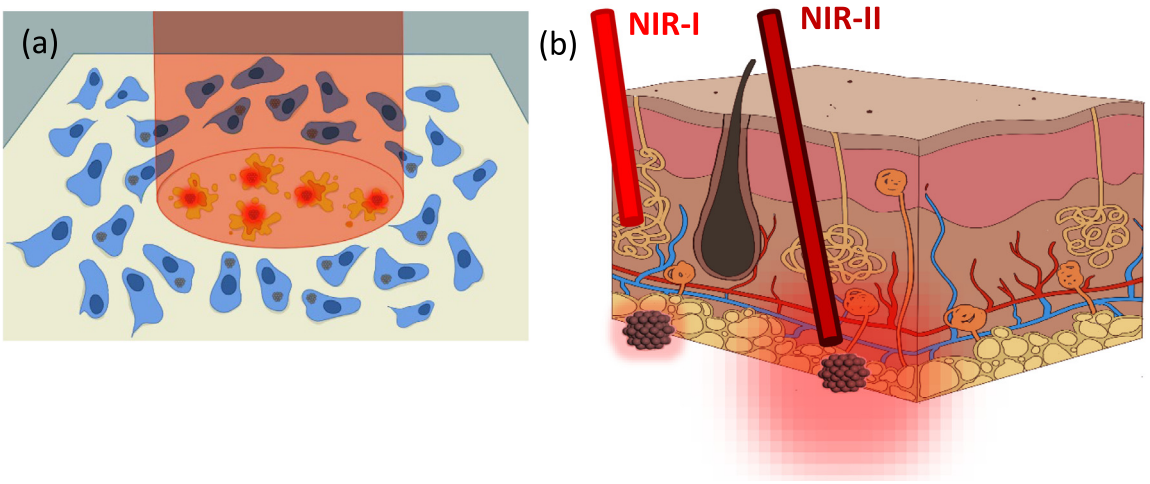

Fig. 1. (a) Schematic representation of the basic mechanism of the nanoparticle-mediated photothermal therapy. (b) Cartoon summarizing the advantages of using iron oxide nanoparticles in the second biological window (NIR-II).

[47–349]. Interestingly, the optical absorption of Fe_3O_4 in the second optical window (λ between 1000 nm and 1350 nm; NIR-II) is considerably higher than in the first biological window. This has triggered the interest in using iron oxides as photothermal mediators in the second NIR window, typically using $\lambda = 1064$ nm (although other wavelengths have been reported, e.g., 1000, 1053, 1090 or 1280 nm) [54,346–360]. Note also that although there are other biological windows (e.g., the third biological window, λ between 1550 nm and 1870 nm; NIR-III or even a possible fourth biological window, $\lambda \sim$2100 nm–2300 nm; NIR-IV) [361–363] no photothermal treatments using iron oxides in the NIR-III or NIR-IV ranges have been reported.

Notably, there is a range of potential benefits of using iron oxide nanoparticles as stand-alone photothermal mediators instead of being one of the moieties in multicomponent particles, such as: (i) reduced complexity of the synthesis compared to composite, making the synthetic approach simpler, more reproducible and easier to scale-up [364–372] (ii) biodegradability, and avoidance of toxic materials [373] or materials not approved by the US Food and Drug Administration (FDA) or the European Medicines Agency (EMA) [374–376]; (iii) larger averaged magnetization, making easier the magnetic manipulation of the particles (e.g., magnetic targeting and magnetic concentration inside the tumors) using lower fields than for composite materials; (iv) low cost and abundance of Fe (in contrast to, for example, Au); (v) robustness and endurance of oxide nanoparticles (particularly compared to, for example, organic or polymeric nanoparticles); (vi) far weaker sensitivity of the photothermal performance of iron oxide particles to size or shape dispersion than in other heat mediators (particularly, plasmonic nanoparticles); (vii) capacity to be used not only as heat mediators in magnetic hyperthermia [44,45], and photothermia [32,33,46], but also in microwave- or ultrasound-based hyperthermia [377–381]; (viii) capability of iron oxides for multimode imaging and sensing, which make them very powerful "single-particle" theranostic agents (therapy + diagnostic); (ix) long tradition of laser therapies (particularly in the NIR) for a myriad of health and cosmetic issues, ranging from neurological or retinal diseases to teeth cleaning or acne removal, in contrast to the therapeutic use of magnetic fields (e.g., magnetic hyperthermia); (x) additional mechanical therapeutic mode to induce cell lysis, by using non-spherical morphologies (particularly nanorods or platelets) of iron oxide nanoparticles that be efficiently rotated by magnetic fields [347]; (xi) enhanced internalization by cancer cells since they use iron for growth [382]; (xii) the additional ferroptosis-programmed cell death mechanism of Fe-based nanomaterials, which in combination with photothermally induced apoptosis can enhance nanoparticle-mediated cell death [46,383–385]; and (xiii) the very broad range of therapeutic uses of iron oxide nanoparticles, such as anti-bacterial, anti-inflammatory, anti-anemia, anti-viral, or even for neurological diseases, among others [386–392].

Interestingly, high quality iron oxide nanoparticles can be easily synthesized in a broad range of sizes and shapes (e.g., spheres, cubes, platelets, nanorods) and morphologies (like clusters, porous particles, urchin-like particles, hollow particles or chains of particles) [393–398]. However, the controlled growth of composite nanoparticles (e.g., dimers or core/shell structures) can be rather cumbersome and often difficult to scale up [364–372]. It is also important to emphasize that iron oxides (Fe_3O_4 and γ-Fe_2O_3) have already been extensively used in different biomedical applications [399–422] and are highly biocompatible and biodegradable, being their metabolic and secretion routes inside the body well known [423–425]. In fact, they are the only magnetic materials approved by the FDA and EMA for their use in humans [374–376]. Actually, iron oxides have already been proposed for the treatment of a great number of diseases and as diagnosis tools. As a matter of fact, several iron oxide-based treatments have been commercialized for diverse diagnostic and therapeutic uses [400,407,426,427].

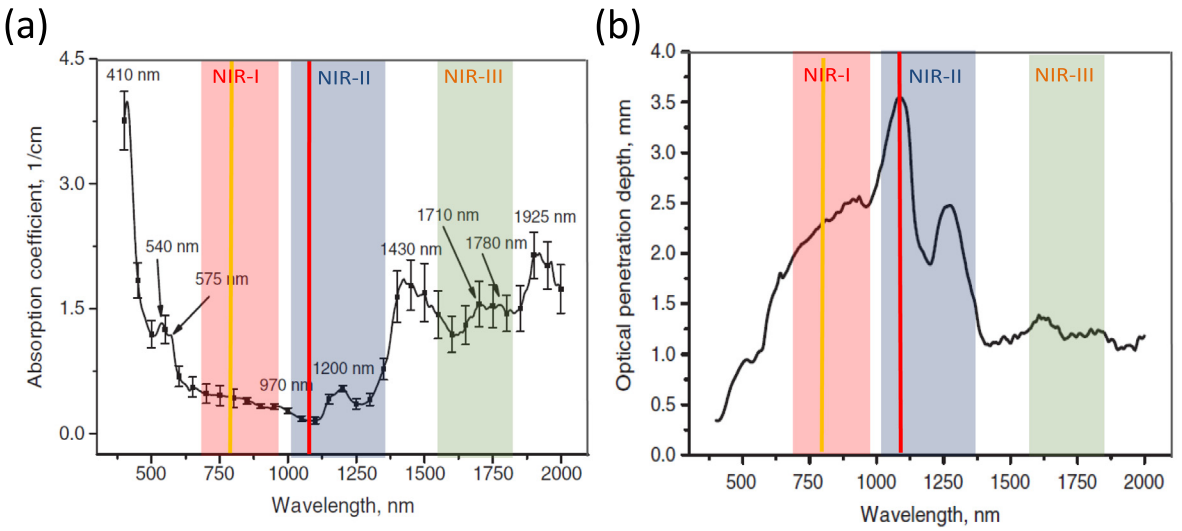

Fig. 2. Dependence of (a) the absorption coefficient, μ_A, and (b) the optical penetration depth, δ, of the skin on the light wavelength. The shaded areas represent the first (NIR-I), second (NIR-II) and third (NIR-III) biological windows. The typical wavelengths used experimentally in photothermia in the NIR-I and NIR-II regions ($\lambda = 808$ nm and 1064 nm, respectively) are highlighted by vertical lines.
Source: Adapted from Ref. [432].

Here, we review the use of iron oxide nanoparticles as independent photothermal mediators (for a broad range of applications) and discuss the advantages of Fe_3O_4 and FeO/Fe_3O_4 nanoparticles for photothermal applications in the second biological window.

2. Optical considerations for photothermia

2.1. Optical absorption of the skin

As a first step for any photothermal cancer treatment it is important to establish how deeply light will penetrate into the organ of interest, since this will establish the viability of photothermia to treat the cancer. Since NIR light does not enter significantly into human tissues and organs, photothermia would be best suited for subcutaneous cancers. Nevertheless, for other types of cancers minimally invasive catheters with optical fibres to guide the light into the area of interest could be used. Remarkably, it is worth mentioning that novel approaches to enhance the penetration of light in biological tissues (like larger laser spots or optical clearing technology) are being investigated [428,429].

In the literature there are numerous studies of the optical properties (absorption, scattering, refractive index) of human skin, other organs and tissue components (e.g., blood, fat, bone) [430,431]. To a first approximation, the absorption coefficient would provide an indication of the penetration depth of light in the body, although tissue light scattering should also be considered. It is well established that NIR light penetrates deeper into the human body than visible light, which has led to the concept of NIR biological windows. In the particular case of the skin, light presents low absorption in the NIR-I and NIR-II ranges ($\lambda = 600$ nm–1300 nm; see Figure 2a) [432–435]. Interestingly, the absorption at $\lambda = 808$ nm (first biological window) is larger than at $\lambda = 1064$ nm (second biological window), where absorption has a local minimum. The lower absorption combined with the weaker scattering at $\lambda = 1064$ nm translates into a considerably higher penetration of light through the skin at this wavelength compared to $\lambda = 808$ nm (see Fig. 2b). Note that the optical penetration depth is given by

$$\delta = \frac{1}{\sqrt{3\mu_A(\mu_A + \mu_S')}}$$

where μ_A is the absorption coefficient and μ'_S is the reduced scattering coefficient given by

$$\mu_S' = \mu_S(1 - g)$$

where μ_S the scattering coefficient and g the anisotropy factor [432].

However, it has to be taken into account that different skin pigmentations and other tissues and organs may have different light absorption and scattering properties [430,431,434–436].

Thus, from the purely optical viewpoint of light penetration into the skin, $\lambda = 1064$ nm would be favoured over $\lambda = 808$ nm for photothermal treatments.

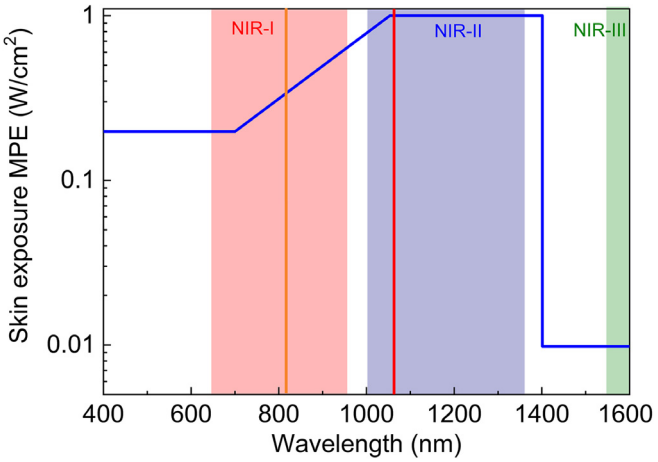

Fig. 3. Dependence of the skin maximum permissible exposure, MPE, of skin on the laser wavelength, λ. The shaded areas represent the first (NIR-I), second (NIR-II) and third (NIR-III) biological windows. The typical wavelengths used experimentally in photothermia in the NIR-I and NIR-II regions (λ = 808 nm and 1064 nm, respectively) are highlighted by vertical lines.
Source: Adapted from Ref. [438].

Concerning the use of light on the skin (or other tissues) another factor which must be taken into account is the maximum permissible exposure (MPE). Namely, the highest light power which has a negligible probability for inducing damage to the irradiated region. It is important to highlight that the power used to excite the nanoparticles will determine the maximum heat that they can generate. According to the standard of the American National Standard for Safe Use of Lasers [437], the MPE depends on the wavelength and the duration of the irradiation exposure. As can be seen in Fig. 3, for human skin, in the NIR range and for durations longer than 10 s, the MPE is given by $0.2 \times 10^{2(\lambda/1000-0.7)}$ W/m^2 in the 700 nm–1050 nm range and 1 W/m^2 (in the 1050 nm–1400 nm range) [438]. This implies that the MPE for λ = 808 nm (MPE = 0.33 W/cm^2) is significantly lower than for λ = 1064 nm (MPE = 1.0 W/cm^2) (see Fig. 3). Consequently, from the MPE viewpoint λ = 1064 nm would, again, be favoured over λ = 808 nm, since it allows the use of higher laser powers and, thus, the possibility of inducing a larger temperature increase.

Consequently, from purely optical considerations of the human skin, the use of lasers in the second biological window (e.g., λ = 1064 nm) should be more efficient for photothermal treatments (Fig. 1b). Moreover, note that from the skin optics perspective, the use of the third biological window would, in principle, not be especially beneficial due to the limited light penetration (Fig. 2b) and the low MPE at these wavelengths (Fig. 3).

2.2. Optical absorption of the heat mediator: Fe_3O_4 versus γ-Fe_2O_3

Another important factor to take into consideration for photothermal applications is how much light the heat mediators can absorb since this will determine in the first instance the induced heat, although other factors like the scattering should also be considered [5–23].

Firstly, for Fe_3O_4 and γ-Fe_2O_3, one has to bear in mind that although the two materials are structurally very similar (inverse spinel structure for both iron oxides), some of their physicochemical properties can differ considerably. In particular, while γ-Fe_2O_3 is a semiconductor with a band gap of 2.0 eV, Fe_3O_4 is almost metallic with a band gap of 0.1 eV [439].

Concerning their optical absorption, from a theoretical viewpoint, we have simulated (see Annex A for details) the absorption and scattering cross-sections of Fe_3O_4 and γ-Fe_2O_3 nanoparticles based on their bulk dielectric constants [440]. Notably, the simulations show remarkable differences between the two materials. Particularly, the absorption cross section, μ_A, for γ-Fe_2O_3 decreases steadily in the NIR region. On the other hand, for Fe_3O_4, while the absorption decreases in the first NIR biological window, it increases considerably in the second NIR range, having a maximum around λ ∼1400 nm and slowly decreasing for longer wavelengths (in the third window) (Fig. 4a).

Additionally, the scattering cross section (μ_S) for γ-Fe_2O_3 is remarkably larger than for Fe_3O_4 in all the NIR regions (Fig. 4b). These marked differences between the two materials stem from the presence of Fe^{2+} ions in Fe_3O_4, where the charge-transfer transitions between Fe^{2+} and Fe^{3+} ions provide a wide and intense absorption band in the NIR region, which is not present in γ-Fe_2O_3 [441,442].

It is also important to emphasize that experimentally, usually the extinction, μ_E, (absorption + scattering; $\mu_E = \mu_A + \mu_S$) rather than the absorption is measured. Moreover, although the experimental optical absorption/extinction of iron oxide nanoparticles (Fe_3O_4 and γ-Fe_2O_3) has been extensively studied, there are rather few studies extending over the three NIR biological windows. Nevertheless, some of the available experimental results confirm our simulation studies in

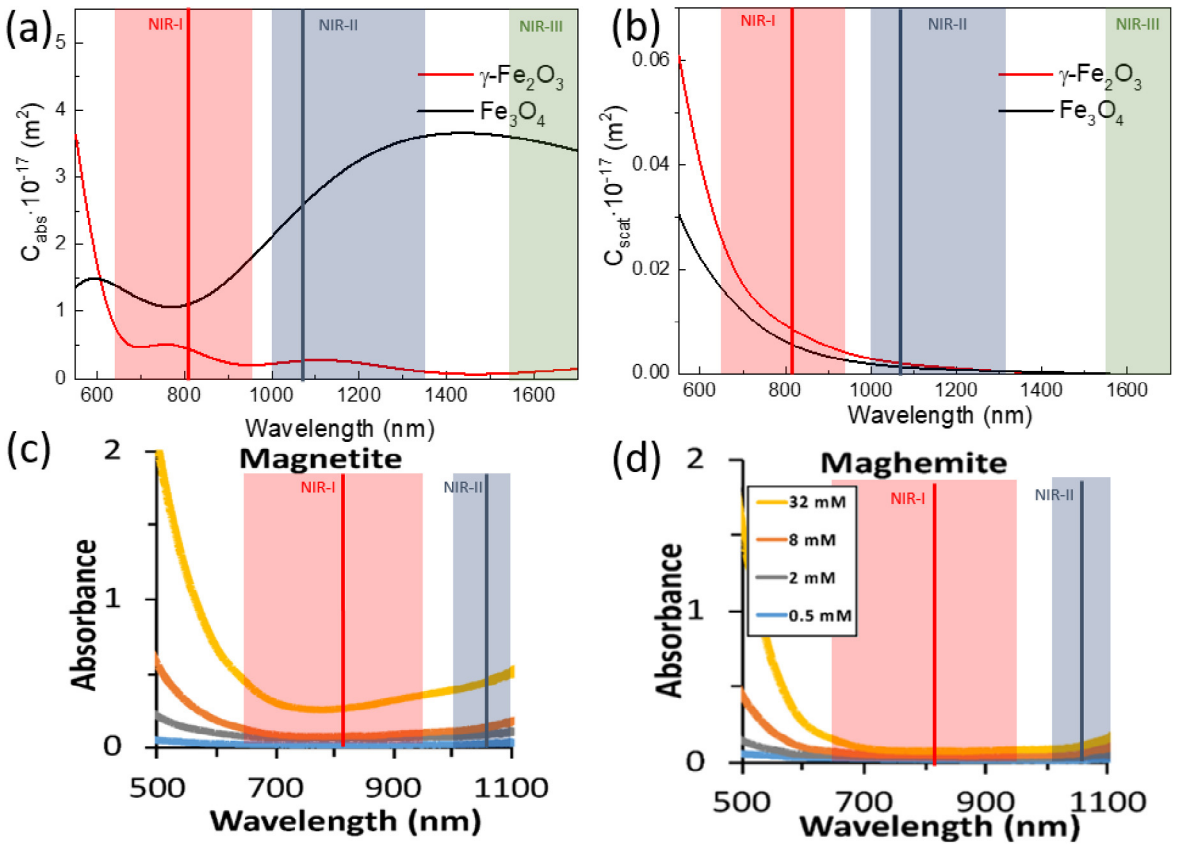

Fig. 4. Dependence of the simulated (a) absorption, μ_A (C_{abs}), and (b) scattering, μ_S (C_{scat}), cross-sections for γ-Fe_2O_3 and Fe_3O_4. (c,d) Experimental wavelength dependence of the extinction, μ_E, for 12.7 nm spherical nanoparticles of (c) Fe_3O_4 and (d) γ-Fe_2O_3 [352]. The shaded areas represent the first (NIR-I), second (NIR-II) and third (NIR-III) biological windows. The typical wavelengths used experimentally in photothermia in the NIR-I and NIR-II regions ($\lambda = 808$ nm and 1064 nm, respectively) are highlighted by vertical lines.

the NIR-I and NIR-II ranges [54,346,351–353,443,444]. Namely, the extinction of γ-Fe_2O_3 steadily decreases in the NIR region (Fig. 4c). On the other hand, although the extinction of Fe_3O_4 decreases in the NIR-I, it shows a significant upturn in the NIR-II range (Fig. 4c). Notably, both the simulated μ_A and the experimental extinction of Fe_3O_4 show a dip in the 700–800 nm region, which covers a large part of the NIR-I range.

However, it is worth mentioning that in iron oxides the absorption in the NIR-I and NIR-II ranges could be enhanced by potential plasmonic effects, particularly for very small non-stoichiometric $Fe_{3-x}O_4$ nanoparticles [444].

The simulated and experimental absorption and extinction results have significant for photothermal applications. Namely, (i) γ-Fe_2O_3 is expected to show poor light-induced heating in the whole NIR range, and (ii) a much higher temperature increase is expected for Fe_3O_4 in the whole NIR region, with an important enhancement in the NIR-II/III regions.

Consequently, based on these optical properties of iron oxides, Fe_3O_4 would be favoured over γ-Fe_2O_3 for photothermal applications. In addition, in the case of Fe_3O_4, NIR-II would be, in principle, more appealing for photothermal treatments. Importantly, given the rather strong dependence of the absorption in the NIR-II on the oxidation state of the iron oxide (see Figure 4) [440,441,445–447], the quality of the Fe_3O_4 nanoparticles (e.g., degree of oxidation, vacancies, antiphase boundaries) may play a fundamental role on their photothermal performance. Interestingly, from the absorption viewpoint, the third biological window in Fe_3O_4 may be an appealing alternative for certain applications, although, in principle it may not be so favourable from the skin optics perspective (Figures 2 and 3).

Finally, it is important to highlight that comparing Fe_3O_4 to Au nanoparticles (i.e., a typical PTT heat mediator), the complex refractive index, $n = n' + in''$, of Fe_3O_4 relative to water ($n' \gtrsim 1.6$) [448] is much higher than that of Au ($n' \approx 10^{-1}$) [449]. Moreover, in the NIR the imaginary part for Fe_3O_4 (relative to water), $n'' \gtrsim 0.4$, is lower than that of Au, $n'' \gtrsim 1.5$. These differences in n between Fe_3O_4 and Au imply that while light penetrates in Fe_3O_4 leading to an enhanced energy absorption, Au presents higher light scattering [450]. Consequently, even if μ_A is moderate for Fe_3O_4 compared to other conventional photothermal heat mediators, its overall optical properties make it very attractive for photothermia.

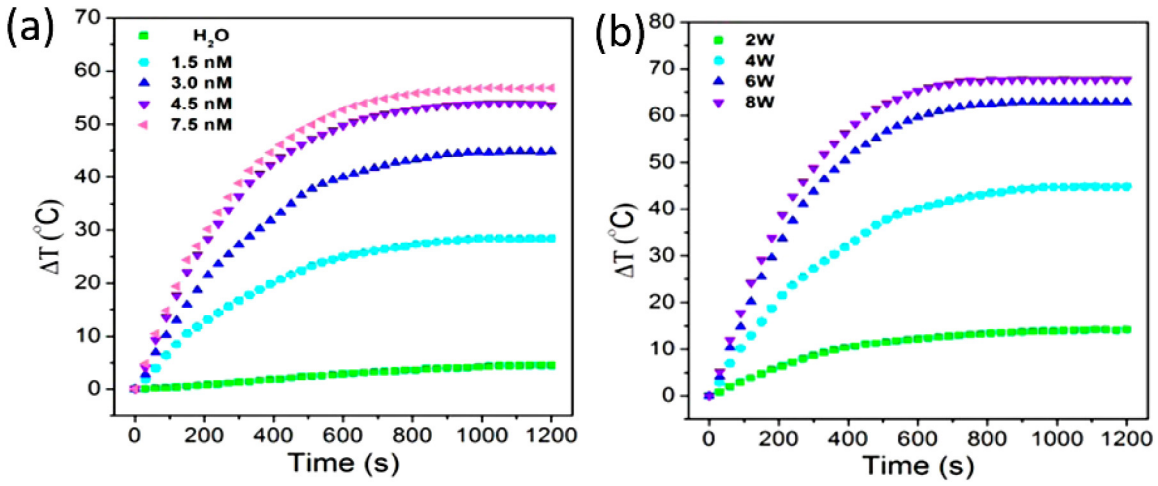

Fig. 5. Dependence of the increased temperature, ΔT, for (a) different concentrations (at 4 W/cm^2) and (b) laser powers (at 3 nM; $1.68 \cdot 10^{-7}$mg/mL) for Fe_3O_4 clusters ($\sim$64 nm) using $\lambda = 808$ nm irradiation [50].

3. Photothermal performance of Fe_3O_4 in the first, second and third optical windows

3.1. First biological window

There is a large number of studies of the photothermal efficiency of iron oxide nanoparticles (mostly Fe_3O_4) in the first biological window (mostly using $\lambda = 808$ nm, although other wavelengths have also been used). Importantly, these studies do not only involve cancer treatment, but a myriad of other applications [47–349]. It is important to emphasize that many investigations, although they involve composite nanoparticles combining iron oxides and other heat mediators, show that the iron oxide counterpart accounts for a significant part of the heating properties of the composite [53,58,71,78,94,102,107,110,115,116,120,122,125–128,130,132–134,138,143,147,149,150,158,166–168,170,172,173,178,189,191,197,221,223,225,238,242,243,250,257,261,262,276,277,282,288,292,302,303,306,308,312,313,323,325,328,334,339,341–343]. In fact, many studies show that Fe_3O_4 nanoparticles are relatively good heat mediators in the first optical window, with temperature increases, ΔT, typically above 20 °C [47–51,56,59,61,63,69,71,75,77,79,84–97,101,102,105,107–109,113–117,119,123,124,126,129,131,133,137,143,144,146–149,152–157,160–162,165,170–174,176,177,179,180,182,184,187,188,192,193–196,198,199,203,207–211,213–219,222,224,227,230,232,237,241–244,247,250,252,253,255,258,260,261,263,264,268–272,278–281,283,287,288,291,292,296,299,302,305–308,310,312,314,316,319–323,326,329,331,334,336,338,341,344,345,347]. However, ΔT values expanding from 0 °C to above 100 °C can be found in the literature, depending on the experimental conditions (e.g., type of particle, concentration, laser power and so on) [47–349].

Interestingly, although ΔT increases linearly with nanoparticle concentration at low concentrations [53,61,82,92,95,110,135,136,147,151,152,156,157,159,162,165,174,180,195,199,205,215,217,224,227,246,269,271,301,313,319,347] it tends towards saturation for higher concentrations (see Fig. 5a) [47–50,54,62,63,68,69,77,79,83,85–87,90–93,97,101,117,123,131,137,141,146,153,155,156,159,162,168,176,180,182,185,193,195,199,203,213,215,217,219,222,227,250,252,253,255,260,269,279,291,296,303,314,319,328,331,344,345]. This stems from the fact that at higher concentrations most of the light is absorbed before reaching the particles further away from the light source. Consequently, not all the particles contribute equally to ΔT at high concentrations.

Nanoparticle size and shape could potentially affect ΔT, since both factors can affect the absorption and, particularly, the scattering of the nanoparticles. However, Chu et al. showed that the nanoparticle shape (spherical, hexagonal, nanorods) has little influence on ΔT despite the changes in the absorption among the different shapes [47,348]. Similarly, Wen et al. showed that for small spherical Fe_3O_4 nanoparticles (2.1–9.5 nm), size had virtually no effect on ΔT [56], while Zhang et al., Guo et al., Gadora et al. and Lozano-Pedraza et al. evidenced that for larger particles, size had a only a small effect on ΔT [131,148,180,348]. Nevertheless, Peng et al. showed that 5 nm spherical nanoparticles had considerably smaller ΔT than 20 nm nanoparticles [213]. One possible origin of this effect may be because, as the size of Fe_3O_4 nanoparticles is reduced, the surface of the particle, which is prone to oxidation to γ-Fe_2O_3, plays a much important role. However, additional systematic studies would be necessary to establish a clear correlation between size or shape and ΔT. In fact, one has to bear in mind that since the different nanoparticles being compared are often produced using diverse approaches, their oxidation state or number and type of defects could be distinctly different. In fact, the degree of crystallinity and the number and type of particle defects (which can strongly affect the optical properties) have been shown to influence ΔT, where more crystalline particles perform better [348,355]. In fact, it has been proposed that defects may have stronger impact on photothermia than other factors such as size or oxidation state [345,355]. In addition, Guo

et al. showed that, in contrast to *in vitro*, the *in vivo* heating efficiency depended strongly on the nanoparticle size, probably due to the different degree of internalization or the extent of the aggregation of the nanoparticles inside the tumors [180].

Another parameter which influences ΔT is the degree of nanoparticle aggregation. Namely, in some cases the effect of the controlled aggregation of nanoparticles, which form small reproducible clusters, on photothermia has been investigated. Interestingly, most of the studies show that controlled aggregation improves ΔT [50,55,59,83,84,97,108,113,144,149,164,219,289,348], although exceedingly large aggregates may be detrimental [51,55,59,111,162,169,219]. The improvement of ΔT for aggregates may arise from the larger absorption of the aggregates as compared to individual particles, although there is probably a trade-off between enhanced absorption and increased scattering. Namely, larger aggregates should have stronger scattering, which is detrimental to the photothermal performance. However, as mentioned earlier, it has to be taken into account that the performance of nanoparticles or aggregates in suspension can be different than *in vitro* or *in vivo*, since smaller particles tend to agglomerate uncontrollably when they are inside the cells [169], which can drastically affect their photothermal behaviour [169].

In addition, ΔT is clearly influenced by the laser intensity. Most studies show that increasing the intensity of the laser results in larger ΔT. However, although usually ΔT is roughly proportional to the intensity [52,54,68,69,83,85,101,103,119,129,136,147,152,165,171,223,224,227,266,269,283,291,316,319,344,348], in other cases the relationship is non-linear (Figure 5b) [48,50,62,75,78,79,109,164,172,185,190,218,246,278,287,292,331].

Nevertheless, it is important to highlight that most of the studies use laser powers well above the established MPE for $\lambda = 808$ nm of 0.33 W/cm^2.

Given the non-linear dependence of ΔT on diverse parameters, it is somewhat complex to compare the various studies since they use different nanoparticle size and shape, degree of aggregation, capping layers, concentrations, laser power, initial temperatures, irradiated areas or irradiation times. However, to try to quantitatively compare the efficiencies of heat mediators under diverse conditions one can use the photothermal conversion efficiency parameter:

$$\eta = \frac{hA\,(T_{max} - T_{amb}) - Q_0}{I(1 - 10^{-A_\lambda})},$$

where h is the heat transfer coefficient, A is the irradiated area, $T_{\max}$ is the highest temperature obtained, T_{amb} is the ambient temperature, Q_0 is heat dissipated from light absorbed by the sample holder and the medium, I is the incident laser power and A_λ is absorbance of the sample at the wavelength λ [451].

Namely, η gives an indication of how good a given material is in converting light into heat. However, η is not an intrinsic property of the material and depends on intrinsic and extrinsic factors, like the volume of the nanoparticle, the degree of aggregation or the coating of the particles, among other factors, indicating that parameters like light scattering may play an important role in η. Namely, there is a correlation between η and the ratio between the absorption and the extinction (absorption+scattering) at the given wavelength [55,452,453].

Despite the possibility of having a more quantitative comparison between samples than that given by ΔT, only a relatively small number of the studies evaluate η for Fe_3O_4 nanoparticles. Remarkably, the reported conversion efficiency values for Fe_3O_4 nanoparticles show a very broad variety of values, ranging between $\eta = 2.2\%$ and 90% [50,51,55,59,62,68,79,83,85,89,95,97,100–103,108,113,126,127,137,149,151,152,158,159,162,165,166,178,197,204,213,214,217,219,227,231,233,238,248,250,254,259,285,288,291,294,297,298,301,313,314,319,331,342,348]. This implies that this parameter is not an intrinsic property of Fe_3O_4, but depends on the specific optical properties of the nanoparticles, which are related to the oxidation state and defects, and to some extent to the concentration, size, shape and degree of aggregation of the particles or other extrinsic parameters such as the capping layers or even the measurement conditions or the details of the efficiency calculations [51,55,62,66,68,97,108,113,149,162,165,227,297,348].

Nevertheless, it is important to highlight that many of the reported values for Fe_3O_4 are similar or better than most of the state-of-the-art proposed heat mediators such as Au nanorods, carbon nanotubes or metal chalcogenides, among others [11].

Interestingly, in addition to the oxidation state or defects that affect the optical properties, doping or substitutions in Fe_3O_4 nanoparticles with different ions can be used to tune their absorption spectrum, which can be used to enhance η; e.g., S doping has been reported to lead to $\eta = 58\%$ [454], or $Zn_xFe_{3-x}O_4$ has been shown to have a higher η than similar Fe_3O_4 nanoparticles [95].

However, it is important to emphasize that the figure of merit for photothermal treatments is the ΔT obtained for a given condition, where the aim is to minimize the laser power, the duration of the treatment and the concentration of the nano heat mediators.

Notably, ΔT depends in a complex way on both μ_A (which is how much light is absorbed by the material) and η (which is how efficient is the material in converting the absorbed light into heat). Interestingly, a systematic study of the photothermal heating capacity of Fe_3O_4 nanoparticles in the $\lambda = 730$ nm–840 nm spectral region has shown that there is not a one-to-one correlation between the experimental extinction and the ΔT [52]. In fact, the lack of a clear correlation between the absorption (extinction) and ΔT is corroborated in other studies comparing different wavelengths within the NIR-I [47,48,50,51,54,59,62,63,68,297,348]. This seems to indicate a complex correlation between the heating efficiency and not only to the absorption, but also to the scattering. Nevertheless, the role of the exact oxidation state of the nanoparticles, which determines both the absorption and the scattering, should also be considered when comparing different systems [348].

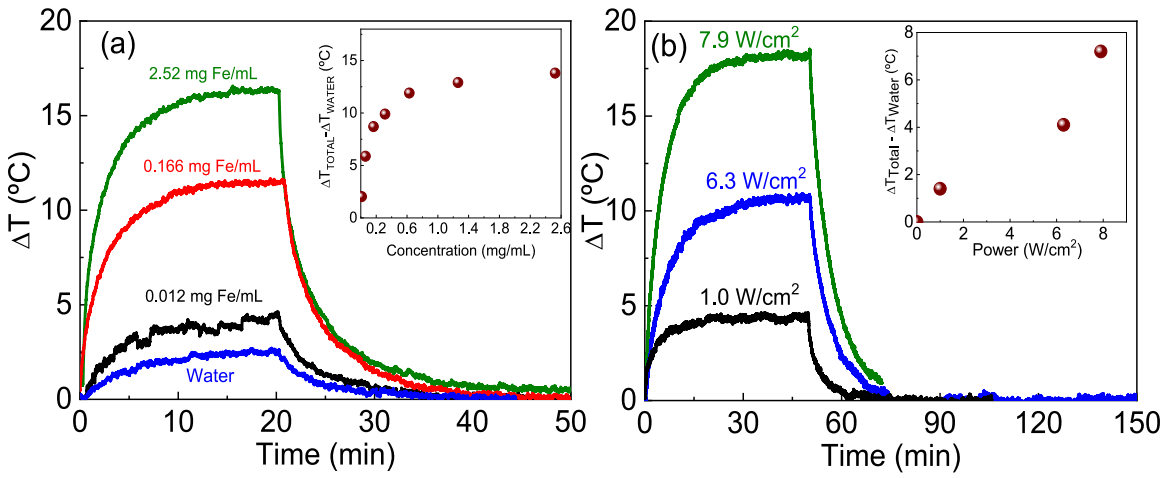

Fig. 6. Heating curves (Annex C) for different (a) concentrations (at 0.1 W/cm^2) and (b) laser powers (at 0.1 mg/mL) for 16 nm Fe_3O_4 nanocubes (see Annex B [394]) using $\lambda = 1064$ nm irradiation. Shown in the insets is the dependence of the intrinsic heating of the particles (ΔT_{Total} - ΔT_{Water}) on the respective conditions. Note that ΔT_{Water} is different at different powers.

3.2. Second biological window

Remarkably, despite the rather promising optical properties of Fe_3O_4 in the NIR-II and the advantages of using this wavelength range from the skin perspective (i.e., light penetration and MPE), there are relatively few studies of the heating efficiency of Fe_3O_4 nanoparticles in the NIR-II range [54,346–360].

Similar to the studies in the NIR-I, there is a rather large spread of the reported ΔT values in the second biological window, ranging $\Delta T \sim 1$ °C to 50 °C [54,346–360], depending on the conditions (laser power, nanoparticle concentration, duration of the actuation, type of particles and so on). However, it is important to emphasize that the conditions used in the second biological windows are usually milder than the ones used in the NIR-I, for example, with small concentrations of nanoparticles or lower laser powers, within the MPE (1 W/cm^2 for $\lambda = 1064$ nm) [54,346,347,352,355,360]. Our own measurements using 16 nm Fe_3O_4 nanocubes (see Annex B [394]) evidence that, in concordance with the NIR-I experiments, ΔT depends on the concentration and the laser power (see Fig. 6). As, expected, the dependence of ΔT on the concentration shows that, while ΔT is proportional to the concentration for small concentrations [358], it tends to saturate for large concentrations (inset in Fig. 6a). On the other hand, in the range of powers used in our experiment the ΔT remains rather linear (inset in Fig. 6b), similar to other studies [358].

Concerning the efficiency, η, only a few studies have evaluated this parameter, with rather different η values, in the range 11%–90% [297,346,347,353,355]. To try to understand this broad range of η values, we studied the photothermal properties of three different iron oxide systems (16 nm nanocubes, 27 × 6 nm nanorods and 50 nm clusters composed of 5 nm particles; see Annex B). As can be seen in Fig. 7a, although the three systems were measured in the same conditions (0.35 mg/mL and 0.793 W/cm^2) the heating is quite different, where the nanocubes heat considerably more than the other two systems. Interestingly, the evaluation of η values from the ΔT curves leads to rather different values for the three systems. While the nanocubes have a moderate efficiency ($\eta = 53\%$), nanorods and nanoclusters have lower efficiency ($\eta = 24\%$ and 20%, respectively).

To clarify this issue, the extinction spectra were measured for the three systems (Fig. 7b). Although all three systems are nominally Fe_3O_4, their extinction spectra are quite different. As discussed earlier, this probably stems from the degree of oxidation towards γ- Fe_2O_3, different amounts and types of defects, and the contribution of the scattering, which is size and shape dependent. Interestingly, the ΔT and η values for the three samples show some degree of correlation between the extinction and their photothermal properties. Namely, the nanocubes with a larger extinction at $\lambda = 1064$ nm have a better photothermal performance. However, the correlation between the different parameters is not straightforward.

Interestingly, Cabana et al. and Bertuit et al. have compared the performance of Fe_3O_4 and γ-Fe_2O_3 in the NIR-II range [352,355]. The results show that, in equal conditions of nanoparticle concentration and laser intensity, the ΔT reached by the γ-Fe_2O_3 nanoparticles is considerably lower than for the Fe_3O_4 ones, particularly at low concentrations, as expected from the difference in μ_E between both materials at $\lambda = 1064$ nm (see Fig. 4). However, Bertuit et al. emphasized the importance of the defects, rather than the stoichiometry, in the difference observed in their oxidized (γ-Fe_2O_3-like) nanoparticles [355].

Diverse studies measured the photothermal properties of the same type of particle under the same conditions (nanoparticle concentration and laser intensity) both at $\lambda = 808$ nm and 1064 nm [54,346–349]. Several of the results show that the heating power of the Fe_3O_4 nanoparticles is considerably better in the second biological window [54,346, 347]. For example, Espinosa et al. found ΔT (808 nm) ~6 °C < ΔT (1064 nm) ~8.5 °C (using [Fe] 0.672 mg Fe/mL and 0.8

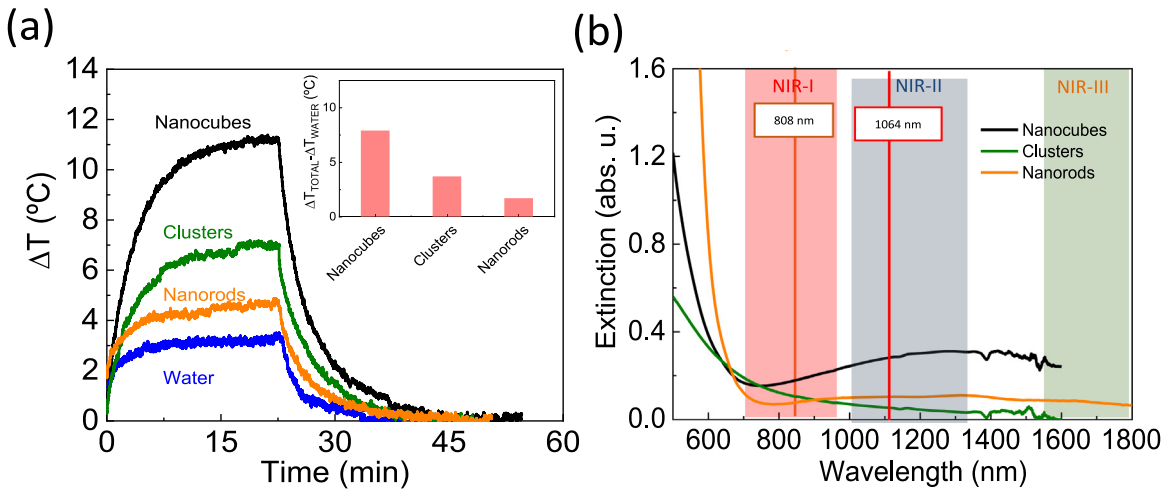

Fig. 7. (a) Heating curves (Annex C) for 16 nm nanocubes, 27 × 6 nm nanorods and 50 nm clusters (see Annex B [394,455,456]) (using 0.35 mg/mL at 0.79 W/cm^2) using $\lambda = 1064$ nm irradiation. Shown in the inset is the dependence of the intrinsic particle heating (ΔT_{Total} - ΔT_{Water}) for the three systems. (b) Extinction spectra (Annex C) for the three systems. The shaded areas represent the first (NIR-I), second (NIR-II) and third (NIR-III) biological windows. The wavelengths used in the photothermia experiments ($\lambda = 808$ nm and 1064 nm, respectively) are highlighted by vertical lines.

W/cm^2 for 30 s) [54]. On the other hand, Huang et al. have reported an even greater ΔT improvement, ΔT (808 nm) ~7 °C << ΔT (1064 nm) ~33 °C (with a concentration about 0.375 mg Fe/mL and using 0.38 W/cm^2 for 480 s) [346]. Similarly, Zhao et al. have reported ΔT (808 nm) ~22 °C < ΔT (1064 nm) ~27 °C (using 2 mg/mL and 1 W/cm^2 during 600 s) [347]. However, Arranz et al. showed that ΔT is quite similar at either $\lambda = 800$ nm or 1053 nm [349]. Our own results, using 0.35 mg/mL of 16 nm Fe_3O_4 nanocubes and 0.79 W/cm^2, show ΔT(808 nm) ~7.6 °C < ΔT (1064 nm) ~11.2 °C, similar to other studies. However, when the effect of water on ΔT is considered at the two wavelengths, the intrinsic heating of the particles becomes similar $\Delta T_{Total} - \Delta T_{Water}$(808 nm) ~7.3 °C < $\Delta T_{Total} - \Delta T_{Water}$ (1064 nm) ~7.9 °C. In contrast, the difference in ΔT (after water correction) at $\lambda = 808$ nm and 1064 nm for the Fe_3O_4 clusters is negligible (3.6 °C vs 3.7 °C), while for the nanorods, in fact, the heating is better at $\lambda = 808$ nm than at 1064 nm (4.1 °C vs 1.7 °C). Comparison the extinction of the nanocubes, nanocluster and nanorods (Fig. 7b), reveals no clear correlation between the extinction and ΔT, implying that other parameters apart for the absorption properties must enter into the ΔT of the different iron oxides.

However, it is worth emphasizing that the laser power used for the two wavelengths is the same in all the studies. However, since the MPE for $\lambda = 1064$ nm is larger than that for $\lambda = 808$ nm, the difference in ΔT could be further enhanced if the MPEs corresponding to each λ were used.

Lozano-Pedraza et al. studied η in the first and second biological widows and observed a larger η in the NIR-II, in agreement with the increased extinction of the nanoparticles in this range [348]. Our own study comparing η for the 16 nm nanocubes, 27 × 6 nm nanorods and 50 nm clusters (see Annex B) at 808 nm and 1064 nm show that our results do not follow the same trend, where, for example, for the nanocubes and the clusters η(808 nm) = 55% > η(1064 nm) = 52 % (nanocubes) and η(808 nm) = 40% > η(1064 nm) = 24% (clusters), respectively. Consequently, the results seem to indicate that the photothermal conversion efficiency of Fe_3O_4 depends in a complex way on the extinction of the materials, and more systematic studies are necessary to understand these effects. However, since, ΔT (and not η) is what will ultimately determine the laser power and nanoparticle concentration required for an efficient treatment, it is clearly advantageous to use $\lambda = 1064$ nm for photothermal therapy for most iron oxide systems.

3.3. Third biological window

Although from the skin optics perspective the third biological window does not appear optimal, more recent studies seem to indicate that, to properly account for the light penetration in the human body, subcutaneous tissues also need to be taken into account [361,362,434]. Consequently, the penetration of NIR-III light into the body may be adequate for photothermal applications. Thus, for the sake of completeness, we studied the performance of the Fe_3O_4 nanocubes, nanorods and clusters (see Annex B) at $\lambda = 1670$ nm (in the NIR-III range) using 0.35 mg Fe/mL and 0.793 W/cm^2. As can be seen in Fig. 8, the ΔT of all the three systems is rather high, better that in the second biological window (Fig. 6). However, one should consider the heating of water which, in fact, for $\lambda = 1670$ nm accounts for greater part of ΔT. Although for some applications the effect of water heating would not be a problem, for biomedical uses, such a large heating of the medium surrounding the particles could induce unwanted side effects in healthy cells and tissues. Thus,

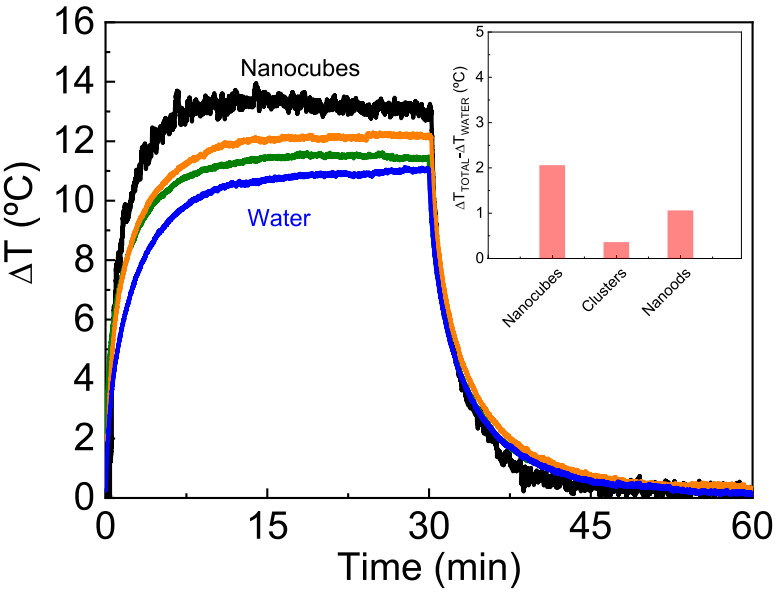

Fig. 8. Heating curves (Annex C) for 16 nm nanocubes, 27 × 6 nm nanorods and 50 nm clusters (see Annex B) (0.35 mg/mL at 0.79 W/cm^2) using $\lambda = 1670$ nm irradiation (NIR-III). The inset shows the dependence of the intrinsic particle heating (ΔT_{Total} - ΔT_{Water}) for the three systems.

although $\lambda = 1670$ nm is in the third biological window, implying that light absorption by water has a minimum in this range, its absorption is still considerably high (compared to 808 and 1064 nm; see Annex D), leading to a rather large temperature increase of water in this wavelength.

Note that despite the somewhat low intrinsic heating of the three Fe_3O_4 heat mediators, the efficiency of the Fe_3O_4 nanocubes is rather good, reaching about $\eta \sim 70\%$ for the current conditions.

4. *In vitro* and *in vivo* photothermal therapies of Fe_3O_4 in the first and second optical windows

There are numerous studies of the effects of photothermal treatments using iron oxide nanoparticles on cancerous cells in the first biological window. These *in vitro* NIR-I studies evidence that photothermia is an efficient way to destroy cancer cells [47,48,52,59–62,68,76,77,84–88,90,92–94,97,98,101,108,113,119,124,133,137,141,151,153,155,157,162,169,175,177,180,184,193,194,213,214,218,221,224,231,233,246,258,284,285,292,332]. For example, cancer cell death beyond 90% (i.e., cell viabilities below 10%) is achieved in many cases after laser irradiation [48,61,77,85,86,93,119,153,162,184,193,213,224,258,285,332], even under rather mild irradiation conditions [85]. Some systematic studies evidence that the cell viability after the photothermal treatment is closely related to the nanoparticle concentration, the irradiation time and the laser power [47,52,56,59,61,87,88,90,92,94,97,98,113,117,124,137,153,155,157,162,184,193,194]. Importantly, many studies show that by controlling the irradiation conditions, apoptosis cell death (rather than necrosis, which can lead to side effects) can be induced [82,83,87,97,98,101,113,116,124,153,180,193,213,214,224,233,246,289,306,313,332].

Remarkably, many *in vivo* studies using Fe_3O_4 nanoparticles or nanoparticle clusters show that the photothermal treatments in the NIR-I range can induce tumor growth inhibition, strong tumor regression, or even complete tumor removal, just a few days after the treatments [47–49,59,65,69,76,77,84–88,92,97,108,113,114,119,123,124,129,142,144,152,155,157,158,177,180,193,194,196,213,222,224,233,247,258,285,286,301,313]. However, since the conditions of the diverse studies (e.g., different types of tumors, nanoparticle concentration, capping layers, laser power and spot size, laser wavelength, or irradiation duration) are not readily comparable, it is difficult to reach any general conclusions from these studies. Moreover, it is important to highlight that virtually all the *in vivo* studies use laser powers high above the recommended MPE of 0.33 W/cm^2 at 808 nm, often above 1 W/cm^2 and reaching values as high as 6.6 W/cm^2 [48,49,59,84,86,88,97,108,113,114,119,123,124,129,141,144,151,155,157,158,177,180,193,194,196,213,224,233,246,258,285,286,301] (with a few exceptions [47,69,87,221]).

In contrast, despite the very promising perspectives of photothermal treatments in the NIR-II window, there are only a few *in vitro* studies in this range [346,347,352,354,356,359,360]. In agreement with what has been observed for the NIR-I, photothermia in the NIR-II range is an excellent approach to kill cancerous cells *in vitro*. For example, Huang et al. used ~200 nm Fe_3O_4 nanoclusters to treat HeLa cancer cells by irradiating with a $\lambda = 1064$ nm laser (0.38 W/cm^2) for 10 min [346]. The treatment resulted in a decrease of the cell viability to 59% after one day, which was further reduced after 3 days to 18%. This significant decrease in cell viability after a few days suggests an apoptotic cell death rather than necrotic. Moreover, it is worth emphasizing that rather mild irradiation conditions were used, with a laser intensity

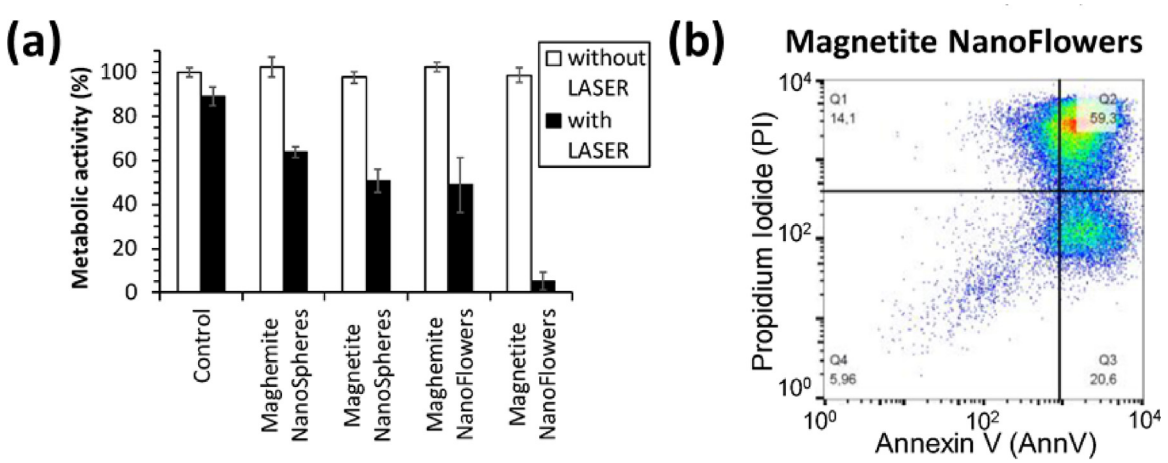

Fig. 9. (a) Metabolic/cytotoxicity tests of PC3 prostatic cancer cells treated with a $\lambda = 1064$ nm laser at a power density of 0.3 W/cm^2 for 10 min using four different types of iron oxide nanoparticles as heat mediators; 12.7 nm γ-Fe_2O_3 nanoparticles — **Maghemite NanoSpheres**; 27 nm γ-Fe_2O_3 clusters — **Maghemite NanoFlowers**; 12.7 nm Fe_3O_4 nanoparticles — **Magnetite NanoSpheres**; 27 nm Fe_3O_4 clusters — **Magnetite NanoFlowers**. (b) Annexin V/propidium iodide apoptosis assay for cells treated with magnetite nanoflowers after laser irradiation.
Source: Adapted from Ref. [352].

well below the MPE for $\lambda = 1064$ nm (1 W/cm^2) [346]. Interestingly, the cell mortality can be further increased when using a magnet to concentrate the nanoparticles in the irradiation area [346]. On the other hand, Cabana et al. used four different types of particles (Fe_3O_4 and γ-Fe_2O_3; see Fig. 9) to treat PC3 cancer cells with a $\lambda = 1064$ nm laser (0.3 W/cm^2) for 10 min [352]. The results using Fe_3O_4 nanoclusters show that a cell viability as low as 5% can be obtained after one day [352]. This is rather remarkable considering that the laser power was only 0.3 W/cm^2, i.e., below the 1 W/cm^2 MPE for $\lambda = 1064$ nm. However, in this case the cell death was found to be mostly by necrosis (60%). Notably, the treatments using γ-Fe_2O_3-based particles (nanoparticles and clusters) resulted in poorer results than the corresponding particles based on Fe_3O_4 (Fig. 9), consistent with the worse photothermal performance of the former [352]. Zhao et al. have shown a reduction of the cell viability to 65% after $\lambda = 1064$ nm irradiation when using chains of Fe_3O_4 nanoparticle aggregates. Interestingly, the cell viability can be further reduced (to 25%) when NIR-II irradiation, anticancer drugs and mechanical cell lysis using alternating magnetic fields are combined [347]. Finally, Wang et al. have reported cell viabilities of about 18% after using hollow ~200 nm Fe_3O_4 nanoclusters, again, under rather mild conditions (i.e., $\lambda = 1064$ nm laser power at 0.8 W/cm^2 and 0.5 mg Fe/mL) [354]. Interestingly, Li et al. formed soft robots using Fe_3O_4 nanoparticles and used them to effectively kill cancerous cells. However, the power used (2.5 W/cm^2) was well above the MPE for $\lambda = 1064$ nm [356].

Unfortunately, there are very few *in vivo* investigations based on Fe_3O_4 nanoparticles in the NIR-II range. Zhao et al. have shown that using chains of Fe_3O_4 nanoparticle aggregates, irradiation at 1064 nm irradiation produces a reduction of the tumor growth rate (Fig. 10).

However, to induce complete tumor destruction, additional therapeutic modes (anticancer drugs and mechanical cell lysis) are required [347]. Yet, note that the extinction of these aggregates does not show the expected increase in the NIR-II region [347], which may indicate the presence γ-Fe_2O_3 rather than Fe_3O_4. This may explain the somewhat weak effect of the NIR-II irradiation in these particles, both *in vitro* and *in vivo*.

On the other hand, Wang et al. have again reported a substantial tumor growth inhibition using hollow ~200 nm Fe_3O_4 nanoclusters and $\lambda = 1064$ nm irradiation at 0.8 W/cm^2. To completely eradicate the tumor, they needed to encapsulate the anticancer drug DOX inside the hollow structure of the clusters [354]. On the other hand, Qin et al. have shown only a rather small tumor growth reduction WHEN ~116 nm Fe_3O_4 nanoparticles and $\lambda = 1064$ nm irradiation at 0.75 W/cm^2 were used [359]. Unfortunately, similar to the study by Zhao et al. [347], the extinction of the nanoparticles in Wang et al. and Quin et al. studies does not show an increase in the second biological window, which may explain the limited efficiency of the NIR-II treatment when Fe_3O_4 nanoparticles are used alone [354,359].

In view of the rather few *in vitro* and *in vivo* studies for NIR-II, this is certainly a field with great potential yet to be explored.

5. FeO (wüstite) as a potential photothermal heat mediator

FeO (wüstite) is another interesting constituent of the family of iron oxides. However, contrary to Fe_3O_4 or γ-Fe_2O_3, it is not ferrimagnetic at room temperature. Although FeO has been far less studied than other iron oxides, FeO-based nanoparticles have been assessed for their use in diverse biomedical applications [360,457–464]. However, from the optic viewpoint, the simulated absorption properties of FeO (see Annex A) [465] are quite appealing since they present a rather

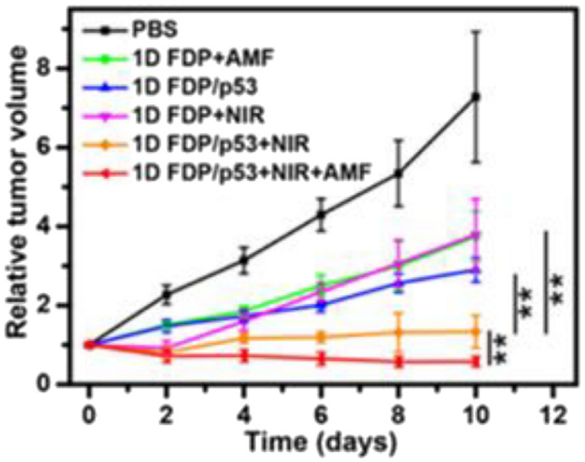

Fig. 10. Evolution of the relative tumor volume after different treatments using one-dimensional polycation-coated nanohybrids Fe_3O_4@Dex-PGEA (1D FDP) [347]. [AFM — alternating magnetic field; p53 — antioncogene p53; NIR — 1064 nm irradiation].

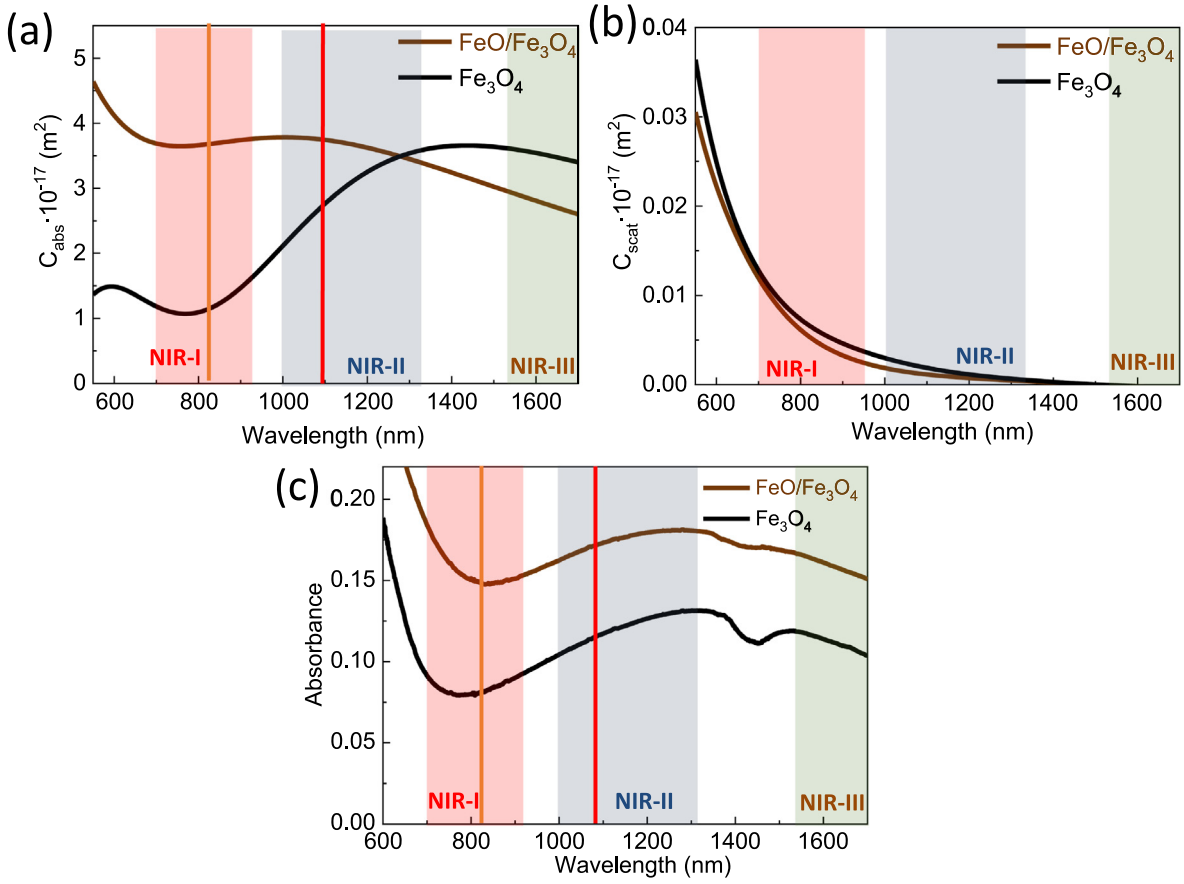

Fig. 11. Dependence of the theoretical (a) absorption, μ_A (C_{abs}), and (b) scattering, μ_S (C_{scat}), cross-sections for spherical FeO and Fe_3O_4 nanoparticles (diameter 25 nm). (c) Experimental wavelength dependence of the extinction (Annex C), for 40 nm FeO/Fe_3O_4 nanocubes and 16 nm Fe_3O_4 nanocubes (see Annex B) [394,466,467]. The shaded areas represent the first (NIR-I), second (NIR-II) and third (NIR-III) biological windows. The typical wavelengths used experimentally in photothermia in the NIR-I and NIR-II regions (λ = 808 nm and 1064 nm, respectively) are highlighted by vertical lines.

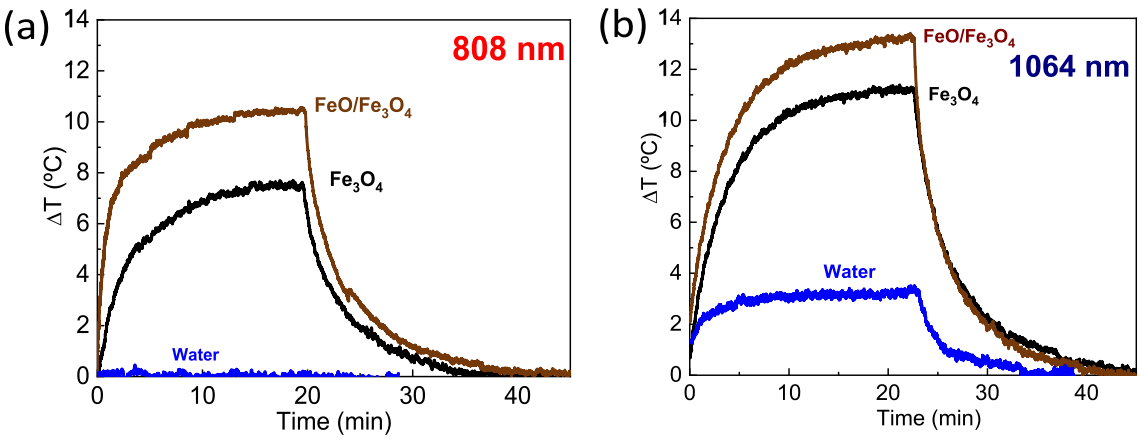

Fig. 12. Heating curves (Annex C) for 40 nm FeO/Fe_3O_4 core/shell nanocubes and 16 nm Fe_3O_4 nanocubes (see Annex B) [394,466] (0.35 mg/mL and 0.79 W/cm^2) using (a) $\lambda = 808$ nm and (b) $\lambda = 1064$ nm irradiation.

high μ_A in both the first, second and third biological windows, significantly better than Fe_3O_4 (Fig. 11). Additionally, the scattering, μ_S is also rather low for small (25 nm) FeO nanospheres.

Remarkably, FeO is not stable under ambient conditions, and in nanoparticle form it partially oxidizes to Fe_3O_4, typically leading to FeO/Fe_3O_4 core/shell nanoparticles [466,468–471], which is a rather stable structure for sufficiently large particles [466]. This fact offers the possibility of exploiting the appealing optical absorption properties of both FeO and Fe_3O_4 while maintaining the overall magnetic character due to the presence of Fe_3O_4. In fact, this type of particle can be easily manipulated using magnets [467] (see Annex E) or can be used in magnetic hyperthermia [457,458].

The FeO/Fe_3O_4 core/shell nanoparticles indeed show experimentally a rather strong extinction spectrum [471]. Our results show that the shape of the extinction curve of FeO/Fe_3O_4 core/shell nanoparticles is similar to that of pure Fe_3O_4 since it combines the properties of the Fe_3O_4 shell and the FeO core. However, due to the presence of the FeO core, the extinction of the FeO/Fe_3O_4 nanoparticles is considerably stronger than that of the pure Fe_3O_4 nanocubes (Fig. 11c).

Remarkably, as can be seen in Fig. 12, the FeO/Fe_3O_4 nanoparticles outperforms the pure Fe_3O_4 nanocubes in terms of ΔT both in the NIR-I and NIR-II ranges. In addition, the efficiency extracted from Fig. 12 shows that η of the FeO/Fe_3O_4 nanocubes is rather high in both biological windows, surpassing many state-of-the-art photothermal mediators [15]. In fact, its efficiency is clearly better than that for the Fe_3O_4 nanocubes both at $\lambda = 808$ nm (55% - Fe_3O_4 vs 68% - FeO/Fe_3O_4) and at $\lambda = 1064$ nm (53% - Fe_3O_4 vs 79% - FeO/Fe_3O_4). Thus, the photothermal performance (ΔT and η) correlates nicely to the higher extinction coefficient of the FeO/Fe_3O_4 nanocubes.

These results clearly reveal the great potential of FeO/Fe_3O_4 nanoparticles for different types of photothermal-based applications, thus encouraging *in vitro* and *in vivo* investigations.

6. Other potential uses of iron oxide nanoparticles in the second biological window

Although we have focused on the use of photothermia for cancer therapy using iron oxide nanoparticles (mainly Fe_3O_4) exploiting the enhanced light absorption and the excellent heating performance of the Fe_3O_4 and FeO/Fe_3O_4 nanoparticles in the second biological window and the overall advantages of this wavelength range, other possible applications of iron oxide nanoparticles using NIR-II light can be envisaged.

6.1. Combined photothermal treatments for oncology

Combining photothermal treatments in the NIR-II range with other therapy modes can lead to an enhancement of the therapeutic effect. For example, combining photothermia and magnetic hyperthermia has been shown to be a very powerful synergetic combination for cancer treatment. However, although the enhanced efficiency of the photo/magnetic-hyperthermia has been demonstrated in the NIR-I region [54,82,98,136,140,312], it has not been systematically explored in the second biological window.

An additional interesting cancer (or other diseases) treatment which could be improved using NIR-II light, is the controlled photo-induced drug delivery in nanoparticle-based chemotherapy approaches [56,96,99,101,105,117,123,137,144,146,156,176,182,184,195,203,204,214,218,231,258–260,267,271,279,295,320,321,325,347,354]. Namely, the enhanced heat induced by the NIR-II light would probably allow more efficient on-demand triggering of the drug release carried by the Fe_3O_4 nanoparticles when they reach the site of action [472]. In fact, it has been proposed that the heat induced in Fe_3O_4-based photothermal experiments could lead to cell poration, which would lead to a better absorption of the drugs carried by the heat mediators [261].

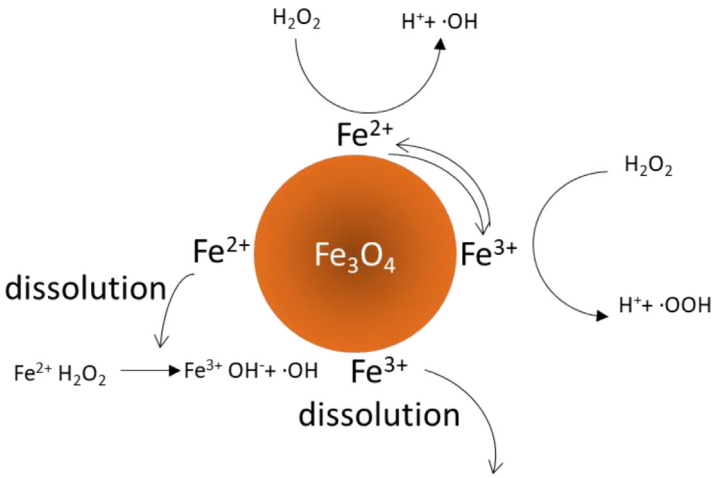

Fig. 13. Schematic diagram of the free radicals or reactive oxygen species (ROS) by Fe_3O_4 nanoparticles [477].

Moreover, another approach often used in cancer treatment is photodynamic therapy, where free radicals or reactive oxygen species (ROS) are used to kill malignant cells [473,474]. Fe_3O_4 nanoparticles have also the potential to generate photodynamic effects (Fig. 13) [475–477]. Namely, the Fenton reaction can be triggered by the Fe^{2+} ions that react with H_2O_2 (usually present inside cells) leading to highly reactive hydroxyl ($^{\bullet}OH$) and superoxide ($O_2^{-\cdot}$) radicals though the Haber–Weiss reaction [476,477]. In fact, these reactions are enhanced at higher temperatures [478–480] as observed also for Fe_3O_4 nanoparticles [215,318,345]. Therefore, the enhanced photothermia in the second biological window could be beneficial for ROS generation. In principle, the larger amount of Fe^{2+} ions in FeO nanoparticles could enhance the photodynamic and photothermal synergistic actuation, although this effect has not been explored yet.

Additionally, as shown for NIR-I, iron oxides are often combined with other materials to increase the production of H_2O_2 or to hinder the reduction of the Fenton reaction with time and, thus, enhance the efficiency of the photodynamic treatments [57,81,110,116,118,119,140,277,291,295].

Interestingly, the ferroptosis cell death mechanism has also been proposed to be enhanced by photothermal temperature increases [215,252], which could potentially be enhanced in the second biological window.

6.2. Non-oncological biomedical applications of photothermal therapy

The first obvious uses of iron oxide-photothermia would be in other biomedical applications beyond cancer, like the treatment of other diseases, where the application of local heat may be advantageous, such as atherosclerosis or even neurological diseases [481].

Interestingly, iron oxide-based photothermia can be used for antibacterial treatments, including biofilm eradication or wound disinfection, which have already been demonstrated in the first optical window using Fe_3O_4 nanoparticles [91, 131,159,167,173,190,198,237,243,257,263,276,287,288,291,311,314,325,345,482,483].

6.3. Diagnosis: Imaging agents and sensing

The second biological window could not only improve the therapy aspects of iron oxide nanoparticles, but also their diagnostic characteristics. For example, the increased induced heat in the NIR-II could improve different light-induced imaging modes proposed for Fe_3O_4 nanoparticles, which have already been demonstrated in the first biological window, like photoacoustic imaging [123,133,177,180,222,233], photothermal optical coherence tomography [484,485], or photothermal microscopy [213,486]. A different diagnostic feature of Fe_3O_4 nanoparticles which may be improved is sensing, for example, in thermal sensing [135,154,166,174,238,283,303,483,487]. In addition, given their strong absorption in the NIR-II and their magnetic character, Fe_3O_4 nanoparticles could potentially be used for *in situ* photo-magnetic temperature sensing in the second biological window [488].

6.4. Environment-related applications

Beyond biomedical applications there are other fields where the enhanced NIR absorption and the outstanding photothermal performance of Fe_3O_4 nanoparticles in the second biological window may be appealing. For example, Fe_3O_4 nanoparticles have long been used for environmental remediation *via*, for example, the Fenton reaction (Fig. 13), where the free radicals or reactive oxygen species (ROS) degrade many organic pollutants [489–491]. In principle, the heat induced by

the NIR-II irradiation could improve the efficiency of these processes [318,345]. In addition, iron oxide nanoparticles can absorb metal ions in solution [492,493]. Since this process is thermally activated [494], it could potentially be enhanced by the photoinduced temperature increase.

Another proposed use of Fe_3O_4 nanoparticles as photothermal mediators is as insecticides, where the generated heat is used to kill insect larvae [292].

Iron oxide nanoparticles have been used for solar water heating, purification, sterilization, desalinization or even anti-freezing or de-icing coatings [280,287,495–500]. Given that solar light is composed of about 50% infrared irradiation, raising the absorption in the NIR-II region using Fe_3O_4 nanoparticles, rather than γ-Fe_2O_3, would enhance the absorption of solar light for diverse applications [495–500]. Notably, the intense and rather flat absorption spectrum of the FeO nanoparticles in the visible and NIR could also find environmental applications exploiting the whole sunlight spectrum.

6.5. Energy-related applications

The photothermal effect could also be exploited in the broad concept of photothermal catalysis, in which light-induced heat is used to drive chemical reactions [501–503], and the strong NIR-II heating can be used to activate certain reactions [331,358].

In addition, the strong absorption of Fe_3O_4 or FeO/Fe_3O_4 nanoparticles in the NIR-II range may be beneficial for non-linear optics and absorbing applications [504–506], where the robustness of oxides compared to other optically non-linear materials [507] may be an advantage for many optical applications. The local photothermal heating can also be exploited to drive the movement of Fe_3O_4-based nanomotors [283]. Moreover, the enhanced absorption in the NIR of Fe_3O_4 has also been used to design more efficient windows [53,508,509].

On the other hand, the photothermal heat generated by Fe_3O_4 nanoparticles when they are embedded in different types of thermosensitive matrices can be used for very widespread applications, ranging from friction control to energy storage in phase-change materials [160,179,187,188,202,207,216,220,230,232,236,240,241,247,263,264,268,275,278,281,305,307,326,329,337,338,340,346,356,510,511]. These applications are based on the photothermally induced generation of physiochemical changes in the matrix [512] (e.g., a solid–liquid phase transition, changes in viscosity) that can be exploited for diverse uses, like soft robots, actuators, shape-memory materials, energy storage, light-controlled ferrofluids, tribological applications, artificial muscles, wireless-controlled switches or energy harvesters among many others.

In fact, there are probably many other uses of Fe_3O_4 nanoparticles which could benefit from an enhanced absorption and/or large photothermal effects in the NIR-II.

7. Conclusions

Summarizing, iron oxides (Fe_3O_4, γ-Fe_2O_3 and FeO) are excellent photothermal agents for biomedical and other applications both in the first (NIR-I) and second (NIR-II) biological windows. Iron oxides are biocompatible and biodegradable, and their metabolic route is very well known. As iron is an abundant element in the Earth's crust, the synthesis of these nanoparticles is relatively cheap. Moreover, due to their magnetophoretic properties, they can be guided inside the body and concentrated at the target organ/tissue boosting the efficiency of the photothermally activated treatment. However, the spread of the photothermal performance results, both in terms of ΔT and η, indicates that the correlation between the physicochemical properties of the iron oxide nanoparticles and photothermia is not straightforward, and more systematic studies are needed to fully elucidate the efficiency of this type of system. There are several parameters that seems to affect the photothermal performance of the iron oxides for photothermal applications. On the one hand, there are intrinsic properties of the particles such as the iron oxide phase, particle size, morphology, aggregate size and defects which clearly affect their performance. On the other hand, the wide spread of the conditions used in the measurement settings reported in the literature (defined by the laser intensity, spot size and wavelength, among others) represent the main drawback for the comparison of the results reported in the results, i.e., the lack of standardization.

Remarkably, despite the evident advantages of Fe_3O_4 and FeO/Fe_3O_4 nanoparticles in the NIR-II region for a broad range of photothermal applications, this field is still relatively unexplored. The enhanced absorption at the NIR-II and the higher MPE limit are, in principle, sufficient arguments to encourage work in this wavelength range. However, more studies are necessary to unravel the full potential of iron oxides beyond the first biological window.

Declaration of competing interest

The authors declare that they have no known competing financial interests or personal relationships that could have appeared to influence the work reported in this paper.

Acknowledgements

This work was financially supported form grants No MAT2016-77391-R, PID2019-106229RB-I00, PDC2021-121303-I00, PDC2022-133036-I00, RTI2018-095495-J-I00 and RYC2019-027449-I funded by MCIN/AEI/10.13039/501100011033. We thank the Ramon Areces foundation through grant CIVP19A5922. Funding from Generalitat de Catalunya through the 2021-SGR-00651 project is also acknowledged. FÖ acknowledges the support of TUBITAK (The Scientific and Technological Research Council of Turkey) through the Project No. 1059B192000021. ICN2 is funded by the CERCA programme/Generalitat de Catalunya. The ICN2 is supported by the Severo Ochoa Centres of Excellence programme, Grant CEX2021-001214-S, funded by MCIN/AEI/10.13039.501100011033. The authors thank Iris Nogués for preparing Fig. 1.

Annex A. Simulation of the absorption and scattering cross sections of different iron oxides

The absorption and scattering cross section simulations of spherical γ-Fe_2O_3, Fe_3O_4 and FeO nanoparticles with a diameter of 25 nm were carried out by finite different time domain (FDTD) simulations using the Lumerical software, using literature values for their optical constants [440,465]. A mesh size of 1 nm was imposed in the nanoparticle region. As external medium in the calculations, it was assumed water (refractive index 1.33), without considering the water absorption coefficient to show just the spectral contribution of the nanoparticles.

Annex B. Sample preparation

B.1. Preparation of the nanoparticles.

All the nanoparticles were prepared through thermal decomposition, which leads to uniform and highly crystalline nanoparticles with well-defined morphology.

The **16 nm magnetite nanocubes** were synthesized following the method reported by Muro-Cruces et al. [394]. Iron (III) acetylacetonate (0.446 g; 1.27 mmol), sodium oleate (0.23 g; 0.80 mmol) and oleic acid (1.48 g; 5.20 mmol) were dissolved to a mixture of 1-octadecene (10 mL), benzyl ether (10 mL) and 1-tetradecene (3 mL) in a 100 mL three-neck round flask. This mixture was sonicated and then heated up to 60 °C under vacuum for one hour. Next, the reaction mixture was heated to 190 °C at 3 °C/min under Ar flow. Finally, Ar was removed and the reaction was kept at reflux for 1 h being cooled down to room temperature afterwards by removing the heating mantle.

The magnetite nanocubes were purified by centrifugation. The reaction mixture was mixed with a mixture of isopropanol, ethanol and methanol and centrifuged for 10 min at 10600 g. Then, the supernatant was discarded and the pellet redispersed in chloroform, mixed with isopropanol and methanol and centrifuged again (10 min, 10600 g).

To obtain a dispersion stable in water, the magnetite nanocubes were coated by PMAO [poly (maleic anhydride-alt-1-octadecene)]. Magnetite nanocubes were redispersed and sonicated in 50 mL of chloroform. In parallel, 20 mg PMAO were dissolved in 5 mL in chloroform and added to the nanocube solution. The dispersion was gently stirred and 50 mL of buffer borate (pH 9) was added to the solution. The suspension was sonicated for several minutes using an ultrasonic probe until a milky solution (denoting the formation of a microemulsion) was formed. Then, the suspension was rota-evaporated at 45 °C for several minutes until the chloroform was evaporated and the nanocubes were transferred to water. Finally, the suspension was centrifuged for 1 h at 10600 g to remove the excess of PMAO and the pellet was redispersed in water.

The **40 nm core/shell FeO/Fe_3O_4** nanocubes were synthesized following the procedure reported by Ichikawa et al. [466]. This procedure consists of two steps: (1) synthesis of iron (III) oleate and (2) thermal decomposition of iron (III) oleate in eicosane under the presence of oleic acid and sodium oleate. The iron (III) oleate was synthesized refluxing iron (III) chloride and sodium oleate in a mixture of hexane, water and ethanol [393]. In the second step, iron (III) oleate (10.25 g, 11.4 mmol), oleic acid (1.44 g, 5.12 mmol) and sodium oleate (1.56 g, 5.12 mmol) were mixed with 26 g of eicosane and degassed at room temperature prior to heating up to 70 °C for 2 h under Ar atmosphere to dissolve the sodium oleate. Then, the reaction mixture was heated up to 350 °C at 3 °C/min under Ar flow and kept for 30 min. Finally, the reaction was cooled down to room temperature under Ar flow. Purification of the particles was carried out by several cycles of centrifugation with ethanol. Finally, the particles were dispersed in chloroform.

The FeO/Fe_3O_4 nanocubes were transferred to water following the same procedure described for the Fe_3O_4 nanocubes.

The **hydrophilic 50 nm magnetic nanoclusters** were synthesized using the solvothermal method [94]. In a typical process, 0.8 g sodium acetate, 0.03 g polyacrylic acid, 0.27 g iron(III) chloride hexahydrate were dissolved in a solvent mixture composed by 4 mL diethylene glycol and 6 mL N- methyldiethanolamine. The mixture was transferred to Teflon-lined autoclave and maintained at 200 °C for 12 h. After the autoclave was cooled to room temperature, the nanoclusters were obtained by magnetic separation using a magnet and then washed with ethanol and water for several times.

Note that the as obtained nanoclusters are readily dispersible in water, thus there no extra steps are required to transfer them to water.

The synthesis approach for the growth of the **27 ×6 nm magnetic nanorods** is based on the method published by Sun et al. [455]. A mixture of 1.79 g oleic acid, 0.83 g hexadecylamine and 11 mL 1-octanol is stirred and heated up to 55 °C for 30 min to completely dissolve the hexadecylamine. Subsequently, the mixture is cooled down to room temperature

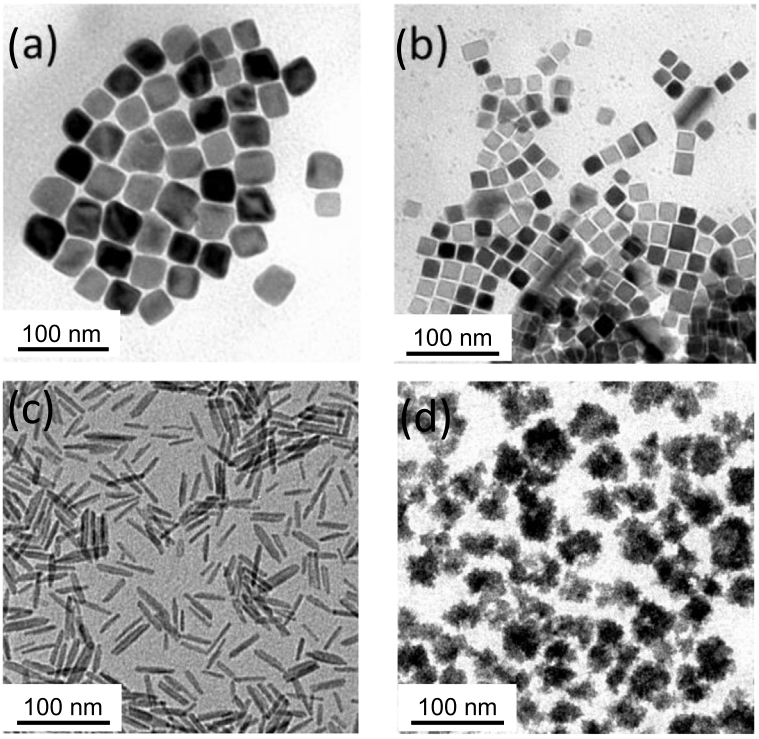

Fig. 14. TEM images (Annex C) of the FeO/Fe_3O_4 nanocubes, (b) the Fe_3O_4 nanocubes, (c) the Fe_3O_4 nanorods and (d) the Fe_3O_4 clusters.

and 2.75 mL iron(0) pentacarbonyl is added to the system and stirred for an additional 30 min. Then, the reaction mixture is transferred to a 23 mL autoclave with a Teflon lining and heated up to 200 °C for 6 h. After cooling the reactor to room temperature, the sample was washed with ethanol and centrifuged for 10 min at 10600 g twice. Then the nanorods are redispersed in chloroform and separated with a magnet.

The nanorods were transferred to water following the same procedure described for the Fe_3O_4 nanocubes.

B.2. Morphological characterization

The average particle size and the corresponding size distribution was estimated from the dimensions obtained from at least 200 particles. In the case of the FeO/Fe_3O_4 nanocubes the particle dimension was defined as the edge length. The average size of the nanocubes was 40 nm with a standard deviation of 5 nm (see Fig. 14). The thickness of the Fe_3O_4 shell is around 7 nm. In the case of the Fe_3O_4 nanocubes, the average particle size (edge length) was 16.5 nm with a standard deviation of 1.9 nm (see Fig. 14). The nanorod dimensions were defined by their length and diameter, being 27 $\pm$ 8 nm for the length and 5.6 $\pm$ 1.5 nm for the diameter, respectively (see Fig. 14). This leads to an aspect ratio of around 5. Finally, the dimensions of the nanoclusters were defined by the diameter of a circle completely comprising the cluster. Thus, the average cluster diameter was 50 $\pm$ 8 nm. Moreover, the size of the nanoparticles forming the cluster was about 5.3 $\pm$ 1.0 nm.

Annex C. Methods

C.1. Transmission electron microscopy

Transmission electron microscopy (TEM) images were collected in a JEM 1400 (JEOL) microscope operating at 120 keV. A small amount of particles was suspended in hexane and a few drops were placed on a carbon-coated copper grid.

C.2. Extinction measurements

The visible-near-infrared (vis–NIR) spectroscopy studies of the nanoparticle dispersions were carried out using a UV–VIS Cary 5 (Agilent) in the 400 to 1800 nm range, covering the visible light and near-infrared regions. Measurements were carried out using 0.7 mL quartz cuvettes with an optical length of 0.2 mm. The nanoparticle dispersion concentration was 0.350 mg Fe/mL.

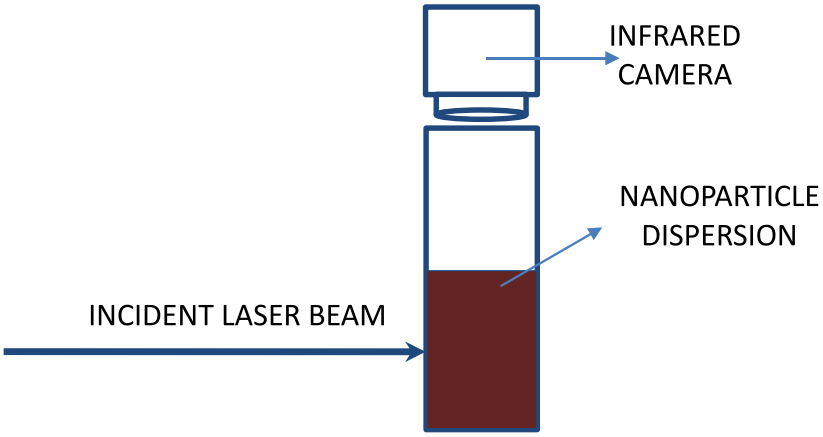

Fig. 15. Experimental setup designed to performed photothermal measurements.

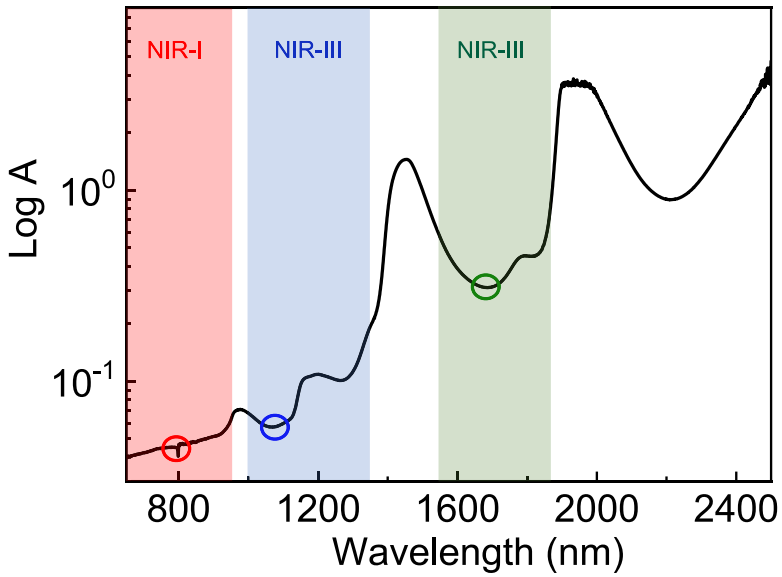

Fig. 16. Experimental absorbance (Annex C) of pure liquid water. The shaded areas represent the first (NIR-I), second (NIR-II) and third (NIR-III) biological windows. The circles highlight the absorption at the wavelengths used in our experiments (λ = 808 nm, 1064 nm and 1670 nm, respectively).

C.3. Photothermal measurements

The heating curves under laser irradiation were obtained using a custom-made photothermal testing system. The system consisted of: (i) a NIR laser diode with the selected emission wavelength (808 nm, K808F11FA, BWT Beijing Ltd; 1064 nm, KA64FAMFA, BWT Beijing Ltd.; and 1670 nm 4PN-135, Seminex) driven by a laser diode controller (ITC4005, Thorlabs), (ii) an optical collimating and aligning system, (iii) an infrared camera (ETS320, FLIR) to monitor the temperature variations at the liquid surface, (iv) a power meter (PM100D, Thorlabs), and (v) a computer with the data acquisition software.

The laser incident power upon the samples was typically set to 100 mW and the laser spot size was about 4 mm in diameter leading to a laser intensity of 0.793 W/m^2. The laser beam incident perpendicularly to the cuvette wall, and the infrared camera is located on top of the cuvette to measure the temperature at the liquid interface. The nanoparticle suspension was placed onto a 1.5 mL polystyrene cuvette. The photothermal laser set up schematics is represented in Fig. 15. The total volume of the dispersion was 0.75 mL. The ambient temperature was set to 23 $\pm$ 1 °C.

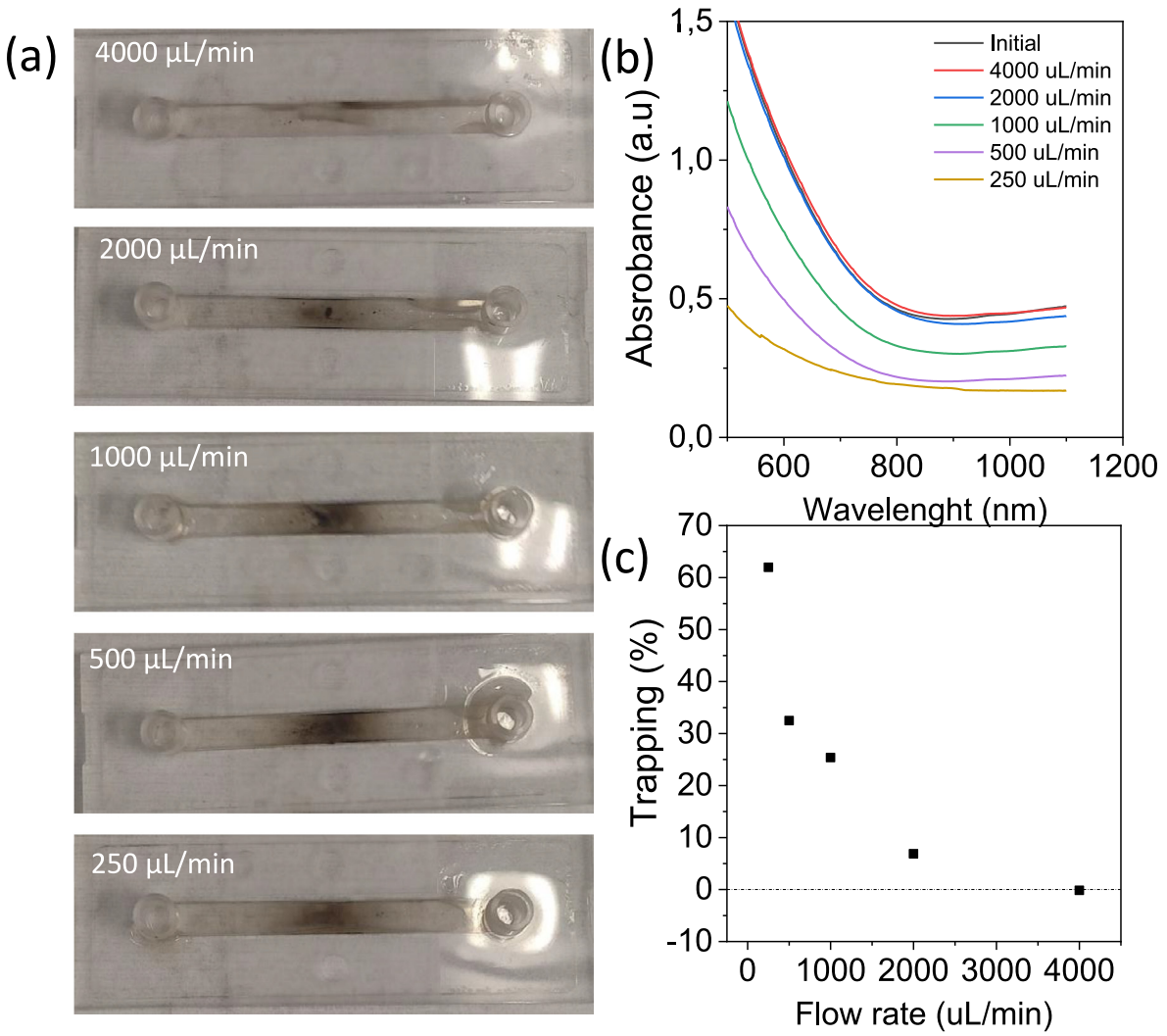

Fig. 17. (a) Different mages showing the trapping of FeO/Fe_3O_4 nanocubes by a magnet after flowing the nanoparticle suspension at different rates. (b) UV–VIS spectra of the nanoparticle suspension after flowing through the magnet at different rates. (c) Trapping efficiency calculated for the different flowing rates.

The photothermal conversion efficiency η was calculated as follows [451]:

$$\eta = \frac{hS(T_{max} - T_{amb}) - Q_{dis}}{I(1 - 10^{-A_x})} \tag{1}$$

where h is the heat transfer coefficient, S the laser irradiating surface, T_{max} is the maximum optically induced temperature change, T_{amb} is the temperature in the lab, Q_{dis} the heat dissipation due to the experimental set up, I the laser incident power (100 mW) and A_x the absorbance at the irradiated wavelength (x = 808 nm, 1064 nm or 1670 nm).

In order to get the value of η, hS for heat dissipation should be calculated. During the cooling process, since there is no light irradiating the nanoparticles, the dispersion will reach T_{amb}:

$$Q_{diss} = \sum_i m_i C_{p,i} \frac{dT}{dt} = hS\,(T - T_{amb}) \tag{2}$$

Here we can define the time constant τ_s and the dimensionless parameter θ to simplify the integral as follows:

$$\tau_s = \frac{\sum_i m_i C_{p,i}}{hS} \text{ and } \theta = \frac{T - T_{amb}}{T_{max} - T_{amb}}$$
$$\frac{d\theta}{dt} = \frac{1}{\tau_s}\theta \tag{3}$$

Setting the boundary conditions for the cooling process: $t = 0$, $\theta = 1$, the equation can be solved as (4) from which a linear relationship can be deduce to obtain τ_s value, consequently, hS can be calculated and introduced in (1) to calculate the photothermal efficiency.

$$\theta = e^{\frac{1}{\tau_s}t} \tag{4}$$

Annex D. Water absorbance spectrum

See Fig. 16.

Annex E. Remote manipulation of the FeO/Fe_3O_4 nanocubes by a magnetic gradient

To demonstrate that the FeO/Fe_3O_4 nanoparticle can be easily manipulated using magnetic fields, magnetic trapping experiments were performed by setting a spherical 19 mm diameter FeNdB permanent magnet (7.1 kOe at the surface) attached to a narrow microfluidic channel (3 mm in diameter) (see Fig. 17) [472]. A FeO/Fe_3O_4 nanoparticle dispersion of 0.3 mg Fe/mL (total volume of 1 mL) was controllably flowed by a syringe pump through the microfluidic channel at different flow rates. Optical spectra of the sample before and after the trapping experiments were carried out to establish the concentration of particles in the dispersion.

In Annex E it is shown how the nanoparticles are efficiently trapped in the magnet, even at high flow rates (i.e., 4000 μL/min). The percentage of the trapped FeO/Fe_3O_4 nanocubes by the magnet was quantified by UV–VIS, measuring the relative absorption lost ($\Delta A/A$) of the nanoparticle dispersions flowing through the microfluidic channel. It has been observed a high trapping efficiency of around 33% with flow rates around 500 μL/min. For comparison, 14 nm Fe_3O_4 nanocubes have a trapping efficiency of about 5% at 500 μL/min [472].

References

[1] H.P. Koka, E.N.K. Cressman, W. Ceelenc, C.L. Braced, R. Ivkove, H. Grülli, G. ter Haarj, P. Wustk, J. Crezeea, Heating technology for malignant tumors: A review, Int. J. Hyperthermia 37 (1) (2020) 711–741.
[2] A. Szasz, N. Iluri, O. Szasz, in: N. Huilgol (Ed.), Local Hyperthermia in Oncology – to Choose or Not to Choose? (Chapt. 1) in Hyperthermia, Intech, Rijeka, Croatia, 2013.
[3] S. Kumari, N. Sharma, S.V. Sahi, Advances in cancer therapeutics: Conventional thermal therapy to nanotechnology-based photothermal therapy, Pharmaceutics 13 (8) (2021) 1174.
[4] L. Farzin, R. Saber, S. Sadjadi, E. Mohagheghpour, A. Sheini, Nanomaterials-based hyperthermia: A literature review from concept to applications in chemistry and biomedicine, J. Therm. Biol. 104 (2022) 103201.
[5] J. Chen, C. Ning, Z. Zhou, P. Yu, Y. Zhu, G. Tan, C. Mao, Nanomaterials as photothermal therapeutic agents, Prog. Mater. Sci. 99 (2019) 1–26.
[6] T.-M. Liu, J. Conde, T. Lipiński, A. Bednarkiewicz, C.-C. Huang, Smart NIR linear and nonlinear optical nanomaterials for cancer theranostics: Prospects in photomedicine, Prog. Mater. Sci. 88 (2017) 89–135.
[7] J.-J. Hu, Y.-J. Cheng, X.-Z. Zhang, Recent advances in nanomaterials for enhanced photothermal therapy of tumor, Nanosclae 10 (48) (2018) 22657–22672.
[8] D. Zhi, T. Yang, J. O'Hagan, S. Zhang, R.F. Donnelly, Photothermal therapy, J. Controll. Rel. 325 (2020) 52–71.
[9] N.S. Rejinold, G. Choi, J.-H. Choy, Recent trends in nano photo-chemo therapy approaches and future scopes, Coord. Chem. Rev. 411 (2020) 213252.
[10] Z. Ashikbayeva, D. Tosi, D. Balmassov, E. Schena, P. Saccomandi, V. Inglezakis, Application of nanoparticles and nanomaterials in thermal ablation therapy of cancer, Nanomaterials 9 (9) (2019) 1195.
[11] T.-M. Liu, J. Conde, T. Lipiński, A. Bednarkiewicz, C.-C. Huang, Revisiting the classification of NIR-absorbing/emitting nanomaterials for *in Vivo* bioapplications, NPG Asia Mater. 8 (2016) e295.
[12] I. Koryakina, D.S. Kuznetsova, D.A. Zuev, V.A. Milichko, A.S. Timin, M.V. Zyuzin, Optically responsive delivery platforms: from the design considerations to biomedical applications, Nanophotonics 9 (1) (2020) 39–74.
[13] A. Cuello, S. Bongiovanni Abel, C.A. Barbero, I. Yslas, M. Molina, Nanomaterials as photothermal agents for biomedical applications, Sci. Rev. End. World 1 (3) (2020) 24–46.
[14] L. Marciniak, K. Kniec, K. Elzbieciak, A. Bednarkiewicz, in: A. Benayas, E. Hemmer, G. Hong, D. Jaque (Eds.), Non-Plasmonic NIR-Activated Photothermal Agents for Photothermal Therapy (Chap. 12) in Near Infrared-Emitting Nanoparticles for Biomedical Applications, Springer, Cham, Switzerland, 2020.
[15] H. Wen, K. Tamarov, E. Happonen, V.-P. Lehto, W. Xu, Inorganic nanomaterials for photothermal-based cancer theranostics, Adv. Ther. 4 (2) (2021) 2000207.
[16] Y. Lyu, J. Li, K. Pu, Second near-infrared absorbing agents for photoacoustic imaging and photothermal therapy, Small Methods 3 (11) (2019) 1900553.
[17] D. Jaque, L. Martínez Maestro, B. del Rosal, P. Haro-Gonzalez, A. Benayas, J.L. Plaza, E. Martín Rodríguez, J. García Solé, Nanoparticles for photothermal therapies, Nanoscale 6 (16) (2014) 9494–9530.
[18] P. Xu, F. Liang, Nanomaterial-based tumor photothermal immunotherapy, Int. J. Nanomed. 15 (2020) 9159–9180.
[19] C. Xu, K. Pu, Second near-infrared photothermal materials for combinational nanotheranostics, Chem. Soc. Rev. 50 (2) (2021) 1111–1137.
[20] M.R. Younis, G. He, B. Gurram, J. Lin, P. Huang, Inorganic cancer phototheranostics in second biowindow, APL Mater. 9 (7) (2021) 070901.
[21] S. Wang, Y. Hou, Photothermal therapy based on magnetic nanoparticles in cancer, J. Appl. Phys. 130 (7) (2021) 070902.
[22] J. Kadkhoda, A. Tarighatnia, J. Barar, A. Aghanejad, S. Davaran, Recent advances and trends in nanoparticles based photothermal and photodynamic therapy, Photodiagn. Photodyn. Ther. 37 (2022) 102697.
[23] X. Cui, Q. Ruan, X. Zhuo, X. Xia, J. Hu, R. Fu, Y. Li, J. Wang, H. Xu, Photothermal nanomaterials: A powerful light-to-heat converter, Chem. Rev. 123 (11) (2023) 6891–6952.
[24] X. Liu, Y. Zhang, Y. Wang, W. Zhu, G. Li, X. Ma, Y. Zhang, S. Chen, S. Tiwari, K. Shi, S. Zhang, H.M. Fan, Y.X. Zhao, X.-J. Liang, Comprehensive understanding of magnetic hyperthermia for improving antitumor therapeutic efficacy, Theranostics 10 (8) (2020) 3793–3815.

[25] I.M. Obaidat, V. Narayanaswamy, S. Alaabed, S. Sambasivam, C.V.V. Muralee Gopi, Principles of magnetic hyperthermia: A focus on using multifunctional hybrid magnetic nanoparticles, Magnetochemistry 5 (4) (2019) 67.
[26] H. Etemadi, P.G. Plieger, Magnetic fluid hyperthermia based on magnetic nanoparticles: Physical characteristics, historical perspective, clinical trials, technological challenges, and recent advances, Adv. Therap. 3 (11) (2020) 2000061.
[27] D. Rahban, M. Doostan, A. Salimi, Cancer therapy; Prospects for application of nanoparticles for magnetic-based hyperthermia, Cancer Invest. 38 (8–9) (2020) 507–521.
[28] G.C. Lavorato, R. Das, J. Alonso Masa, M.-H. Phan, H. Srikanth, Hybrid magnetic nanoparticles as efficient nanoheaters in biomedical applications, Nanoscale Adv. 3 (4) (2021) 867–888.
[29] H. Gavilán, S.K. Avugadda, T. Fernández-Cabada, N. Soni, M. Cassani, B.T. Mai, R. Chantrell, T. Pellegrino, Magnetic nanoparticles and clusters for magnetic hyperthermia: Optimizing their heat performance and developing combinatorial therapies to tackle cancer, Chem. Soc. Rev. 50 (20) (2021) 11614–11667.
[30] S.K. Sharma, N. Shrivastava, F. Rossi, L.D. Tung, N.T.K. Thanhc, Nanoparticles-based magnetic and photo induced hyperthermia for cancer treatment, Nano Today 29 (2019) 100795.
[31] X.Y. Wong, A. Sena-Torralba, R. Álvarez-Diduk, K. Muthoosamy, A. Merkoçi, Nanomaterials for nanotheranostics: Tuning their properties according to disease needs, ACS Nano 14 (3) (2020) 2585–2627.
[32] J. Estelrich, M.A. Busquets, Iron oxide nanoparticles in photothermal therapy, Molecules 23 (7) (2018) 1567.
[33] M. Chu, in: D. Shi (Ed.), Magnetic Fe_3O_4 Nanoparticles for Cancer Photothermal Therapy (Chap. 4) in Frontiers in Nanobiomedical Research — 4. Bio-Inspired Nanomaterials and Applications. Nano Detection, Drug/Gene Delivery, Medical Diagnosis and Therapy, World Scientific, Publishing, Singapore, 2015.
[34] L.L. Israel, A. Galstyan, E. Holler, J.Y. Ljubimova, Magnetic iron oxide nanoparticles for imaging, targeting and treatment of primary and metastatic tumors of the brain, J. Control. Release 320 (2020) 45–62.
[35] M. Bietenbeck, A. Florian, C. Faber, U. Sechtem, A. Yilmaz, Remote magnetic targeting of iron oxide nanoparticles for cardiovascular diagnosis and therapeutic drug delivery: Where are we now? Int. J. Nanomed. 11 (2016) 3191–3203.
[36] Wahajuddin S. Arora, Superparamagnetic iron oxide nanoparticles: Magnetic nanoplatforms as drug carriers, Int. J. Nanomed. 7 (2012) 3445–3471.
[37] N. Lee, T. Hyeon, Designed synthesis of uniformly sized iron oxide nanoparticles for efficient magnetic resonance imaging contrast agents, Chem. Rev. 41 (7) (2012) 2575–2589.
[38] M. Jeon, M.V. Halbert, Z.R. Stephen, M. Zhang, Iron oxide nanoparticles as T-1 contrast agents for magnetic resonance imaging: Fundamentals, challenges, applications, and prospectives, Adv. Mater. 33 (23) (2021) 1906539.
[39] R.M. Ferguson, K.R. Minard, K.M. Krishnan, Optimization of nanoparticle core size for magnetic particle imaging, J. Magn. Magn. Mater. 321 (10) (2009) 1548–1551.
[40] H. Arami, E. Teeman, A. Troksa, H. Bradshaw, K. Saatchi, A. Tomitaka, S.S. Gambhir, U.O. Häfeli, D. Liggittg, K.M. Krishnan, Tomographic magnetic particle imaging of cancer targeted nanoparticles, Nanoscale 9 (47) (2017) 18723–18730.
[41] C. Lu, L. Han, J. Wang, J. Wan, G. Song, J. Rao, Engineering of magnetic nanoparticles as magnetic particle imaging tracers, Chem. Rev. 50 (14) (2021) 8102–8146.
[42] G. Hu, B. He, Magnetoacoustic imaging of magnetic iron oxide nanoparticles embedded in biological tissues with microsecond magnetic stimulation, Appl. Phys. Lett. 100 (1) (2012) 013704.
[43] P.-H. Ting, C.-C. Huang, M.-L. Li, NIR-activated iron oxides as a new multi-functional contrast agent of photoacoustic imaging, Proc. SPIE 8943 (2014) 89434E.
[44] S. Laurent, S. Dutz, U.O. Häfeli, M. Mahmoudi, Magnetic fluid hyperthermia: Focus on superparamagnetic iron oxide nanoparticles, Adv. Colloid Interface Sci. 166 (2011) 8–23.
[45] C. Blanco-Andujar, A. Walter, G. Cotin, C. Bordeianu, D. Mertz, D. Felder-Flesch, S. Begin-Colin, Design of iron oxide-based nanoparticles for MRI and magnetic hyperthermia, Nanomedicine (London) 11 (14) (2016) 1889–1910.
[46] A. Van de walle, A. Figuerola, A. Espinosa, A. Abou-Hassan, M. Estrader, C. Whilelm, Emergence of magnetic nanoparticles in photothermal and ferroptotic therapies, Mater. Horiz. (2023) http://dx.doi.org/10.1039/D3MH00831B, in press.
[47] M. Chu, Y. Shao, J. Peng, X. Dai, H. Li, Q. Wu, D. Shi, Near-infrared laser light mediated cancer therapy by photothermal effect of Fe_3O_4 magnetic nanoparticles, Biomaterials 34 (16) (2013) 4078–4088.
[48] F. Wang, X. Li, W. Li, H. Bai, Y. Gao, J. Ma, W. Liu, G. Xi, Dextran coated Fe_3O_4 nanoparticles as a near-infrared laser-driven photothermal agent for efficient ablation of cancer cells *in vitro* and *in Vivo*, Mater. Sci. Eng. C 90 (2018) 46–56.
[49] H. Chen, J. Burnett, F. Zhang, J. Zhang, H. Paholaka, D. Sun, Highly crystallized iron oxide nanoparticles as effective and biodegradable mediators for photothermal cancer therapy, J. Mater. Chem. B 2 (7) (2014) 757–765.
[50] X. Zhang, X. Xu, T. Li, M. Lin, X. Lin, H. Zhang, H. Sun, B. Yang, Composite photothermal platform of polypyrrole-enveloped Fe_3O_4 nanoparticle self-assembled superstructures, ACS Appl. Mater. Interfaces 6 (16) (2014) 14552–14561.
[51] M.E. Sadat, M.K. Baghbador, A.W. Dunn, H.P. Wagner, R.C. Ewing, J. Zhang, H. Xu, G.M. Pauletti, D.B. Mast, D. Shi, Photoluminescence and photothermal effect of Fe_3O_4 nanoparticles for medical imaging and therapy, Appl. Phys. Lett. 105 (9) (2014) 091903.
[52] K. Bilici, A. Muti, F.D. Duman, c.A. Sennaroğlua, H.Y. Acar, Investigation of the factors affecting the photothermal therapy potential of small iron oxide nanoparticles over the 730–840 nm spectral region, Photochem. Photobiol. Sci. 17 (11) (2018) 1787–1793.
[53] J. Lin, Y. Zhao, D. Shi, Optical thermal insulation via the photothermal effects of Fe_3O_4 and Fe_3O_4@Cu2–xS thin films for energy-efficient single-pane windows, MRS Commun. 10 (1) (2020) 155–163.
[54] A. Espinosa, R. Di Corato, J. Kolosnjaj-Tabi, P. Flaud, T. Pellegrino, C. Wilhelm, Duality of iron oxide nanoparticles in cancer therapy: Amplification of heating efficiency by magnetic hyperthermia and photothermal bimodal treatment, ACS Nano 10 (2) (2016) 2436–2446.
[55] M.E. Sadat, D.B. Mast, J. Sookoor, H. Xu, A.W. Dunn, D. Shi, Effects of nanoscale structures on photothermal heating behaviors of surface-modified Fe_3O_4 nanoparticles, Nano Life 9 (1 & 2) (2019) 1950001.
[56] W. Wen, L. Wu, Y. Chen, X. Qi, J. Cao, X. Zhang, W. Ma, Y. Ge, S. Shen, Ultra-small Fe_3O_4 nanoparticles for nuclei targeting drug delivery and photothermal therapy, J. Drug Deliv. Sci. Technol. 58 (2020) 101782.
[57] K. Zhang, Z. Yang, X. Meng, Y. Cao, Y. Zhang, W. Dai, H. Lu, Z. Yu, H. Dong, X. Zhanga, Peroxidase-like Fe_3O_4 nanocomposite for activatable reactive oxygen species generation and cancer theranostics, Mater. Chem. Front. 2 (6) (2018) 1184–1194.
[58] A. Tewari, R. Gupta, D. Sharma, Near-infrared-responsive silver-capped magnetic nanoclusters for cancer therapy, J. Radiat. Cancer Res. 11 (2) (2020) 45–51.
[59] W.-J. Syu, C.-C. Huang, J.-K. Hsiao, Y.-C. Lee, Y.-T. Huang, P. Venkatesan, P.-S. Lai, Co-precipitation synthesis of near-infrared iron oxide nanocrystals on magnetically targeted imaging and photothermal cancer therapy via photoablative protein denature, Nanotheranostics 3 (3) (2019) 236–254.
[60] A.W. Dunn, Y. Zhang, D. Mast, G.M. Pauletti, H. Xue, J. Zhang, R.C. Ewing, D. Shi, In-vitro depth-dependent hyperthermia of human mammary gland adenocarcinoma, Mater. Sci. Eng. C 69 (2016) 12–16.

[61] A.W. Dunn, S.M. Ehsan, D. Mast, G.M. Pauletti, H. Xu, J. Zhang, R.C. Ewing, D. Shi, Photothermal effects and toxicity of Fe_3O_4 nanoparticles via near infrared laser irradiation for cancer therapy, Mater. Sci. Eng. C 46 (2015) 97–102.
[62] S. Fu, Y. Man, F. Jia, Photothermal effect of superparamagnetic Fe_3O_4 nanoparticles irradiated by near-infrared laser, J. Nanomater. 2020 (2020) 2832347.
[63] G.-Z. Liu, J.-P. Ma, J.-Q. Liu, Photothermal effect for Fe_3O_4 nanoparticles contained in micelles induced by near-infrared light, J. Shanghai Jiaotong Univ. (Sci.) 17 (6) (2012) 730–733.
[64] G. Brennan, N.D. Thorat, M. Pescio, S. Bergamino, J. Bauer, N. Liu, S.A.M. Tofail, C. Silien, Spectral drifts in surface textured Fe_3O_4-Au, core–shell nanoparticles enhance spectra-selective photothermal heating and scatter imaging, Nanoscale 12 (23) (2020) 12632–12638.
[65] J. Feng, W.-X. Ren, J.-L. Gao, F. Li, F. Kong, B.-J. Yao, Y.-B. Dong, Core-shell-structured covalent-organic framework as a nanoagent for single-laser-induced phototherapy, ACS Appl. Mater. Interfaces 13 (15) (2021) 17243–17254.
[66] R. Guo, H. Peng, Y. Tian, S. Shen, W. Yang, Mitochondria-targeting magnetic composite nanoparticles for enhanced phototherapy of cancer, Small 12 (33) (2016) 4541–4552.
[67] K. Ma, G.-J. Liu, L. Yan, S. Wen, B. Xu, W. Tian, E.M. Goldys, G. Liu, AIEgen based poly(L-lactic-co-glycolic acid) magnetic nanoparticles to localize cytokine VEGF for early cancer diagnosis and photothermal therapy, Nanomedicine 14 (9) (2019) 1191–1201.
[68] S. Fu, Y. Man, F. Jia, Photothermal effect of superparamagnetic Fe_3O_4 nanoparticles irradiated by near-infrared laser, J. Nanomater. 2020 (2020) 2832347.
[69] R. Amatya, S. Hwang, T. Park, K.A. Min, M.C. Shin, In vitro and in Vivo evaluation of PEGylated starch-coated iron oxide nanoparticles for enhanced photothermal cancer therapy, Pharmaceutics 13 (6) (2021) 871.
[70] F. Yang, A. Skripka, M.S. Tabatabaei, S.H. Hong, F. Ren, A. Benayas, J.K. Oh, S. Martel, X. Liu, F. Vetrone, D. Ma, Multifunctional self-assembled supernanoparticles for deep-tissue bimodal imaging and amplified dual-mode heating treatment, ACS Nano 13 (1) (2019) 408–420.
[71] X. Jiang, N. Yan, M. Wang, M. Feng, Q. Guan, L. Xu, Magnetic nanostructure and biomolecule synergistically promoted Suaeda inspired self-healing hydrogel composite for seawater evaporation, Sci. Total Environ. 830 (2022) 154545.
[72] Ferdinandus, M. Suzuki, C.Q. Vu, Y. Harada, S.R. Sarker, S. Ishiwata, T. Kitaguchi, S. Arai, Modulation of local cellular activities using a photothermal dye-based subcellular-sized heat spot, ACS Nano 16 (6) (2022) 9004–9018.
[73] A. Chen, H. Lu, R. Cao, Y. Zhu, Y. Li, R. Ge, S. Zhang, Y. Li, L. Xiao, L. Su, J. Zhao, H. Hu, Z. Wang, A novel MMP-responsive nanoplatform with transformable magnetic resonance property for quantitative tumor bioimaging and synergetic chemo-photothermal therapy, Nano Today 45 (2022) 101524.
[74] Y. Jin, B. Zhao, W. Guo, Y. Li, J. Min, W. Miao, Penetration and photodynamic ablation of drug-resistant biofilm by cationic iron oxide nanoparticles, J. Control. Rel. 348 (2022) 911–923.
[75] C.E. Onyekanne, A.A. Salifu, J.D. Obayemi, C.J. Ani, H.A. Choshali, C.C. Nwazojie, K.C. Onwudiwe, J.C. Oparah, T.C. Ezenwafor, C.C. Ezeala, O.S. Odusanya, N. Rahbar, W.O. Soboyejo, Laser-induced heating of polydimethylsiloxane-magnetite nanocomposites for hyperthermic inhibition of triple-negative breast cancer cell proliferation, J. Biomed. Mater. Res. 110 (12) (2022) 2727–2743.
[76] F.H. Beigi, S.S. Jazi, D. Shahbazi-Gahrouei, P.M. Khaniabadi, H. Hafezi, R. Monajemi, G.R. Amiri, Iron oxide nanoparticles coated with polydopamine as a potential nano-photothermal agent for treatment of melanoma cancer: An in Vivo study, Lasers Med. Sci. 37 (9) (2022) 3413–3421.
[77] R. Amatya, D. Kim, K.A. Min, M.C. Shin, Iron oxide nanoparticles-loaded hydrogels for effective topical photothermal treatment of skin cancer, J. Pharm. Invest. 52 (6) (2022) 775–785.
[78] M. Lázaro, P. Lupiáñez, J.L. Arias, M.P. Carrasco-Jiménez, A.V. Delgado, G.R. Iglesias, Combined magnetic hyperthermia and photothermia with polyelectrolyte/gold-coated magnetic nanorods, Polymers 14 (22) (2022) 4913.
[79] Y. Guo, Y. Rana, Z. Wang, J. Cheng, Y. Cao, C. Yang, F. Liu, H. Ran, Magnetic-responsive and targeted cancer nanotheranostics by PA/MR bimodal imaging-guided photothermally triggered immunotherapy, Biomaterials 219 (2019) 119370.
[80] P. Zhang, Y. Qiao, L. Zhu, M. Qin, Q. Li, C. Liu, Y. Xu, X. Zhang, Z. Gan, Y. Hou, Nanoprobe based on biominerals in protein corona for dual-modality MR imaging and therapy of tumors, ACS Nano 17 (1) (2023) 184–196.
[81] B. Wang, Y. Qin, J. Liu, Z. Zhang, W. Li, G. Pu, Z. Yuanhe, X. Gui, M. Chu, Magnetotactic bacteria-based drug-loaded micromotors for highly efficient magnetic and biological double-targeted tumor therapy, ACS Appl. Mater. Interfaces 15 (2) (2023) 2747–2759.
[82] J. Hai, H. Piraux, E. Mazarío, J. Volatron, N.T. Ha-Duong, P. Decorse, J.S. Lomas, P. Verbeke, S. Ammar, C. Wilhelm, J.-M. El Hage Chahine, M. Hémadi, Maghemite nanoparticles coated with human serum albumin: Combining targeting by the iron-acquisition pathway and potential in photothermal therapies, J. Mater. Chem. B 5 (17) (2017) 3154–3162.
[83] A. Espinosa, J. Kolosnjaj-Tabi, A. Abou-Hassan, A.P. Sangnier, A. Curcio, A.K.A. Silva, R. Di Corato, S. Neveu, T. Pellegrino, L.M. Liz-Marzán, C. Wilhelm, Magnetic (Hyper) thermia or photothermia? Progressive comparison of iron oxide and gold nanoparticles heating in water, in Cells, and in Vivo, Adv. Funct. Mater. 28 (37) (2018) 1803660.
[84] S. Shen, S. Wang, R. Zheng, X. Zhu, X. Jiang, D. Fu, W. Yang, Magnetic nanoparticle clusters for photothermal therapy with near-infrared irradiation, Biomaterials 39 (2015) 67–74.
[85] A.P. Sangniera, S. Preveral, A. Curcio, A.K.A. Silva, C.T. Lefèvre, D. Pignol, Y. Lalatonne, C. Wilhelm, Targeted thermal therapy with genetically engineered magnetite magnetosomes@RGD: Photothermia is far more efficient than magnetic hyperthermia, J. Controll. Rel. 279 (2018) 271–281.
[86] S. Shen, F. Kong, X. Guo, L. Wu, H. Shen, M. Xie, X. Wang, Y. Jin, Y. Ge, CMCTS stabilized Fe_3O_4 particles with extremely low toxicity as highly efficient near-infrared photothermal agents for in Vivo tumor ablation, Nanoscale 5 (17) (2013) 8056–8066.
[87] Z. Zhou, Y. Sun, J. Shen, J. Wei, C. Yu, B. Kong, W. Liu, H. Yang, S. Yang, W. Wang, Iron/iron oxide core/shell nanoparticles for magnetic targeting MRI and near-infrared photothermal therapy, Biomaterials 35 (2014) 7470–7478.
[88] M.-Y. Liao, P.-S. Lai, H.-P. Yu, H.-P. Lin, C.-C. Huang, Innovative ligand-assisted synthesis of NIR-activated iron oxide for cancer theranostics, Chem. Commun. 48 (43) (2012) 5319–5321.
[89] M. Kong, Y. Huang, R. Yu, J. Xi, Coordination bonding-based Fe_3O_4@PDA-Zn^{2+}-doxorubicin nanoparticles for tumor chemo-photothermal therapy, J. Drug Delivery Sci. Technol. 51 (2019) 185–193.
[90] G. Yuan, Y. Yuan, K. Xu, Q. Luo, Biocompatible PEGylated Fe_3O_4 nanoparticles as photothermal agents for near-infrared light modulated cancer therapy, Int. J. Mol. Sci. 15 (10) (2014) 18776–18788.
[91] T.-J. Yu, P.-H. Li, T.-W. Tseng, Y.-C. Chen, Multifunctional Fe_3O_4/alumina core/shell MNPs as photothermal agents for targeted hyperthermia of nosocomial and antibiotic-resistant bacteria, Nanomedicine (London) 6 (8) (2011) 1353–1363.
[92] M. Saeed, M.Z. Iqbal, W. Ren, Y. Xia, C. Liu, W.S. Khan, A. Wu, Controllable synthesis of Fe_3O_4 nanoflowers: Enhanced imaging guided cancer therapy and comparison of photothermal efficiency with black-TiO_2, J. Mater. Chem. B 6 (22) (2018) 3800–3810.
[93] J. Zhang, J. Li, S. Chen, N. Kawazoe, G. Chen, Preparation of gelatin/Fe_3O_4 composite scaffolds for enhanced and repeatable cancer cell ablation, J. Mater. Chem. B 4 (34) (2016) 5664–5672.
[94] J. Yang, L. Fan, Y. Xu, J. Xia, Iron oxide nanoparticles with different polymer coatings for photothermal therapy, J. Nanopart. Res. 19 (10) (2017) 333.
[95] K. Wang, P. Yang, R. Guo, X. Yao, W. Yang, Photothermal performance of MFe_2O_4 nanoparticles, Chin. Chem. Lett. 30 (12) (2019) 2013–2016.

[96] M.M. Fathy, Multifunctional thymoquinone-capped iron oxide nanoparticles for combined chemo-photothermal therapy of cancer, J. Superond. Novel Mag. 33 (7) (2020) 2125–2131.

[97] Y. Wang, X. Li, P. Chen, Y. Dong, G. Liang, Y. Yu, Enzyme-instructed self-aggregation of Fe_3O_4 nanoparticles for enhanced MRI T_2 imaging and photothermal therapy of tumors, Nanoscale 12 (3) (2020) 1886–1893.

[98] M.S. Jabir, U.M. Nayef, W.K. Abdulkadhim, G.M. Sulaiman, Supermagnetic Fe_3O_4-PEG nanoparticles combined with NIR laser and alternating magnetic field as potent anti-cancer agent against human ovarian cancer cells, Mater. Res. Express 6 (11) (2019) 115412.

[99] M. Sharifi, A. Hasan, N.M.Q. Nanakali, A. Salihi, F.A. Qadir, H.A. Muhammad, M.S. Shekha, F.M. Aziz, K.M. Amen, F. Najafi, H. Yousefi-Manesh, M. Falahati, Combined chemo-magnetic field-photothermal breast cancer therapy based on porous magnetite nanospheres, Sci. Rep. 10 (2020) 5925.

[100] B. Getiren, Z. Çıplak, C. Gökalp, N. Yıldız, NIR-responsive Fe_3O_4@PPy nanocomposite for efficient potential use in photothermal therapy, J. Appl. Polym. Sci. 137 (44) (2020) 49343.

[101] Y. Oh, J.Y. Je, M.S. Moorthy, H. Seo, W.H. Choe, pH and NIR-light-responsive magnetic iron oxide nanoparticles for mitochondria-mediated apoptotic cell death induced by chemo-photothermal therapy, Int. J. Pharma. 531 (1) (2017) 1–13.

[102] X. Wang, K. Wang, J. Liu, X. Hong, Mesoporous -structure enhnced photothermal effect of Fe_3O_4 superlatices@mesoporous silica, Chem. J. Chin. Univ. 40 (8) (2019) 1586–1592.

[103] S. Wang, Y. Yin, W. Song, Q. Zhang, Z. Yang, Z. Dong, Y. Xu, S. Cai, K. Wang, W. Yang, X. Wang, Z. Pang, L. Feng, Red-blood-cell-membrane-enveloped magnetic nanoclusters as a biomimetic theranostic nanoplatform for bimodal imaging-guided cancer photothermal therapy, J. Mater. Chem. B 8 (4) (2020) 803–812.

[104] S. Chen, B. Huang, W. Pei, Y. Xu, Z. Jiang, J. Li, L. Wang, C. Niu, Magnetically targeted nanoparticles for imaging-guided photothermal therapy of cancer, RSC Avd. 9 (65) (2019) 38154–38164.

[105] S. Shen, Y. Chen, S. Qi, X. Zhang, C. Qiao, L. Wu, Erythrocyte membrane coated Fe_3O_4 nanoparticles for near infrared light responsive drug delivery, Chem. Lett. 48 (11) (2019) 1414–1416.

[106] L. Wang, M. Wang, B. Zhou, F. Zhou, C. Murray, R.A. Towner, N. Smith, D. Saunders, G. Xie, W.R. Chen, PEGylated reduced-graphene oxide hybridized with Fe_3O_4 nanoparticles for cancer photothermal-immunotherapy, J. Mater. Chem. B 7 (46) (2019) 7406–7414.

[107] D. Liu, J. Lai, R. Wang, L. Ye, Y. Tian, Reverse microemulsion synthesis of Fe_3O_4-Ag_2S heteronanocrystals for dual-modal imaging-guided photothermal tumor ablation, ACS Biomater. Sci. Eng. 5 (11) (2019) 6196–6206.

[108] X. Wang, Z. Lia, Y. Ding, K. Wang, Z. Xing, X. Sun, W. Guo, X. Hong, X. Zhu, Y. Liu, Enhanced photothermal-photodynamic therapy for glioma based on nearinfrared dye functionalized Fe_3O_4 superparticles, Chem. Eng. J. 381 (2020) 122693.

[109] S. Saber-Samandari, M. Mohammadi-Aghdama, S. Saber-Samandari, A novel magnetic bifunctional nanocomposite scaffold for photothermal therapy and tissue engineering, Int. J. Biol. Macromol. 138 (2019) 810–818.

[110] X. Ma, Y. Wang, X.-L. Liu, H. Ma, G. Li, Y. Li, F. Gao, M. Peng, H.M. Fan, X.-J. Liang, Fe_3O_4–Pd Janus nanoparticles with amplified dual-mode hyperthermia and enhanced ROS generation for breast cancer treatment, Nanoscale Horiz. 4 (6) (2019) 1450–1459.

[111] M. Liu, J. Zhang, X. Li, C. Cai, X. Cao, X. Shi, R. Guo, A polydopamine-coated LAPONITE® -stabilized iron oxide nanoplatform for targeted multimodal imaging-guided photothermal cancer therapy, J. Mater. Chem. B 7 (24) (2019) 3856–3864.

[112] Y. Yao, D. Zhao, N. Li, F. Shen, J. Ong'achwa Machuki, D. Yang, J. Li, D. Tang, Y. Yu, J. Tian, H. Dong, F. Gao, Multifunctional Fe_3O_4@Polydopamine@DNA-fueled molecular machine for magnetically targeted intracellular Zn^{2+} imaging and fluorescence/MRI guided photodynamic-photothermal therapy, Anal. Chem. 91 (12) (2019) 7850–7857.

[113] H. Peng, S. Tang, Y. Tian, R. Zheng, L. Zhou, W. Yang, Highly ligand-directed and size-dependent photothermal properties of magnetite particles, Part. Part. Syst. Charact. 33 (6) (2016) 332–340.

[114] L.-L. Bu, L. Rao, G.-T. Yu, L. Chen, W.-W. Deng, J.-F. Liu, H. Wu, Q.-F. Meng, S.-S. Guo, X.-Z. Zhao, W.-F. Zhang, G. Chen, Z. Gu, W. Liu, Z.-J. Sun, Cancer stem cell-platelet hybrid membrane-coated magnetic nanoparticles for enhanced photothermal therapy of head and neck squamous cell carcinoma, Adv. Funct. Mater. 29 (10) (2019) 1807733.

[115] M. Kang, Y. Kim, Au-coated Fe_3O_4@SiO_2 core–shell particles with photothermal activity, Colloids Surf. A 600 (2020) 124957.

[116] Y.M. Kwon, J.-Y. Je, S.H. Cha, Y. Oh, W.H. Cho, Synergistic combination of chemo-phototherapy based on temozolomide/ICG-loaded iron oxide nanoparticles for brain cancer treatment, Oncol. Rep. 42 (5) (2019) 1709–1724.

[117] S. Shen, D. Huang, J. Cao, Y. Chen, X. Zhang, S. Guo, W. Ma, X. Qi, Y. Ge, L. Wu, Magnetic liposomes for light-sensitive drug delivery and combined photothermal–chemotherapy of tumors, J. Mater. Chem. B 7 (7) (2019) 1096–1106.

[118] H. Wu, K. Cheng, Y. He, Z. Li, H. Su, X. Zhang, Y. Sun, W. Shi, D. Ge, Fe_3O_4-Based multifunctional nanospheres for amplified magnetic targeting photothermal therapy and fenton reaction, ACS Biomater. Sci. Eng. 5 (2) (2019) 1045–1056.

[119] K. Qiu, J. Wang, T.W. Rees, L. Ji, Q. Zhang, H. Chao, A mitochondria-targeting photothermogenic nanozyme for MRI-guided mild photothermal therapy, Chem. Commun. 54 (100) (2018) 14108–14111.

[120] L. Wang, S. Chen, Y. Zhu, M. Zhang, S. Tang, J. Li, W. Pei, B. Huang, C. Niu, Triple-modal imaging-guided chemo-photothermal synergistic therapy for breast cancer with magnetically targeted phase-shifted nanoparticles, ACS Appl. Mater. Interfaces 10 (49) (2018) 42102–42114.

[121] P. Xue, M. Hou, L. Sun, Q. Li, L. Zhang, Z. Xu, Y. Kang, Calcium-carbonate packaging magnetic polydopamine nanoparticles loaded with indocyanine green for near-infrared induced photothermal/photodynamic therapy, Acta Biomater. 81 (2018) 242–255.

[122] S. Song, Y. Chong, H. Fu, X. Ning, H. Shen, Z. Zhang, HP-β-CD functionalized Fe_3O_4/CNPs-based theranostic nanoplatform for pH/NIR responsive drug release and MR/NIRFL imaging-guided synergetic chemo/photothermal therapy of tumor, ACS Appl. Mater. Interfaces 10 (40) (2018) 33867–33878.

[123] S. Shen, B. Ding, S. Zhang, X. Qi, K. Wang, J. Tian, Y. Yan, Y. Ge, L. Wu, Near-infrared light-responsive nanoparticles with thermosensitive Yolk-Shell structure for multimodal imaging and chemo-photothermal therapy of tumor, Nanomed. - Nanotechnol. 13 (5) (2017) 1607–1616.

[124] S.Peng B. Ouyang, Y. Men, Yang. Du, Y. Cao, R. Xie, Z. Pang, S. Shen, W. Yang, Biodegradable zwitterionic polymer membrane coating endowing nanoparticles with ultra-long circulation and enhanced tumor phototherma therapy, Biomaterials 231 (2020) 119680.

[125] Y.-T. Yu, S.-W. Shi, Y. Wang, Q.-L. Zhang, S.-H. Gao, S.-P. Yang, J.-G. Liu, A ruthenium nitrosyl-functionalized magnetic nanoplatform with near-infrared light-controlled nitric oxide delivery and photothermal effect for enhanced antitumor and antibacterial therapy, ACS Appl. Mater. Interfaces 12 (1) (2020) 312–321.

[126] K. Tao, S. Liu, L. Wang, H. Qiu, B. Li, M. Zhang, M. Guo, H. Liu, X. Zhang, Y. Liu, Y. Hou, H. Zhang, Targeted multifunctional nanomaterials with MRI, chemotherapy and photothermal therapy for the diagnosis and treatment of bladder cancer, Biomater. Sci. 8 (1) (2020) 342–352.

[127] W.-E. Hong, I-L. Hsu, S.-Y. Huang, C.-W. Lee, H. Ko, P.-J. Tsai, D.-B. Shieh, C.-C. Huang, Assembled growth of 3D Fe_3O_4@Au nanoparticles for efficient photothermal ablation and SERS detection of microorganisms, J. Mater. Chem. B 6 (36) (2018) 5689–5697.

[128] Y.-M. Yang, M.-X. Ji, Y. Yang, A.-J. Xie, Y.-H. Shen, Construction of synergistic anticancer efficacy of sandwich-like rGO/Fe_3O_4@mSiO_2 drug carriers, Chin. J. Inorg. Chem. 34 (6) (2018) 1095–1102.

[129] Q.-F. Meng, L. Rao, M. Zan, M. Chen, G.-T. Yu, X. Wei, Z. Wu, Y. Sun, S.-S. Guo, X.-Z. Zhao, Macrophage membrane-coated iron oxide nanoparticles for enhanced photothermal tumor therapy, Nanotechnology 29 (13) (2018) 134004.

[130] C. Niu, Y. Xu, S. An, M. Zhang, Y. Hu, L. Wang, Q. Peng, Near-infrared induced phase-shifted ICG/Fe_3O_4 loaded PLGA nanoparticles for photothermal tumor ablation, Sci. Rep. 7 (2017) 5490.

[131] S. Zhang, L. Wu, J. Cao, K. Wang, Y. Ge, W. Ma, X. Qi, S. Shen, Effect of magnetic nanoparticles size on rheumatoid arthritis targeting and photothermal therapy, Colloids Surfaces B 170 (2018) 224–232.

[132] Y. Yang, B. Gong, Y. Yang, A. Xie, Y. Shen, M. Zhu, Construction and synergistic anticancer efficacy of magnetic targeting cabbage-like Fe_3O_4@MoS_2@ZnO drug carriers, J. Mater. Chem. B 6 (22) (2018) 3792–3799.

[133] W. Wang, C. Hao, M. Sun, L. Xu, C. Xu, H. Kuang, Spiky Fe_3O_4@Au supraparticles for multimodal in Vivo imaging, Adv. Funct. Mater. 28 (22) (2018) 1800310.

[134] S. Yu, G. Li, R. Liu, D. Ma, W. Xue, Dendritic Fe_3O_4@Poly(dopamine)@PAMAM nanocomposite as controllable NO-releasing material: A synergistic photothermal and NO antibacterial study, Adv. Funct. Mater. 28 (20) (2018) 1707440.

[135] G. Fu, S.T. Sanjay, W. Zhou, R.A. Brekken, R.A. Kirken, X. Li, Exploration of nanoparticle-mediated photothermal effect of TMB-H_2O_2 colorimetric system and its application in a visual quantitative photothermal immunoassay, Anal. Chem. 90 (9) (2018) 5930–5937.

[136] P. Pan, Y. Lin, Z. Gan, X. Luo, W. Zhou, N. Zhang, Magnetic field enhanced photothermal effect of Fe_3O_4 nanoparticles, J. Appl. Phys. 123 (11) (2018) 115115.

[137] Y. Hu, H. Hu, J. Yan, C. Zhang, Y. Li, M. Wang, W. Tan, J. Liu, Y. Pan, Multifunctional porous iron oxide nanoagents for MRI and photothermal/chemo synergistic therapy, Bioconjug. Chem. 29 (4) (2018) 1283–1290.

[138] Y. Chen, F. Zhang, Q. Wang, H. Lin, R. Tong, N. An, F. Qu, The synthesis of LA-Fe_3O_4@PDA-PEG-DOX for photothermal therapy–chemotherapy, Dalton Trans. 47 (7) (2018) 2435–2443.

[139] Y. Wang, G. Wei, X. Zhang, X. Huang, J. Zhao, X. Guo, S. Zhou, Multistage targeting strategy using magnetic composite nanoparticles for synergism of photothermal therapy and and chemotherapy, Small 14 (12) (2018) 1702994.

[140] R. Pązik, A. Lewińska, J. Adamczyk-Grochala, M. Kulpa-Greszta, P. Kłoda, A. Tomaszewska, A. Dziedzic, G. Litwinienko, M. Noga, D. Sikora, M. Wnuk, Energy conversion and biocompatibility of surface functionalized magnetite nanoparticles with phosphonic moieties, J. Phys. Chem. B 124 (24) (2020) 4931–4948.

[141] R.-M. Yang, C.-P. Fu, J.-Z. Fang, X.-D. Xu, X.-H. Wei, W.-J. Tang, X.-Q. Jiang, L.-M. Zhang, Hyaluronan-modified superparamagnetic iron oxide nanoparticles for bimodal breast cancer imaging and photothermal therapy, Int. J. Nanomed. 12 (2017) 197–206.

[142] P. Xue, L. Sun, Q. Li, L. Zhang, Z. Xu, C.M. Li, Y. Kang, PEGylated magnetic prussian blue nanoparticles as a multifunctional therapeutic agent for combined targeted photothermal ablation and pH-triggered chemotherapy of tumor cells, J. Colloid Interface Sci. 509 (2018) 384–394.

[143] C.-W. Chen, W.-J. Syu, T.-C. Huang, Y.-C. Lee, J.-K. Hsiao, K.-Y. Huang, H.-P. Yu, M.-Y. Liao, P.-S. Lai, Encapsulation of Au/Fe_3O_4 nanoparticles into a polymer nanoarchitecture with combined near infrared-triggered chemo-photothermal therapy based on intracellular secondary protein understanding, J. Mater. Chem. B 5 (29) (2017) 5774–5782.

[144] X. Guo, W. Li, L. Luo, Z. Wang, Q. Li, F. Kong, H. Zhang, J. Yang, C. Zhu, Y. Du, J. You, External magnetic field-enhanced chemo-photothermal combination tumor therapy via iron oxide nanoparticles, ACS Appl. Mater. Interfaces 9 (19) (2017) 16581–16593.

[145] X.-R. Song, S.-H. Li, J. Dai, L. Song, G. Huang, R. Lin, J. Li, G. Liu, H.-H. Yang, Polyphenol-inspired facile construction of smart assemblies for ATP- and pH-responsive tumor MR/Optical imaging and photothermal therapy, Small 13 (20) (2017) 1603997.

[146] X. Qi, L. Xiong, J. Peng, D. Tang, Near infrared laser-controlled drug release of thermoresponsive microgel encapsulated with Fe_3O_4 nanoparticles, RSC Adv. 7 (32) (2017) 19604–19610.

[147] J. Du, J. Liu, P. Gong, M. Tian, L. Sun, S. Ji, L. Zhang, Z. Liu, Construction of a novel fluorinated graphene-based magnetic nanocomposite and its application in cancer photo-chemotherapy, Mater. Lett. 196 (2017) 165–167.

[148] K.M. Gadora, D. Huang, B.A. Yousef, S. Song, In Vivo biodistribution and photothermal properties of Fe_3O_4 magnetic nanoparticle: effect of different size, World J. Pharm. Res. 5 (4) (2016) 152–162.

[149] R. Ge, X. Li, M. Lin, D. Wang, S. Li, S. Liu, Q. Tang, Y. Liu, J. Jiang, L. Liu, H. Sun, H. Zhang, B. Yang, Fe_3O_4@polydopamine composite theranostic superparticles employing preassembled Fe_3O_4 nanoparticles as the core, ACS Appl. Mater. Interfaces 8 (35) (2016) 22942–22952.

[150] C. Wang, L. Zhang, S. Li, M. Zhang, T. Wang, L. Li, C. Wang, Z. Su, A designed synthesis of multifunctional Fe_3O_4@carbon/zinc phosphate nanoparticles for simultaneous imaging and synergic chemo-photothermal cancer therapy, J. Mater. Chem. B 4 (35) (2016) 5809–5813.

[151] J. Wang, H. Zhao, Z. Zhou, P. Zhou, Y. Yan, M. Wang, H. Yang, Y. Zhang, S. Yang, MR/SPECT imaging guided photothermal therapy of tumor-targeting Fe@Fe_3O_4 nanoparticles in Vivo with low mononuclear phagocyte uptake, ACS Appl. Mater. Interfaces 8 (31) (2016) 19872–19882.

[152] C. Koo, H. Hong, P.W. Im, H. Kim, C. Lee, X. Jin, B. Yan, W. Lee, H.- J. Im, S.H. Paek, Y. Piao, Magnetic and near-infrared derived heating characteristics of dimercaptosuccinic acid coated uniform Fe@Fe_3O_4 core–shell nanoparticles, Nano Convergence 7 (2020) 20.

[153] Y. Yin, S. Wang, D. Hu, J. Cai, F. Chen, B. Wang, Y. Gao, Magnetic-, acoustic-, and optical-triple-responsive microbubbles for magnetic hyperthermia and pothotothermal combination cancer therapy, J. Visual. Exp. 159 (2020) e61208.

[154] T.-J. Li, C.-M. Chang, P.-Y. Chang, Y.-C. Chuang, C.-C. Huang, W.-C. Su, D.-B. Shieh, Handheld energy-efficient magneto-optical real-time quantitative PCR device for target DNA enrichment and quantification, NPG Asia Mater. 8 (2016) e277.

[155] M. Wu, Q. Guo, F. Xu, S. Liu, X. Lu, J. Wang, H. Gao, P. Luo, Engineering phosphopeptide-decorated magnetic nanoparticles as efficient photothermal agents for solid tumor therapy, J. Colloid Interface Sci. 476 (2016) 158–166.

[156] L. Chen, L. Wu, F. Liu, X. Qi, Y. Ge, S. Shen, Azo-functionalized Fe_3O_4 nanoparticles: A near-infrared light triggered drug delivery system for combined therapy of cancer with low toxicity, J. Mater. Chem. B 4 (21) (2016) 3660–3669.

[157] X. Ren, R. Zheng, X. Fang, X. Wang, X. Zhang, W. Yang, X. Sha, Red blood cell membrane camouflaged magnetic nanoclusters for imaging-guided photothermal therapy, Biomaterials 92 (2016) 13–24.

[158] R. Zheng, S. Wang, Y. Tian, X. Jiang, D. Fu, S. Shen, W. Yang, Polydopamine-coated magnetic composite particles with an enhanced photothermal effect, ACS Appl. Mater. Interfaces 7 (29) (2015) 15876–15884.

[159] C.J. Jeong, S.M. Sharker, I. In, S.Y. Park, Iron Oxide@PEDOT-based recyclable photothermal nanoparticles with poly(vinylpyrrolidone) sulfobetaines for rapid and effective antibacterial activity, ACS Appl. Mater. Interfaces 7 (18) (2015) 9469–9478.

[160] C.-H. Zhu, Y. Lu, J.-F. Chen, S.-H. Yu, Photothermal poly(N-isopropylacrylamide)/Fe_3O_4 nanocomposite hydrogel as a movable position heating source under remote control, Small 10 (14) (2014) 2796–2800.

[161] Z. Dai, W. Wen, Z. Guo, X.-Z. Song, K. Zheng, X. Xu, X. Qia, Z. Tan, SiO_2-coated magnetic nano-Fe_3O_4 photosensitizer for synergistic tumor-targeted chemo-photothermal therapy, Colloids Surfaces B 195 (2020) 111274.

[162] J. Ling, S. Gong, Y. Xia, Monodisperse Fe_2O_3 supraparticles: Eco-friendly fabrication, gallic acid modification, size-dependent photothermal conversion efficiency, and cellular uptake, Adv. Mater. Interfaces 7 (18) (2020) 2000804.

[163] Y. Hu, L. Meng, L. Niu, Q. Facile, Synthesis of superparamagnetic Fe_3O_4@polyphosphazene@Au shells for magnetic resonance imaging and photothermal therapy, ACS Appl. Mater. Interfaces 5 (11) (2013) 4586–4591.

[164] A. Jędrzak, B.F. Grześkowiak, K. Golba, E. Coy, K. Synoradzki, S. Jurga, T. Jesionowski, R. Mrówczyński, Magnetite nanoparticles and spheres for chemo- and photothermal therapy of hepatocellular carcinoma in vitro, Int. J. Nanomed. 15 (2020) 7923–7936.

[165] I.B. Yeboah, S.W.K. Hatekah, Y.K. Konku-Asase, A. Yaya, K. Kan-Dapaah, Destruction of fibroadenomas using photothermal heating of Fe_3O_4 nanoparticles: Experiments and models, Appl. Sci. 10 (17) (2020) 5844.

[166] H. Guo, X. Su, Q. Su, W. Zhuang, Z. You, Au-coated Fe_3O_4 core–shell nanohybrids with photothermal activity for point-of-care immunoassay for lipoprotein-associated phospholipase A_2 on a digital near-infrared thermometer, Anal. Bioanal. Chem. 413 (2021) 235–244.
[167] F. Wei, X. Cui, Z. Wang, C. Dong, J. Li, X. Han, Recoverable peroxidase-like Fe_3O_4@MoS_2-Ag nanozyme with enhanced antibacterial ability, Chem. Eng. J. 408 (2021) 127240.
[168] S. Shen, J. Ren, X. Zhu, Z. Pang, X. Lu, C. Deng, R. Zhang, X. Jiang, Monodisperse magnetites anchored onto carbon nanotubes: A platform for cell imaging, magnetic manipulation and enhanced photothermal treatment of tumors, J. Mater. Chem. B 1 (14) (2013) 1939–1946.
[169] A. Nicolas-Boluda, Z. Yang, T. Guilbert, L. Fouassier, F. Carn, F. Gazeau, M.P. Pileni, Self-assemblies of Fe_3O_4 nanocrystals: Toward nanoscale precision of photothermal effects in the tumor microenvironment, Adv. Funct. Mater. 31 (4) (2021) 2006824.
[170] B. Li, T. Gong, N. Xu, F. Cui, B. Yuan, Q. Yuan, H. Sun, L. Wang, J. Liu, Improved stability and photothermal performance of polydopamine-modified Fe_3O_4 nanocomposites for highly efficient magnetic resonance imaging-guided photothermal therapy, Small 16 (45) (2020) 2003969.
[171] V.A. Tran, V.G. Vo, K. Shim, S.-W. Lee, S.S.A. An, Multimodal mesoporous silica nanocarriers for dual stimuli-responsive drug release and excellent photothermal ablation of cancer cells, Int. J. Nanomed. 15 (2020) 7667–7685.
[172] J. Ren, S. Shen, Z. Pang, X. Lu, C. Deng, X. Jiang, Facile synthesis of superparamagnetic Fe_3O_4@Au nanoparticles for photothermal destruction of cancer cells, Chem. Commun. 47 (42) (2011) 11692–11694.
[173] Z. Shi, Y. Zhang, R. Dai, S. Chen, M. Zhang, L. Jin, J. Wang, W. Zhaoa, C. Zhao, Rationally designed magnetic poly(catechol-hexanediamine) particles for bacteria removal and on-demand biofilm eradication, Colloids Surfaces B 186 (2020) 110728.
[174] T. Zhang, L. Lei, M. Tian, J. Ren, Z. Lu, Y. Liu, Y. Liu, Multifunctional Fe_3O_4@Au supraparticle as a promising thermal contrast for an ultrasensitive lateral flow immunoassay, Talanta 222 (2021) 121478.
[175] S. Fu, Y. Ding, T. Cong, X. Yang, X. Hong, B. Yu, Y. Li, Y. Liu, Multifunctional $NaYF_4$:Yb, Er@PE_3@Fe_3O_4 nanocomposites for magnetic-field-assisted upconversion imaging guided photothermal therapy of cancer cells, Dalton Trans. 48 (34) (2019) 12850.
[176] D.-H. Huang, X.-Y. Qi, Y.-R. Ge, S. Shen, Application of magnetic iron oxide nanoparticles in magnetic resonance/ photothermal dual-modal imaging, Acta Pharm. Sinica 52 (3) (2017) 481–487.
[177] J. Wang, H. Liu, Y. Liu, C. Chu, Y. Yang, Y. Zeng, W. Zhang, G. Liu, Eumelanin–Fe_3O_4 hybrid nanoparticles for enhanced MR/PA imaging-assisted local photothermolysis, Biomater. Sci. 6 (3) (2018) 86–595.
[178] C. Gökalp, Z. Çıplak, B. Getiren, N. Yıldız, Photoluminescence, photothermal and magnetic properties of nitrogen doped graphene quantum dots based ternary nanocomposite, Colloids Surf. A 605 (2020) 125370.
[179] G. Liu, M. Cai, Y. Feng, X. Wang, F. Zhou, W. Liu, Photothermally actuated interfacial hydration for fast friction switch on hydrophilic polymer brush modified PDMS sheet incorporated with Fe_3O_4 nanoparticles, Chem. Commun. 52 (18) (2016) 3681–3683.
[180] X. Guo, Z. Wu, W. Li, Z. Wang, Q. Li, F. Kong, H. Zhang, X. Zhu, Y.P. Du, Y. Jin, Y. Du, J. You, Appropriate size of magnetic nanoparticles for various bioapplications in cancer diagnostics and therapy, ACS Appl. Mater. Interfaces 8 (5) (2016) 3092–3106.
[181] G. Fu, W. Liu, Y. Li, Y. Jin, L. Jiang, X. Liang, S. Feng, Z. Dai, Magnetic prussian blue nanoparticles for targeted photothermal therapy under magnetic resonance imaging guidance, Bioconjug. Chem. 25 (9) (2014) 1655–1663.
[182] S. Shen, L. Wu, C.-R. Wang, X.-Y. Qi, Y.-R. Ge, Y. Jin, Preparation and in vitro evaluation of doxorubicin-loaded magnetic iron oxide nanoparticles, Acta Pharma. Sinica 48 (12) (2013) 1844–1849.
[183] S. Li, X. Shi, H. Wang, L. Xiao, A multifunctional dual-shell magnetic nanocomposite with near-infrared light response for synergistic chemo-thermal tumor therapy, J. Biomed. Mater. Res. 109 (6) (2021) 841–852.
[184] S.Shen L. Wu, X.-Y. Qi, Y.-R. Ge, Y. Jin, Preparation and photothermal effect evaluation of magnetic Fe_3O_4-CMCTS nanoparticles, Chin. Pharm. J. 49 (16) (2014) 1432–1436.
[185] X. Feng, W. Xu, C. Zhang, S. Tan, J. Zhang, P. Zhang, Y. Zhang, Facile synthesis of Yolk-Shell structured Fe_3O_4@C-Au nanoparticles for thermotherapic application, Mater. Lett. 258 (2020) 126809.
[186] Y. Wang, F. Zhang, H. Lin, F. Qu, Biodegradable hollow $MoSe_2$/Fe_3O_4 nanospheres as the photodynamic therapy-enhanced agent for multimode CT/MR/IR imaging and synergistic antitumor therapy, ACS Appl. Mater. Interfaces 11 (47) (2019) 43964–43975.
[187] C. Chen, Z. Huang, L.-A. Shi, Y. Jiao, S. Zhu, J. Li, Y. Hu, J. Chu, D. Wu, L. Jiang, Remote photothermal actuation of underwater bubble toward arbitrary direction on planar slippery Fe_3O_4-doped surfaces, Adv. Funct. Mater. 29 (40) (2019) 1904766.
[188] X. Wang, Q. Dai, H. Zhong, X. Liu, J. Ren, Fast-responsive temperature-sensitive hydrogels, Bioresources 14 (4) (2019) 8543–8558.
[189] P. Xu, R. Yang, L. Sun, Q. Li, L. Zhang, Z. Xu, Y. Kang, Indocyanine green-conjugated magnetic prussian blue nanoparticles for synchronous photothermal/photodynamic tumor therapy, Nano-Micro Lett. 10 (4) (2018) 74.
[190] Y. Yang, L. Ma, C. Cheng, Y. Deng, J. Huang, X. Fan, C. Nie, W. Zhao, C. Zhao, Nonchemotherapic and robust dual-responsive nanoagents with on-demand bacterial trapping, ablation, and release for efficient wound disinfection, Adv. Funct. Mater. 28 (21) (2018) 1705708.
[191] Y.-J. Lu, P.-Y. Lin, P.-H. Huang, C.-Y. Kuo, K.T. Shalumon, M.-Y. Chen, J.-P. Chen, Magnetic graphene oxide for dual targeted delivery of doxorubicin and photothermal therapy, Nanomaterials 8 (4) (2018) 193.
[192] L. Sun, Q. Li, L. Zhang, Z. Xu, Y. Kang, P. Xue, PEGylated polydopamine nanoparticles incorporated with indocyanine green and doxorubicin for magnetically guided multimodal cancer therapy triggered by near-infrared light, ACS Appl. Nano Mater. 1 (1) (2018) 325–336.
[193] Q. Zhang, W. Shan, C. Ai, Z. Chen, T. Zhou, X. Lv, X. Zhou, S. Ye, L. Ren, X. Wang, Construction of multifunctional Fe_3O_4-MTX@HBc nanoparticles for MR imaging and photothermal therapy/chemotherapy, Nanotheranostics 2 (1) (2018) 87–95.
[194] L. Rao, B. Cai, L.-L. Bu, Q.-Q. Liao, S.-S. Guo, X.-Z. Zhao, W.-F. Dong, W. Liu, Microfluidic electroporation-facilitated synthesis of erythrocyte membrane-coated magnetic nanoparticles for enhanced imaging-guided cancer therapy, ACS Nano 11 (4) (2017) 3496–3505.
[195] L. Wu, L. Chen, F. Liu, X. Qi, Y. Ge, S. Shen, Remotely controlled drug release based on iron oxide nanoparticles for specific therapy of cancer, Colloids Surfaces B 152 (2017) 440–448.
[196] L. Rao, L.-L. Bu, Q.-F. Meng, B. Cai, W.-W. Deng, A. Li, K. Li, S.-S. Guo, W.-F. Zhang, W. Liu, Z.-J. Sun, X.-Z. Zhao, Antitumor platelet-mimicking magnetic nanoparticles, Adv. Funct. Mater. 27 (9) (2017) 1604774.
[197] Y. Shan, X.-G. Yu, X.-Z. Yuan, Z. Wang, Preparation and photothermal property of Fe_3O_4@Au composites: Senior undergraduate material chemistry comprehensive experiment, J. Lab. Chem. Educ. 8 (2) (2020) 23–27.
[198] B. Chen, F. Li, X.K. Zhu, W. Xie, X. Hu, M.H. Zan, X. Li, Q.-Y. Li, S.-S. Guo, X.-Z. Zhao, Y.-A. Jiang, Z. Cao, W. Liu, Highly biocompatible and recyclable biomimetic nanoparticles for antibiotic-resistant bacteria infection, Biomater. Sci. 9 (3) (2021) 826–834.
[199] S. Nemec, S. Kralj, C. Wilhelm, A. Abou-Hassan, M.-P. Rols, J. Kolosnjaj-Tabi, Comparison of iron oxide nanoparticles in photothermia and magnetic hyperthermia: Effects of clustering and silica encapsulation on nanoparticles' heating yield, Appl. Sci. 10 (20) (2020) 7322.
[200] E.-J. Nam, Y. Kwon, Y. Ha, S.R. Paik, Fabrication of a dual stimuli-responsive assorted film comprising magnetic- and gold-nanoparticles with a self-assembly protein of α-synuclein, ACS Appl. Bio Mater. 4 (2) (2021) 1863–1875.
[201] Z. Huang, C. Chen, X. Wang, R. Li, Y. Bian, S. Zhu, Y. Hu, J. Li, D. Wu, J. Chu, Light-driven locomotion of underwater bubbles on ultrarobust paraffin-impregnated laser-ablated Fe_3O_4-doped slippery surfaces, ACS Appl. Mater. Interfaces 13 (7) (2021) 9272–9280.
[202] X. Bai, J. Yong, C. Shan, Y. Fang, X. Hou, F. Chen, Remote, selective, and in situ manipulation of liquid droplets on a femtosecond laser-structured superhydrophobic shape-memory polymer by near-infrared light, Sci. China Chem. 64 (5) (2021) 861–872.

[203] M.M. Fathy, L. Nasser, G. El-Sokkary, M.S. Rasheedy, Combined chemo-photothermal therapy of metastatic mammary adenocarcinoma using curcumin-coated iron oxide nanoparticles, BioNanoScience 11 (2) (2021) 447–453.
[204] H. Belkahla, E. Mazarío, A.P. Sangnier, J.S. Lomas, T. Gharbi, S. Ammar, O. Micheau, C. Wilhelm, M. Hémadi, TRAIL acts synergistically with iron oxide nanocluster-mediated magneto- and photothermia, Theranostics 9 (20) (2019) 5924–5936.
[205] X. Yao, J. Jing, F. Liang, Z. Yang, Polymer-Fe_3O_4 composite Janus nanoparticles, Macromolecules 49 (24) (2016) 9618–9625.
[206] Y. Zhang, T. Zhou, J. Li, N. Xu, M. Cai, H. Zhang, Q. Zhao, S. Wang, Au catalyzing control release NO in Vivo and tumor growth-inhibiting effect in chemo-photothermal combination therapy, Int. J. Nanomed. 16 (2021) 2501–2513.
[207] F. Wang, C. Zhang, A. Tan, H. Chen, S. Weng, Q. Xie, C. Li, Z. Cai, X. Wan, Photothermal and magnetocaloric-stimulated shape memory and self-healing via magnetic polymeric composite with dynamic crosslinking, Polymer 223 (2021) 123677.
[208] X. Li, Z. Wang, M. Ma, Z. Chen, X.-L. Tang, Z. Wang, Self-assembly iron oxide nanoclusters for photothermal-mediated synergistic chemo/chemodynamic therapy, J. Immunol. Res. 2021 (2021) 995839.
[209] M. Xing, J. Mohapatra, J. Beatty, J. Elkins, N.K. Pandey, A. Chalise, W. Chen, M. Jin, J.P. Liu, Iron-based magnetic nanoparticles for multimodal hyperthermia heating, J. Alloys Compd. 871 (2021) 159475.
[210] S. Zheng, S. Jin, M. Jiao, W. Wang, X. Zhou, J. Xu, Y. Wang, P. Dou, Z. Jin, C. Wu, J. Li, X. Ge, K. Xu, Tumor-targeted gd-doped mesoporous Fe_3O_4 nanoparticles for T_1/T_2 MR imaging guided synergistic cancer therapy, Drug Deliv. 28 (1) (2021) 787–799.
[211] W. Nong, W. Guan, Y. Yin, C. Lu, Q. Wang, Y. Luo, B. Zhang, Z. Xu, J. Wu, Y. Guan, Photo-triggered on-demand carvacrol vapor release from nano-generators for non-contact bacterial inactivation between nanomaterials and bacteria, Chem. Eng. J. 420 (2021) 129874.
[212] X. Song, Z. Chen, X. Zhang, J. Xiong, T. Jiang, Z. Wang, X. Geng, U.K. Cheang, Magnetic tri-bead microrobot assisted near-infrared triggered combined photothermal and chemotherapy of cancer cells, Sci. Rep. 11 (2021) 7907.
[213] H. Peng, J. Tang, R. Zheng, G. Guo, A. Dong, Y. Wang, W. Yang, Nuclear-targeted multifunctional magnetic nanoparticles for photothermal therapy, Adv. Healthc. Mater. 6 (7) (2017) 1601289.
[214] R. Ge, C. Liu, X. Zhang, W. Wang, B. Li, J. Liu, Y. Liu, H. Sun, D. Zhang, Y. Hou, H. Zhang, B. Yang, Photothermal-activatable Fe_3O_4 superparticle nanodrug carriers with PD-L1 immune checkpoint blockade for anti-metastatic cancer immunotherapy, ACS Appl. Mater. Interfaces 10 (24) (2018) 20342–20355.
[215] S. Xie, W. Sun, C. Zhang, B. Dong, J. Yang, M. Hou, L. Xiong, B. Cai, X. Liu, W. Xue, Metabolic control by heat stress determining cell fate to ferroptosis for effective cancer therapy, ACS Nano 15 (4) (2021) 7179–7194.
[216] D. Wu, L. Ma, F. Zhang, H. Qian, B. Minhas, Y. Yang, X. Han, D. Zhang, Durable deicing lubricant-infused surface with photothermally switchable hydrophobic/slippery property, Mater. Des. 185 (2020) 108236.
[217] A. Kolokithas-Ntoukas, A. Bakandritsos, J. Belza, P. Kesa, V. Herynek, J. Pankrac, A. Angelopoulou, O. Malina, K. Avgoustakis, V. Georgakilas, K. Polakova, R. Zboril, Condensed clustered iron oxides for ultrahigh photothermal conversion and in Vivo multimodal imaging, ACS Appl. Mater. Interfaces 13 (25) (2021) 29247–29256.
[218] Y. Jabalera, A. Sola-Leyva, M.P. Carrasco-Jiménez, G.R. Iglesias, C. Jimenez-Lopez, Synergistic photothermal-chemotherapy based on the use of biomimetic magnetic nanoparticles, Pharmaceutics 13 (5) (2021) 625.
[219] S.K. Shaw, J. Kailashiya, A. Gangwar, S.K. Alla, S.K. Gupta, C.L. Prajapat, S.S. Meena, D. Dash, P. Maiti, N.K. Prasad, γ-Fe_2O_3 nanoflowers as efficient magnetic hyperthermia and photothermal agent, Appl. Surf. Sci. 560 (2021) 150025.
[220] T. Chen, Y. Yang, H. Peng, A.K. Whittaker, Y. Li, Q. Zhao, Y. Wang, S. Zhu, Z. Wang, Cellulose nanocrystals reinforced highly stretchable thermal-sensitive hydrogel with ultra-high drug loading, Carbohydr. Polymers 266 (2021) 118122.
[221] J. Feng, W.-X. Ren, J.-L. Gao, F. Li, F. Kong, B.-J. Yao, Y.-B. Dong, Core-shell-structured covalent-organic framework as a nanoagent for single-laser-induced phototherapy, ACS Appl. Mater. Interfaces 13 (15) (2021) 17243–17254.
[222] T. He, J. He, M.R. Younis, N.T. Blum, S. Lei, Y. Zhang, P. Huang, J. Lin, Dual-stimuli-responsive nanotheranostics for dual-targeting photothermal-enhanced chemotherapy of tumor, ACS Appl. Mater. Interfaces 13 (19) (2021) 22204–22212.
[223] M.A. Antoniak, R. Pązik, U. Bazylińska, K. Wiwatowski, A. Tomaszewska, M. Kulpa-Greszta, J. Adamczyk-Grochala, M. Wnuk, S. Maćkowski, A. Lewińska, M. Nyk, Multimodal polymer encapsulated CdSe/Fe_3O_4 nanoplatform with improved biocompatibility for two-photon and temperature stimulated bioapplications, Mater. Sci. Eng. C 127 (2021) 112224.
[224] Q. Liu, L. Liu, C. Mo, X. Zhou, D. Chen, Y. He, H. He, W. Kang, Y. Zhao, G. Jin, Polyethylene glycol-coated ultrasmall superparamagnetic iron oxide nanoparticles-coupled sialyl Lewis X nanotheranostic platform for nasopharyngeal carcinoma imaging and photothermal therapy, J. Nanobiotechnol. 19 (2021) 171.
[225] X. Wang, Z. Liu, R. Jin, B. Cai, S. Liu, Y. Bai, X. Chen, Multifunctional hierarchical nanohybrids perform triple antitumor theranostics in a cascaded manner for effective tumor treatment, Acta Biomater. 128 (2021) 408–419.
[226] J. Wang, T. Mei, Y. Liu, Y. Zhang, Z. Zhang, Y. Hu, Y. Wang, M. Wu, C. Yang, X. Zhong, B. Chen, Z. Cui, W. Le, Z. Liu, Dual-targeted and MRI-guided photothermal therapy via iron-based nanoparticles-incorporated neutrophils, Biomater. Sci. 9 (11) (2021) 3968–3978.
[227] C. Koo, H. Hong, P.W. Im, H. Kim, C. Lee, X. Jin, B. Yan, W. Lee, H.-J. Im, S.H. Paek, Y. Piao, Magnetic and near-infrared derived heating characteristics of dimercaptosuccinic acid coated uniform Fe@Fe_3O_4 core–shell nanoparticles, Nano Converg. 7 (2020) 20.
[228] T.-W. Chang, H. Ko, W.-S. Huang, Y.-C. Chiu, L.-X. Yang, Z.-C. Chia, Y.-C. Chin, Y.-J. Chen, Y.-T. Tsai, C.-W. Hsu, C.-C. Chang, P.-J. Tsai, C.-C. Huang, Tannic acid-induced interfacial ligand-to-metal charge transfer and the phase transformation of Fe_3O_4 nanoparticles for the photothermal bacteria destruction, Chem. Eng. J. 428 (2022) 131237.
[229] B.S. Dash, Y.-J. Lu, H.-A. Chen, C.-C. Chuang, J.-P. Chen, Magnetic and GRPR-targeted reduced graphene oxide/doxorubicin nanocomposite for dual-targeted chemophotothermal cancer therapy, Mater. Sci. Eng. C 128 (2021) 112311.
[230] N. Wang, Y. Feng, Y. Zheng F. Zhou, D. Wang, Triboelectrification of interface controlled by photothermal materials based on electron transfer, Nano Energy 89 (2021) 106336.
[231] T.M.T. Vo, S. Mondal, V.T. Nguyen, S. Park, J. Choi, N.T. Bui, J. Oh, Rice starch coated iron oxide nanoparticles: A theranostic probe for photoacoustic imaging-guided photothermal cancer therapy, Int. J. Bio. Macromol. 183 (2021) 55–67.
[232] D. Zhang, J. Zhang, Y. Jian, B. Wu, H. Yan, H. Lu, S. Wei, S. Wu, Q. Xue, T. Chen, Multi-field synergy manipulating soft polymeric hydrogel transformers, Adv. Intell. Syst. 3 (4) (2021) 2000208.
[233] H. Huang, G. Yuan, Y. Xu, Y. Gao, Q. Mao, Y. Zhang, L. Bai, W. Li, A. Wu, W. Hu, Y. Pan, G. Zhou, Photoacoustic and magnetic resonance imaging-based gene and photothermal therapy using mesoporous nanoagents, Bioactive Mater. 9 (2022) 157–167.
[234] L. Chen, T. Yang, R. Tian, T. Yin, L. Weng, Y. Bai, Y. Zhang, X. Chen, Near-infrared and tumor environment co-activated nanoplatform for precise tumor therapy in multiple models, Appl. Mater. Today 24 (2021) 101133.
[235] B. Cai, M. Hou, S. Zhang, Z. Xin, J. Huang, J. Yang, Y. Wang, X. Cai, S. Xie, C. Zhang, Y. Huang, Dual targeting of endoplasmic reticulum by redox-deubiquitination regulation for cancer therapy, Int. J. Nanomed. 16 (2021) 5196–5209.
[236] S.B. Li, X. Wang, J. Zhu, Z. Wang, L. Wang, Synthesis and characterization of photothermal antibacterial hydrogel with enhanced mechanical properties, New J. Chem. 45 (36) (2021) 16804–16815.
[237] B. Chen, F. Li, X.K. Zhu, W. Xie, X. Hu, M.H. Zan, X. Li, Q.-Y. Li, S.-S. Guo, X.-Z. Zhao, Y.-A. Jiang, Z. Cao, W. Liu, Highly biocompatible and recyclable biomimetic nanoparticles for antibiotic-resistant bacteria infection, Biomater. Sci. 9 (3) (2021) 826–834.

[238] H. Guo, X. Su, Q. Su, W. Zhuang, Z. You, Au-coated Fe_3O_4 core–shell nanohybrids with photothermal activity for point-of-care immunoassay for lipoprotein-associated phospholipase A_2 on a digital near-infrared thermometer, Anal. Bioanal. Chem. 413 (1) (2021) 235–244.
[239] Q. Cheng, L. Yue, J. Li, C. Gao, Y. Ding, C. Sun, M. Xu, Z. Yuan, R. Wang, Supramolecular tropism driven aggregation of nanoparticles in situ for tumor-specific bioimaging and photothermal therapy, Small 17 (43) (2021) 2101332.
[240] L. Li, B. Zhao, H. Wang, Y. Gao, J. Hu, S. Zheng, Nanocomposites of polyhydroxyurethane with Fe_3O_4 nanoparticles: Synthesis, shape memory and reprocessing properties, Compos. Sci. Technol. 215 (2021) 109009.
[241] X. Bai, J. Yong, C. Shan, Y. Fang, X. Hou, F. Chen, Remote, selective, and in situ manipulation of liquid droplets on a femtosecond laser-structured superhydrophobic shape-memory polymer by near-infrared, Sci. China Chem. 64 (5) (2021) 861–872.
[242] Q. Fang, K. Xu, Q. Xiong, Y. Xu, A. Hui, S. Xuan, Fe_3O_4–Au–polydopamine hybrid microcapsules with photothermal–photodynamic synergistic anti-bacterial performance, CrysEngComm 23 (37) (2021) 6610–6619.
[243] X. Xu, M. Fan, Z. Yu, Y. Zhao, H. Zhang, J. Wang, M. Wu, F. Sun, X. Xu, C. Ding, J. Li, A removable photothermal antibacterial warm paste target for cariogenic bacteria, Chem. Eng. J. 429 (2022) 132491.
[244] Y. Zhang, Y. Yang, J. Shi, L. Wang, A multimodal strategy of Fe_3O_4@ZIF-8/GOx@MnO_2 hybrid nanozyme via TME modulation for tumor therapy, Nanoscale 13 (39) (2021) 16571–16588.
[245] X. Kang, T. Sun, L. Zhang, C. Zhou, Z. Xu, M. Du, S. Xiao, Y. Liu, M. Gong, D. Zhang, Synergistic theranostics of magnetic resonance imaging and photothermal therapy of breast cancer based on the Janus nanostructures Fe_3O_4-Au_{shell}-PEG, Int. J. Nanomed. 16 (2021) 6383–6394.
[246] X. Wang, L. Xuan, Y. Pan, Photothermal ablation of murine melanomas by Fe_3O_4 nanoparticle clusters, Beilstein J. Nanotechnol. 13 (2022) 255–264.
[247] Z. Chen, Y. Feng, N. Zhao, Y. Liu, G. Liu, F. Zhou, W. Liu, Near-infrared-light-modulated lubricating coating enabled by photothermal microgels, ACS Appl. Mater. Interfaces 13 (41) (2021) 49322–49330.
[248] A. Sennaroglu, M. Khan, M. Hashemkhani, H.Y. Acar, Determination of the wavelength-dependent photothermal conversion efficiency of photosensitizers for photothermal therapy: Application to Ag_2S-Glutathione quantum dots, J. Phys. Chem. B 125 (42) (2021) 11650–11659.
[249] M. Xing, J. Mohapatra, J. Beatty, J. Elkins, N.K. Pandey, A. Chalise, W. Chen, M. Jin, J.P. Liu, Iron-based magnetic nanoparticles for multimodal hyperthermia heating, J. Alloys Compd. 871 (2021) 159475.
[250] Z. Deng, J. Lin, S.L. Bud'ko, B. Webster, T.V. Kalin, V.V. Kalinichenko, D. Shi, Dual targeting with cell surface electrical charge and folic acid via superparamagnetic Fe_3O_4@$Cu_{2-x}S$ for photothermal cancer cell killing, Cancers 13 (2021) 5275.
[251] M. Wang, Y. Li, M. Wang, K. Liu, A.R. Hoover, M. Li, R.A. Towner, P. Mukherjee, F. Zhou, J. Qu, W.R. Chen, Synergistic interventional photothermal therapy and immunotherapy using an iron oxide nanoplatform for the treatment of pancreatic cancer, Acta Biomater. 138 (2022) 453–462.
[252] A. Qi, C. Wang, S. Ni, Y. Meng, T. Wang, Z. Yue, K. Yang, Y. Li, Z. Cheng, P. Guo, C. Zhang, Intravesical mucoadhesive hydrogel induces chemoresistant bladder cancer ferroptosis through delivering iron oxide nanoparticles in a three-tier strategy, ACS Appl. Mater. Interfaces 13 (44) (2021) 52374–52384.
[253] L. Zhang, X. Guan, X. Xiao, Y. Chai, Z. Chen, G. Zhou, Y. Fan, Near-infrared triggered injectable ferrimagnetic chitosan thermosensitive hydrogel for photo hyperthermia and precisely controlled drug release in tumor ablation, Eur. Polym. J. 162 (2022) 110879.
[254] S. Wang, H. Shen, Q. Mao, Q. Tao, G. Yuan, L. Zeng, Z. Chen, Y. Zhang, L. Cheng, J. Zhang, H. Dai, C. Hu, Y. Pan, Y. Li, Macrophage-mediated porous magnetic nanoparticles for multimodal imaging and postoperative photothermal therapy of gliomas, ACS Appl. Mater. Interfaces 13 (48) (2021) 56825–56837.
[255] W. Hu, Q. Qi, H. Hu, C. Wang, Q. Zhang, Z. Zhang, Y. Zhao, X. Yu, M. Guo, S. Du, Y. Lu, Fe_3O_4 liposome for photothermal/chemo-synergistic inhibition of metastatic breast tumor, Colloids Surf. A 634 (2022) 127921.
[256] J. Xiong, M. Wu, J. Chen, Y. Liu, Y. Chen, G. Fan, Y. Liu, J. Cheng, Z. Wang, S. Wang, Y. Liu, W. Zhang, Cancer-erythrocyte hybrid membrane-camouflaged magnetic nanoparticles with enhanced photothermal-immunotherapy for ovarian cancer, ACS Nano 15 (12) (2021) 19756–19770.
[257] J. Xiao, L. Hai, Y. Li, H. Li, M. Gong, Z. Wang, Z. Tang, L. Deng, D. He, An ultrasmall Fe_3O_4-decorated polydopamine hybrid nanozyme enables continuous conversion of oxygen into toxic hydroxyl radical via GSH-depleted cascade redox reactions for intensive wound disinfection, Small 18 (9) (2022) 2105465.
[258] A. Yuan, L. Ruan, R. Jia, X. Wang, L. Wu, J. Cao, X. Qi, Y. Wei, S. Shen, Tumor exosome-mimicking iron oxide nanoparticles for near infrared-responsive drug delivery, ACS Appl. Nano Mater. 5 (1) (2022) 996–1002.
[259] Z. Jin, Y. Dun, L. Xie, W. Jiang, X. Sun, P. Hu, S. Zheng, Y. Yu, Preparation of doxorubicin-loaded porous iron Oxide@polydopamine nanocomposites for MR imaging and synergistic photothermal–chemotherapy of cancer, Colloids Surfaces B 208 (2021) 112107.
[260] M.M. Fathy, L. Nasser, G. El-Sokkary, M.S. Rasheedy, Combined chemo-photothermal therapy of metastatic mammary adenocarcinoma using curcumin-coated iron oxide nanoparticles, Bionanoscience 11 (2) (2021) 447–453.
[261] K. Lu, Y. Qu, Y. Lin, L. Li, Y. Wu, Y. Zou, T. Chang, Y. Zhang, Q. Yu, H. Chen, A photothermal nanoplatform with sugar-triggered cleaning ability for high-efficiency intracellular delivery, ACS Appl. Mater. Interfaces 14 (2) (2022) 2618–2628.
[262] P. Ye, F. Li, J. Zou, Y. Luo, S. Wang, G. Lu, F. Zhang, C. Chen, J. Long, R. Jia, M. Shi, Y. Wang, X. Cheng, G. Ma, W. Wei, In situ generation of gold nanoparticles on bacteria-derived magnetosomes for imaging-guided starving/chemodynamic/photothermal synergistic therapy against cancer, Adv. Funct. Mater. 32 (17) (2022) 2110063.
[263] N. Zhao, X. Gao, Z. Chen, Y. Feng, G. Liu, F. Zhou, W. Liu, Super-lubricating hybrid elastomer with rapid photothermal sterilization and strong anti-cell adhesion, Chem. Eng. J. 434 (2022) 134763.
[264] X. Wei, L. Chen, Y. Wang, Y. Sun, C. Ma, X. Yang, S. Jiang, G. Duan, An electrospinning anisotropic hydrogel with remotely-controlled photo-responsive deformation and long-range navigation for synergist actuation, Chem. Eng. J. 433 (2022) 134258.
[265] E.D. Quiñones, T.-Y. Lu, K.-T. Liu, Y.-J. Fan, E.-Y. Chuang, J. Yu, Glycol chitosan/iron oxide/polypyrrole nanoclusters for precise chemodynamic/photothermal synergistic therapy, Int. J. Biol. Macromol. 203 (2022) 268–279.
[266] Y. Jabalera, A. Sola-Leyva, S.C. Gaglio, M.P. Carrasco-Jiménez, G.R. Iglesias, M. Perduca, C. Jimenez-Lopez, Enhanced cytotoxic effect of TAT–PLGA-embedded DOXO carried by biomimetic magnetic nanoparticles upon combination with magnetic hyperthermia and photothermia, Pharmaceutics 13 (8) (2021) 1168.
[267] X. Sun, Y. Xu, Q. Guo, N. Wang, B. Wu, C. Zhu, W. Zhao, W. Qiang, M. Zheng, A novel nanoprobe for targeted imaging and photothermal/photodynamic therapy of lung cancer, Langmuir 38 (4) (2022) 1360–1367.
[268] X. Zheng, Y. Chen, C. Chen, Z. Chen, Y. Guo, H. Li, H. Liu, High-energy-density shape memory materials with ultrahigh strain for reconfigurable artificial muscles, J. Mater. Chem. B 9 (36) (2021) 7371–7380.
[269] X. Lin, T. He, R. Tang, Q. Li, N. Wu, Y. Zhou, H. He, L. Wan, J. Huang, Q. Jiang, Y. Zhong, Z. Xie, Z. Hu, Y. Zhou, P. Li, Biomimetic nanoprobe-augmented triple therapy with photothermal, sonodynamic and checkpoint blockade inhibits tumor growth and metastasis, J. Nanobiotechnol. 20 (2022) 80.
[270] K.L. Ribeiro, I.A.M. Frías, O.L. Franco, S.C. Dias, A.A. Sousa-Junior, O.N. Silva, A.F. Bakuzis, M.D.L. Oliveira, C.A.S. Andrade, Clavanin A-bioconjugated Fe_3O_4/silane core–shell nanoparticles for thermal ablation of bacterial biofilms, Colloids Surfaces B 169 (2018) 72–81.
[271] W. Hu, Q. Qi, H. Hu, C. Wang, Q. Zhang, Z. Zhang, Y. Zhao, X. Yu, M. Guo, S. Du, Y. Lu, Fe3O4 liposome for photothermal/chemo-synergistic inhibition of metastatic breast tumor, Colloids Surfaces B 634 (2022) 127921.

[272] J. Cui, J. Huang, Y. Yan, W. Chen, J. Wen, X. Wu, J. Liu, H. Liu, C. Huang, Ferroferric oxide loaded near-infrared triggered photothermal microneedle patch for controlled drug release, J. Colloid Interface Sci. 617 (2022) 718–729.
[273] I.B. Yeboah, S.W.K. Hatekah, A. Yaya, K. Kan-Dapaah, Photothermally-heated superparamagnetic polymeric nanocomposite implants for interstitial thermotherapy, Nanomaterials 12 (6) (2022) 955.
[274] Z. Tang, W. Tian, H. Long, S. Jiang, J. Zhao, J. Zhou, Q. He, X. Luo, Subcellular-targeted near-infrared-responsive nanomedicine with synergistic chemo-photothermal therapy against multidrug resistant cancer, Mol. Pharmaceutics 19 (12) (2022) 4538–4551.
[275] L. Liu, J. Wu, B. Chen, J. Gao, T. Li, Y. Ye, H. Tian, S. Wang, F. Wang, J. Jiang, J. Ou, F. Tong, F. Peng, Y. Tu, Magnetically actuated biohybrid microswimmers for precise photothermal muscle contraction, ACS Nano 16 (4) (2022) 6515–6526.
[276] H. Wang, S. Gong, X. Li, Y. Chong, Q. Ge, J. Wang, Y. Zhang, Y. Liu, X. Jiao, SDS coated Fe_3O_4@MoS_2 with NIR-enhanced photothermal-photodynamic therapy and antibiotic resistance gene dissemination inhibition functions, Colloids Surfaces B 214 (2022) 112457.
[277] Y. Yang, P. Wang, R. Shi, Z. Zhao, A. Xie, Y. Shen, M. Zhu, Design of the tumor microenvironment-multiresponsive nanoplatform for dual-targeting and photothermal imaging guided photothermal/photodynamic/chemodynamic cancer therapies with hypoxia improvement and GSH depletion, Chem. Eng. J. 441 (2022) 136042.
[278] X. Wei, L. Chen, Y. Wang, Y. Sun, C. Ma, X. Yang, S. Jiang, G. Duan, An electrospinning anisotropic hydrogel with remotely-controlled photo-responsive deformation and long-range navigation for synergist actuation, Chem. Eng. J. 433 (2022) 134258.
[279] X. Wang, X. Tian, K. Zhao, L. Wu, J. Cao, S. Shen, Oxygen-independent free radicals induced by photothermal effect of Fe_3O_4 for hypoxic cancer therapy, Chem. Lett. 51 (6) (2022) 633–635.
[280] N. Zhao, X. Gao, Z. Chen, Y. Feng, G. Liu, F. Zhou, W. Liu, Super-lubricating hybrid elastomer with rapid photothermal sterilization and strong anti-cell adhesion, Chem. Eng. J. 434 (2022) 134763.
[281] X. Ke, S. Tang, Z. Dong, H. Wang, X. Xu, R. Qiu, J. Yang, J. Luo, J. Li, A silk fibroin based bioadhesive with synergistic photothermal-reinforced antibacterial activity, Int. J. Biol. Macromol. 209 (2022) 608–617.
[282] C. Li, Z. Li, Y. Gan, F. Jiang, H. Zhao, J. Tan, Y.Y. Yang, P. Yuan, X. Ding, Selective capture, separation, and photothermal inactivation of Methicillin-Resistant Staphylococcus Aureus (MRSA) using functional magnetic nanoparticles, ACS Appl. Mater. Interfaces 14 (18) (2022) 20566–20575.
[283] Y. Hu, Z. Li, Y. Sun, Ultrasmall enzyme/light-powered nanomotor facilitates cholesterol detection, J. Colloid Interface Sci. 621 (2022) 341–351.
[284] H. Peng, D. Wang, D. Ma, Y. Zhou, J. Zhang, Y. Kang, Q. Yue, Multifunctional Yolk–Shell structured magnetic mesoporous polydopamine/carbon microspheres for photothermal therapy and heterogenous catalysis, ACS Appl. Mater. Interfaces 14 (20) (2022) 23888–23895.
[285] K. Wu, A. Mohsin, W.Q. Zaman, Z. Zhang, W. Guan, M. Chu, Y. Zhuang, M. Guo, Urchin-like magnetic microspheres for cancer therapy through synergistic effect of mechanical force, photothermal and photodynamic effects, J. Nanobiotechnol. 20 (2022) 224.
[286] G. Jiang, D. Fan, J. Tian, Z. Xiang, Q. Fang, Self-confirming magnetosomes for tumor-targeted T_1/T_2 dual-mode MR imaging and MRI-guided photothermal therapy, Adv. Health Mater. 11 (14) (2022) 2200841.
[287] H. Zhang, X. Xu, M. Wu, Y. Zhao, F. Sun, Q. Xin, Y. Zhou, M. Qin, Y. Zhou, C. Ding, J. Li, Virus-like iron oxide minerals inspired by magnetotactic bacteria: Towards an outstanding photothermal superhydrophobic platform on universal substrates, Adv. Funct. Mater. 32 (29) (2022) 2201795.
[288] G. Li, L. Li, Z. Wang, S. Zhong, M. Li, H. Wang, L. Yuan, The construct of triple responsive nanocomposite and its antibacterial effect, Colloids Surfaces B 214 (2022) 112378.
[289] M.P. Pileni, Supraballs as spherical solid 3D superlattices of hydrophobic nanocrystals dispersed in water: Nanoarchitectonics and properties, Phys. Chem. Chem. Phys. 24 (23) (2022) 14140–14149.
[290] X. Yang, J. Xiao, L. Jiang, L. Ran, Y. Fan, M. Zhang, Y. Xu, C. Yao, B. An, Y. Yang, C. Yang, G. Tian, G. Zhang, Y. Zhang, A multifunctional vanadium-iron-oxide nanoparticle eradicates hepatocellular carcinoma via targeting tumor and endothelial cells, ACS Appl. Mater. Interfaces 14 (25) (2022) 28514–28526.
[291] J. Guo, W. Wei, Y. Zhao, H. Dai, Iron oxide nanoparticles (IONPs) with photothermal performance and enhanced nanozyme activity for bacteria-infected wound therapy, Regen. Biomater. 9 (2022) rbac041.
[292] H. Wang, Q. Zhang, X. Zhang, K. Zhang, X. Zhao, R. Zhang, Z. Zhang, NIR laser-activated polydopamine-coated Fe_3O_4 nanoplatform used as a recyclable precise photothermal insecticide, Sustain. Mater. Technol. 33 (2022) e00456.
[293] H. Peng, D. Wang, D. Ma, Y. Zhou, J. Zhang, Y. Kang, Q. Yue, Multifunctional Yolk-Shell structured magnetic mesoporous polydopamine/carbon microspheres for photothermal therapy and heterogenous catalysis, ACS Appl. Mater. Interfaces 14 (20) (2022) 23888–23895.
[294] J. Ma, Y. Zhang, H. Sun, P. Ding, D. Chen, Fabrication of human serum albumin–imprinted photothermal nanoparticles for enhanced immunotherapy, J. Mater. Chem. B 10 (22) (2022) 4226–4241.
[295] S. Chen, Y. Lv, Y. Wang, D. Kong, J. Xia, J. Li, Q. Zhou, Tumor acidic microenvironment-responsive promodulator iron oxide nanoparticles for photothermal-enhanced chemodynamic immunotherapy of cancer, ACS Biomater. Sci. Eng. 9 (2) (2023) 773–783.
[296] X. Wang, X. Tian, K. Zhao, L. Wu, J. Cao, S. Shen, Oxygen-independent free radicals induced by photothermal effect of Fe_3O_4 for hypoxic cancer therapy, Chem. Lett. 51 (6) (2022) 633–635.
[297] A. Pasćiak, R. Marin, L. Abiven, A. Pilch-Wróbel, M. Misiak, W. Xu, K. Prorok, O. Bezkrovnyi, Ł. Marciniak, C. Chanéac, F. Gazeau, R. Bazzi, S. Roux, B. Viana, V.-P. Lehto, D. Jaque, A. Bednarkiewicz, Quantitative comparison of the light-to-heat conversion efficiency in nanomaterials suitable for photothermal therapy, ACS Appl. Mater. Interfaces 14 (29) (2022) 33555–33566.
[298] L. Zhang, X. Guan, X. Xiao, Z. Chen, G. Zhou, Y. Fan, Dual-phase injectable thermosensitive hydrogel incorporating Fe_3O_4@PDA with pH and NIR triggered drug release for synergistic tumor therapy, Eur. Polym. J. 176 (2022) 111424.
[299] H. Wu, Y. Lei, J. Wang, Y. Tan, X. Song, J. Zheng, T. He, X. Zhou, C. Liu, A.-L. Kjøniksend, Y. Zhang, Exploiting CMC@Fe_3O_4 nanoparticles as a multi-functional component for hydrogel fabrication, J. Phys. D Appl. Phys. 55 (40) (2022) 404002.
[300] J.-E. Cun, Y. Pan, Z. Zhang, Y. Lu, J. Li, Q. Pan, W. Gao, K. Luo, B. He, Y. Pu, Photo-enhanced upcycling H_2O_2 into hydroxyl radicals by IR780-embedded Fe_3O_4@MIL-100 for intense nanocatalytic tumor therapy, Biomaterials 287 (2022) 121687.
[301] L. Yu, S. Zhu, K. Qin, X. Fan, L. An, Macrophages loaded with fe nanoparticles for enhanced photothermal ablation of tumors, J. Funct. Biomater. 13 (2022) 94.
[302] X. Huang, Z. Zhang, L. Chen, Y. Lin, R. Zeng, J. Xu, S. Chen, J. Zhang, H. Cai, H. Zhou, P. Sun, Multifunctional au nano-bridged nanogap probes as ICP-MS/SERS dual-signal tags and signal amplifiers for bacteria discriminating, quantitative detecting and photothermal bactericidal activity, Biosens. Bioelectron. 212 (2022) 114414.
[303] L. Li, H. Yang, L. Li, X. Tan, S. Ge, L. Zhang, J. Yu, Y. Zhang, Photothermal-reagent-triggered visual thermoresponsive and quantized photoelectrochemical dual-signal assay, ACS Sens. 7 (8) (2022) 2429–2437.
[304] Z. Xu, J. Chen, Y. Li, T. Hu, L. Fan, J. Xi, J. Han, R. Guo, Yolk-shell Fe_3O_4@Carbon@Platinum-Chlorin e6 nanozyme for MRI-assisted synergistic catalytic-photodynamic-photothermal tumor therapy, J. Colloid Interface Sci. 628 (2022) 1033–1043.
[305] J. Wang, S. Wu, L. Ma, B. Zhao, H. Xu, X. Ding, D. Zhang, Corrosion resistant coating with passive protection and self-healing property based on Fe_3O_4-MBT nanoparticles, Corrosion Commun. 7 (2022) 1–11.
[306] A. Nicolás-Boluda, J. Vaquero, G. Laurent, G. Renault, R. Bazzi, E. Donnadieu, S. Roux, L. Fouassier, F. Gazeau, Photothermal depletion of cancer-associated fibroblasts normalizes tumor stiffness in desmoplastic cholangiocarcinoma, ACS Nano 14 (5) (2020) 5738–5753.

[307] H. Lu, B. Wu, X. Le, W. Lu, Q. Yang, Q. Liu, J. Zhang, T. Chen, Programming shape memory hydrogel to a pre-encoded static deformation toward hierarchical morphological information encryption, Adv. Funct. Mater. 32 (45) (2022) 2206912.
[308] X. Zeng, Y. Ruan, Q. Chen, S. Yan, W. Huang, Biocatalytic cascade in tumor microenvironment with a Fe_2O_3/Au hybrid nanozyme for synergistic treatment of triple negative breast cancer, Chem. Eng. J. 445 (2023) 138422.
[309] T. Wang, X. Hu, Y. Yang, Q. Wu, C. He, X. He, Z. Wang, X. Mao, New insight into assembled Fe_3O_4@PEI@Ag structure as acceptable agent with enzymatic and photothermal properties, Int. J. Mol. Sci. 23 (18) (2022) 10743.
[310] H. Du, F. Yang, C. Yao, Z. Zhong, P. Jiang, S.G. Stanciu, H. Peng, J. Hu, B. Jiang, Z. Li, W. Lv, F. Zheng, H.A. Stenmark, A. Wu, Multifunctional modulation of high-performance $Zn_xfe_{3-x}O_4$ nanoparticles by precisely tuning the zinc doping content, Small 18 (42) (2022) 2201669.
[311] H. Wang, X. Li, Q. Ge, Y. Chong, Y. Zhang, A multifunctional Fe_2O_3@MoS_2@SDS Z-scheme nanocomposite: NIR enhanced bacterial inactivation, degradation antibiotics and inhibiting ARGs dissemination, Colloids Surf. B 219 (2022) 112833.
[312] M. Kulpa-Greszta, A. Tomaszewska, A. Michalicha, D. Sikora, A. Dziedzic, R. Wojnarowska-Nowak, A. Belcarz, R. Pżik, Alternating magnetic field and NIR energy conversion on magneto-plasmonic Fe_3O_4@APTES–Ag heterostructures with SERS detection capability and antimicrobial activity, RSC Adv. 12 (32) (2022) 27396–27410.
[313] L. Yu, S. Zhu, K. Qin, X. Fan, L. An, Macrophages loaded with fe nanoparticles for enhanced photothermal ablation of tumors, J. Funct. Biomater. 13 (3) (2022) 94.
[314] K. Saravanakumar, A. Sathiyaseelan, P. Manivasagan, M.S. Jeong, M. Choi, E.-S. Jang, V.V. Priya, M.-H. Wang, Photothermally responsive chitosan-coated iron oxide nanoparticles for enhanced eradication of bacterial biofilms, Biomater. Adv. 141 (2022) 213129.
[315] Y. Chen, M. Su, L. Jia, Z. Zhang, Synergistic chemo-photothermal and ferroptosis therapy of polydopamine nanoparticles for esophageal cancer, Nanomedicine 17 (16) (2022) 1115–1130.
[316] M. Kulpa-Greszta, M. Wnuk, A. Tomaszewska, J. Adamczyk-Grochala, A. Dziedzic, I. Rzeszutek, B. Zarychta, D. Błoniarz, A. Lewińska, R. Pązik, Synergic temperature effect of star-like monodisperse iron oxide nanoparticles and their related responses in normal and cancer cells, J. Phys. Chem. B 126 (42) (2022) 8515–8531.
[317] A. Abareshi, N. Salehi, The effect of Fe_3O_4 nanoparticles on structural, optical, and thermal properties MoS_2 nanoflakes, J. Mater. Sci.: Mater. Electron. 33 (33) (2022) 25153–25162.
[318] L. Yang, H. Zhu, R. Zhao, Z. Zhang, B. Liu, H. Gong, Y. Zhu, H. Ding, S. Gai, L. Feng, Tumor microenvironment activated glutathione self-depletion theranostic nanocapsules for imaging-directed synergistic cancer therapy, Chem. Eng. J. 450 (2022) 138137.
[319] Y. Wang, D. Wang, Y. Zhang, H. Xu, L. Shen, J. Cheng, X. Xu, H. Tan, X. Chen, J. Li, Tumor microenvironment-adaptive nanoplatform synergistically enhances cascaded chemodynamic therapy, Bioactive Mater. 22 (2023) 239–253.
[320] L. Ruan, K. Zhao, X. Tian, L. Wu, J. Cao, X. Qi, S. Shen, Macrophages exosomes-coated Fe_3O_4 nanoparticles for oxygen independent generation of free radicals and hypoxic cancer therapy, Mater. Today Commun. 33 (2022) 104672.
[321] Q. Chen, S. Liu, Alkyl gallate derived magnetic clusters and photothermal controlled release lipid carrier, Colloids Surf. A 656 (2023) 130518.
[322] H. Du, D. Zhang, R. Xu, J. Xie, S. Guan, S. Chen, F. Peng, S. Qian, X. Liu, Ferric oxide nanosheet-engineered Mg alloy for synergetic osteosarcoma photothermal/chemodynamic therapy, J. Mater. Sci. Technol. 138 (2023) 203–213.
[323] X. Huang, Z. Zhang, L. Chen, Y. Lin, R. Zeng, J. Xu, S. Chen, J. Zhang, H. Cai, H. Zhou, P. Sun, Multifunctional au nano-bridged nanogap probes as ICP-MS/SERS dual-signal tags and signal amplifiers for bacteria discriminating, quantitative detecting and photothermal bactericidal activity, Biosens. Bioelectron. 212 (2022) 114414.
[324] W. Zhu, J. Mei, X. Zhang, J. Zhou, D. Xu, Z. Su, S. Fang, J. Wang, X. Zhang, C. Zhu, Photothermal nanozyme-based microneedle patch against refractory bacterial biofilm infection via iron-actuated Janus ion therapy, Adv. Mater. 34 (51) (2022) 2207961.
[325] X. Yuan, X. Zhao, R. Xia, Z. Xie, Y. Lin, Z. Su, Photothermally responsive magnetic nanoparticles for nitric oxide release to combat staphylococcus aureus biofilms, ACS Appl. Nano. Mater. 5 (12) (2022) 18799–18810.
[326] M. Wang, T. Hu, H.K. Bisoyi, Z. Yu, L. Liu, Y. Song, J. Yang, H. Yang, Q. Li, Rheological tunable magnetic fluids with long-term stability, Small 19 (8) (2023) 2204609.
[327] Y. Gao, X. Chen, B. Wang, S. Wang, J. Wang, L. Ren, W. k. Jin, H. Han, L. Wang, Engineering platelets with PDL1 antibodies and iron oxide nanoparticles for postsurgical cancer immunotherapy, ACS Appl. Bio Mater. 6 (1) (2023) 257–266.
[328] S. Yang, J. Du, M. Wei, Y. Huang, Y. Zhang, Y. Wang, J. Li, W. Wei, Y. Qiao, H. Dong, X. Zhang, Colorimetric-photothermal-magnetic three-in-one lateral flow immunoassay for two formats of biogenic amines sensitive and reliable quantification, Anal. Chim. Acta 1239 (2023) 340660.
[329] X. Luo, X. Dong, H. Zhao, T.S. Hu, X. Lan, L. Ding, J. Li, H. Ni, J.A. Contreras, H. Zeng, Q. Xu, Near-infrared responsive gecko-inspired flexible arm gripper, Mater. Today Phys. 29 (2022) 100919.
[330] Q. Fang, J. Wang, S. Wu, K.C.-F. Leung, Y. Xu, S. Xuan, NIR-induced improvement of catalytic activity and antibacterial performance over AuAg nanorods in Rambutan-like Fe_3O_4@AgAu@PDA magnetic nanospheres, J. Hazard. Mater. 445 (2023) 130616.
[331] T. Zeng, S. Xia, S. Li, X. Hong, Y. Wang, L. Wang, X. Huang, Kinetic and mechanistic investigations of the oxidation of organics by near-infrared light driven thermocatalytic activation of peroxydisulfate with Fe_3O_4, Chem. Eng. J. 455 (1) (2023) 140629.
[332] M. Cândido, P. Vieira, A. Campos, C. Soare, L. Raniero, Gold-coated superparamagnetic iron oxide nanoparticles functionalized to EGF and Ce6 complexes for breast cancer diagnoses and therapy, Pharmaceutics 15 (1) (2023) 100.
[333] Y. Lu, F. Wu, Y. Xu, C. He, S. Luo, X. Sun, Triple functional mild photothermal improves gene editing of PD-L1 for enhanced antitumor immunity, J. Controll. Rel. 354 (2023) 57–68.
[334] K. Xu, Q. Fang, J. Wang, A. Hui, S. Xuan, Magnetic-field-induced improvement of photothermal sterilization performance by Fe_3O_4@SiO_2@Au/PDA nanochains, Materials 16 (1) (2023) 387.
[335] Y. Qian, L. Zhang, N. Li, F. Dong, Z. Yang, H. Dong, Y. Wang, M. Wang, A magnetic cloud bomb for effective biofilm eradication, Adv. Funct. Mater. 33 (15) (2023) 2214330.
[336] H. Ma, G. Yu, J. Cheng, L. Song, Z. Zhou, Y. Zhao, Q. Zhao, L. Liu, X. Wei, M. Yang, Design of an injectable magnetic hydrogel based on the tumor microenvironment for multimodal synergistic cancer therapy, Biomacromolecules 24 (2) (2023) 868–885.
[337] S. Leungpuangkaew, L. Amornkitbamrung, N. Phetnoi, C. Sapcharoenkun, C. Jubsilp, S. Ekgasit, S. Rimdusit, Magnetic- and light-responsive shape memory polymer nanocomposites from bio-based benzoxazine resin and iron oxide nanoparticles, Adv. Ind. Eng. Polym. Res. 6 (3) (2023) 215–225.
[338] C. Lu, Y. Shen, X. Wang, S. Xu, J. Wang, Q. Yong, F. Chu, Biomimetic ultra-strong, ultra-tough, degradable cellulose-based composites for multi-stimuli responsive shape memory, Int. J. Biol. Macromol. 226 (2023) 1468–1476.
[339] Z.Z. Nori, M. Bahadori, M. Moghadam, S. Tangestaninejad, V. Mirkhani, I. Mohammadpoor-Baltork, S.S. Jafari, R. Emamzadeh, H. Alem, Synthesis and characterization of a new gold-coated magnetic nanoparticle decorated with a thiol-containing dendrimer for targeted drug delivery, hyperthermia treatment and enhancement of MRI contrast agent, J. Drug Delivery Sci. Technol. 81 (2023) 104216.
[340] M. Saadli, D.L. Braunmiller, A. Mourran, J.J. Crassous, Thermally and magnetically programmable hydrogel microactuators, Small 19 (16) (2023) 2207035.
[341] S. Hao, J. Zuo, H. Huang, W. Li, H. Guo, M. Liu, H. Zhu, H. Sun, Tumor microenvironment (TME)-modulating nanoreactor for multiply enhanced chemodynamic therapy synergized with chemotherapy, starvation, and photothermal therapy, J. Mater. Chem. B 11 (8) (2023) 1739–1748.

[342] Y. Liu, Y. Zhao, H. Li, X. Zhang, Z. Wang, W. She, F. Jiang, Y. Liu, P. Jiang, Dual-targeting and multimodal imaging-guided photothermal/chemodynamic synergistic therapy boosted by ascorbic acid-induced H_2O_2 in situ self-supply, ACS Appl. Mater. Interfaces 15 (7) (2023) 9841–9852.
[343] Q. Kang, X. y. Xing, S. q. Zhang, L. He, J. z. Li, J. b. Jiao, X. Du, S. Wang, A novel aptamer-induced CHA amplification strategy for ultrasensitive detection of staphylococcus aureus and NIR-triggered photothermal bactericidal activity based on aptamer-modified magnetic Fe_3O_4@aunrs, Sensors Actuators B 382 (2023) 133554.
[344] X. Wei, Q. Wu, L. Chen, Y. Sun, L. Chen, C. Zhang, S. Li, C. Ma, S. Jiang, Remotely controlled light/electric/magnetic multiresponsive hydrogel for fast actuations, ACS Appl. Mater. Interfaces 15 (7) (2023) 10030–10043.
[345] Z. Zhang, J. Sun, X. Chen, Y. Zhao, J. Wen, J. Liu, Q. Yu, L. Liu, Unraveling the role of defect types in Fe_3O_4 for efficient NIR-driven photocatalytic inactivation, Appl. Surf. Sci. 622 (2023) 156860.
[346] C.-C. Huang, P.-Y. Chang, C.-L. Liu, J.-P. Xu, S.-P. Wu, W.-C. Kuo, New insight on optical and magnetic Fe_3O_4 nanoclusters promising for near infrared theranostic applications, Nanoscale 7 (29) (2015) 12689–12697.
[347] N. Zhao, L. Yana, J. Xue, K. Zhang, F.-J. Xu, Degradable one-dimensional dextran-iron oxide nanohybrids for MRI-guided synergistic gene/photothermal/magnetolytic therapy, Nano Today 38 (2021) 101118.
[348] C. Lozano-Pedraza, E. Plaza-Mayoral, A. Espinosa, B. Sot, A. Serrano, G. Salas, C. Blanco-Andujar, G. Cotin, D. Felder-Flesch, S. Begin-Colin, F.J. Teran, Assessing the parameters modulating optical losses of iron oxide nanoparticles under near infrared irradiation, Nanoscale Adv. 3 (22) (2021) 6490–6502.
[349] D. Arranz, R. Weigand, P. de la Presa, Towards the standardization of photothermal measurements of iron oxide nanoparticles in two biological windows, Nanomaterials 13 (3) (2023) 450.
[350] M.-F. Tsai, C. Hsu, C.-S. Yeh, Y.-J. Hsiao, C.-H. Su, L.-F. Wang, Tuning the distance of rattle-shaped IONP@Shell-in-shell nanoparticles for magnetically-targeted photothermal therapy in the second near-infrared window, ACS Appl. Mater. Interfaces 10 (2) (2018) 1508–1519.
[351] P. Kharey, S.B. Dutta, Manikandan M., I.A. Palani, S.K. Majumder, S. Gupta, Green synthesis of near-infrared absorbing eugenate capped iron oxide nanoparticles for photothermal application, Nanotechnology 31 (9) (2020) 095705.
[352] S. Cabana, A. Curcio, A. Michel, C. Wilhelm, A. Abou-Hassan, Iron oxide mediated photothermal therapy in the second biological window: A comparative study between magnetite/maghemite nanospheres and nanoflowers, Nanomaterials 10 (8) (2020) 1548.
[353] M.A. Busquets, J.M. Fernández-Pradas, P. Serra, J. Estelrich, Superparamagnetic nanoparticles with efficient near-infrared photothermal effect at the second biological window, Molecules 25 (22) (2020) 5315.
[354] X. Wang, C. Li, J. Qian, X. Lv, H. Li, J. Zou, J. Zhang, X. Meng, H. Liu, Y. Qian, W. Lin, H. Wang, NIR-II responsive hollow magnetite nanoclusters for targeted magnetic resonance imaging-guided photothermal/chemo-therapy and chemodynamic therapy, Small 17 (31) (2021) 2100794.
[355] E. Bertuit, E. Benassai, G. Mériguet, J.-M. Greneche, B. Baptiste, S. Neveu, C. Wilhelm, A. Abou-Hassan, Structure-property-function relationships of iron oxide multicore nanoflowers in magnetic hyperthermia and photothermia, ACS Nano 16 (1) (2022) 271–284.
[356] Y. Ji, X. Bai, H. Sun, L. Wang, J. Xu, C. Gan, Y. Dai, H. Hui, L. Feng, Biocompatible ferrofluid robot with photothermal property for targeted tumor therapy, IEEE Robot. Autom. Lett. 7 (4) (2022) 11517–11522.
[357] Y. Fernández-Afonso, L. Asín, L. Beola, R.M. Fratila, L. Gutiérrez, Influence of magnetic nanoparticle degradation in the frame of magnetic hyperthermia and photothermal treatments, ACS Appl. Nano Mater. 5 (11) (2022) 16220–16230.
[358] Y. Liao, D. Liu, B. Wang, Z. Wu, M. Ni, M. Wang, C.-H. Wang, Y. Lu, Photothermally modulated magnetic nanochains as swarm nanorobotics for microreaction control, ACS Appl. Nano Mater. 6 (1) (2023) 21–33.
[359] W. Qin, J. Huang, C. Yang, Q. Yue, S. Chen, M. Wang, S. Gao, X. Zhou, X. Yang, Y. Zhang, Protease-activatable nanozyme with photoacoustic and tumor-enhanced magnetic resonance imaging for photothermal ferroptosis cancer therapy, Adv. Funct. Mater. 33 (4) (2023) 2209748.
[360] B. Freis, M.D.L.A. Ramirez, C. Kiefer, S. Harlepp, C. Iacovita, C. Henoumont, C. Affolter-Zbaraszczuk, F. Meyer, D. Mertz, A. Boos, M. Tasso, S. Furgiuele, F. Journe, S. Saussez, S. Bégin-Colin, S. Laurent, Effect of the size and shape of dendronized iron oxide nanoparticles bearing a targeting ligand on MRI, magnetic hyperthermia, and photothermia properties-from suspension to in vitro studies, Pharmaceutics 15 (4) (2023) 1104.
[361] E. Hemmer, A. Benayas, F. Légaré, F. Vetrone, Exploiting the biological windows: Current perspectives on fluorescent bioprobes emitting above 1000 nm, Nanoscale Horiz. 1 (3) (2016) 168–184.
[362] L.A. Sordillo, Y. Pu, S. Pratavieira, Y. Budansky, R.R. Alfano, Deep optical imaging of tissue using the second and third near-infrared spectral windows, J. Biomed. Opt. 19 (5) (2014) 056004.
[363] A. Nexha, J.J. Carvajal, M.C. Pujol, F. Díaz, M. Aguiló, Short-wavelength infrared self-assessed photothermal agents based on Ho, Tm:$KLu(WO_4)_2$ nanocrystals operating in the third biological window (1.45–1.96 nm wavelength range), J. Mater. Chem. C 8 (1) (2020) 180–191.
[364] A. López-Ortega, M. Estrader, G. Salazar-Alvarez, A.G. Roca, J. Nogués, Applications of exchange coupled bi-magnetic hard/soft and soft/hard magnetic core/shell nanoparticles, Phys. Rep. 553 (2015) 1–32.
[365] Y. Song, S. Chen, Janus nanoparticles: Preparation, characterization, and applications, Chem.- Asian J. 9 (2) (2014) 418–430.
[366] S. Talebzadeh, C. Queffélec, D.A. Knight, Surface modification of plasmonic noble metal–metal oxide core–shell nanoparticles, Nanoscale Adv. 1 (12) (2019) 4578–4591.
[367] N. Safaie, R.C. Ferrier Jr., Janus nanoparticle synthesis: Overview, recent developments, and applications, J. Appl. Phys. 127 (17) (2020) 170902.
[368] E. Fantechi, A.G. Roca, B. Sepúlveda, P. Torruella, S. Estradé, F. Peiró, E. Coy, S. Jurga, N.G. Bastús, J. Nogués, V. Puntes, Seeded growth synthesis of Au–Fe_3O_4 heterostructured nanocrystals: Rational design and mechanistic insights, Chem. Mater. 29 (9) (2017) 4022–4035.
[369] P.D. Cozzoli, T. Pellegrino, L. Manna, Synthesis, properties and perspectives of hybrid nanocrystal structures, Chem. Soc. Rev. 35 (11) (2006) 1195–1208.
[370] C. Le, J. Zhai, W.-H. Chiu, P.A. Tran, N. Tran, Janus particles: Recent advances in the biomedical applications, Int. J. Nanomed. 14 (2019) 6749–6777.
[371] R. Singh, R. Bhateria, Core–shell nanostructures: A simplest two-component system with enhanced properties and multiple applications, Environ. Geochem. Health 43 (2021) 2459–2482.
[372] X. Zhang, Q. Fu, H. Duan, J. Song, H. Yang, Janus nanoparticles: From fabrication to (Bio) applications, ACS Nano 15 (4) (2021) 6147–6191.
[373] L. Yan, Y.L. Zhao, Z.J. Gu, Nanotoxicity of near infrared nanomaterials (Chapt. 11) in near infrared nanomaterials, in: F. Zhang (Ed.), Preparation, Bioimaging, and Therapy Applications, The Royal Society of Chemistry, Croydon, UK, 2016.
[374] A.C. Anselmo, S. Mitragotri, Nanoparticles in the clinic, Bioeng. Transl. Med. 1 (1) (2016) 10–29.
[375] A.C. Anselmo, S. Mitragotri, Nanoparticles in the clinic: An update, Bioeng. Transl. Med. 4 (3) (2019) e10143.
[376] D. Bobo, K.J. Robinson, J. Islam, K.J. Thurecht, S.R. Corrie, Nanoparticle-based medicines: A review of FDA-approved materials and clinical trials to date, Pharm. Res. 33 (10) (2016) 2373–2387.
[377] S. Li, Y. Liu, X. Liu, B. Lan, W. Li, F. Guo, Magnetite Fe_3O_4 nanoparticles enhance mild microwave ablation of tumor by activating the IRE1-ASK1-JNK pathway and inducing endoplasmic reticulum stress, Int. J. Nanomed. 16 (2021) 6129–6140.
[378] K. Kim, T. Seo. K. Sim. Y. Kwon, Magnetic nanoparticle-assisted microwave hyperthermia using an active integrated heat applicator, IEEE Trans. Microw. Theory Tech. 64 (7) (2016) 2184–2197.

[379] V.H.B. Ho, M.J. Smith, N.K.H. Slater, Effect of magnetite nanoparticle agglomerates on the destruction of tumor spheroids using high intensity focused ultrasound, Ultrasound Med. Biol. 37 (1) (2011) 169–175.
[380] S.B. Devarakonda, M.R. Myers, D. Giridhar, S. Ahmad R. Dibaji, R.K. Banerjee, Enhanced thermal effect using magnetic nano-particles during high-intensity focused ultrasound, PLoS One 12 (4) (2017) e0175093.
[381] A. Józefczak, K. Kaczmarek, T. Hornowski, M. Kubovčíková, Z. Rozynek, M. Timko, A. Skumiel, Magnetic nanoparticles for enhancing the effectiveness of ultrasonic hyperthermia, Appl. Phys. Lett. 108 (26) (2016) 263701.
[382] D.H. Manz, N.L. Blanchette, B.T. Paul. F. M. Torti, S.V. Torti, Iron and cancer: recent insights, Ann. New York Acad. Sci. 1368 (2016) 149–161.
[383] X. Jiang, B.R. Stockwell, M. Conrad, Ferroptosis: mechanisms, biology and role in disease, Nat. Rev. Mol. Cell Biol. 22 (2021) 266–282.
[384] Z. Li, L. Rong, Cascade reaction-mediated efficient ferroptosis synergizes with immunomodulation for high-performance cancer therapy, Biomater. Sci. 8 (22) (2020) 6272–6285.
[385] X. Tian, L. Ruan, S. Zhou, L. Wu, J. Cao, X. Qi, X. Zhang, S. Shen, Appropriate size of Fe_3O_4 nanoparticles for cancer therapy by ferroptosis, ACS Appl. Bio Mater. 5 (4) (2022) 1692–1699.
[386] J.V. Nuzhina, A.A. Shtil, A.Y. Prilepskii, V.V. Vinogradov, Preclinical evaluation and clinical translation of magnetite-based nanomedicines, J. Drug Delivery Sci. Technol. 54 (2019) 101282.
[387] A.N. Mahmoodabadi, A. Kompany, M. Mashreghi, Characterization, antibacterial and cytotoxicity studies of graphene-Fe_3O_4 nanocomposites and Fe_3O_4 nanoparticles synthesized by a facile solvothermal method, Mater. Chem. Phys. 213 (2018) 285–294.
[388] M. Alavi, N. Karimi, Ultrasound assisted-phytofabricated Fe_3O_4 NPs with antioxidant properties and antibacterial effects on growth, biofilm formation, and spreading ability of multidrug resistant bacteria, Artif. Cells Nanomed. Biotechnol. 47 (1) (2019) 2405–2423.
[389] A.B. Pai, A.O. Garba, Ferumoxytol: A silver lining in the treatment of anemia of chronic kidney disease or another dark cloud? J. Blood Med. 3 (2012) 77–85.
[390] Y. Abo-zeid, N.S.M. Ismail, G.R. McLean, N.M. Hamdy, A molecular docking study repurposes FDA approved iron oxide nanoparticles to treat and control COVID-19 infection, Eur. J. Pharm. Sci. 153 (2022) 105465.
[391] Z. Mao, X. Li, P. Wang, H. Yan, Iron oxide nanoparticles for biomedical applications: An updated patent review (2015–2021), Expert Opin. Ther. Pat. 32 (9) (2022) 939–952.
[392] M.M. El-Hammadi, J.L. Arias, Iron oxide-based multifunctional nanoparticulate systems for biomedical applications: A patent review (2008 – present), Expert Opin. Ther. Pat. 25 (6) (2015) 691–709.
[393] J. Park, K. An, Y. Hwang, J.-G. Park, H.-J. Noh, J.-Y. Kim, J.-H. Park, N.-M. Hwang, T. Hyeon, Ultra-large-scale syntheses of monodisperse nanocrystals, Nature Mater. 3 (12) (2004) 891–895.
[394] J. Muro-Cruces, A.G. Roca, A. López-Ortega, E. Fantechi, D. del Pozo-Bueno, S. Estradé, F. Peiró, B. Sepúlveda, F. Pineider, C. Sangregorio, J. Nogues, Precise size control of the growth of Fe_3O_4 nanocubes over a wide size range using a rationally designed one-pot synthesis, ACS Nano 13 (7) (2019) 7716–7728.
[395] A.G. Roca, L. Gutiérrez, H. Gavilán, M.E. Fortes Brollo, S. Veintemillas-Verdaguer, M.P. Morales, Design strategies for shape-controlled magnetic iron oxide nanoparticles, Adv. Drug Deliv. Rev. 138 (2019) 68–104.
[396] G. Singh, V.S. Myasnichenko, W.R. Glomm, New insights into size-controlled reproducible synthesis of anisotropic Fe_3O_4 nanoparticles: The importance of the reaction environment, Mater. Adv. 1 (5) (2020) 1077–1082.
[397] J. Mohapatra, M. Xing, J. Beatty, J. Elkins, T. Seda, S.R. Mishra, J.P. Liu, Enhancing the magnetic and inductive heating properties of Fe_3O_4 nanoparticles via morphology control, Nanotechnology 31 (27) (2020) 275706.
[398] P. Guardia, N. Pérez, A. Labarta, X. Batlle, Controlled synthesis of iron oxide nanoparticles over a wide size range, Langmuir 26 (8) (2010) 5843–5847.
[399] S. Tanaka, Y.V. Kaneti, N.L.W. Septiani, S.X. Dou, Y. Bando, M.S.A. Hossain, J. Kim, Y. Yamauchi, A review on iron oxide-based nanoarchitectures for biomedical, energy storage, and environmental applications, Small Methods 3 (5) (2019) 1800512.
[400] E. Alphandéry, Iron oxide nanoparticles for therapeutic applications, Drug Discov. Today 25 (1) (2020) 141–149.
[401] A.K. Gupta, M. Gupta, Synthesis and surface engineering of iron oxide nanoparticles for biomedical applications, Biomaterials 26 (18) (2005) 3995–4021.
[402] M. Suciu, C.M. Ionescu, A. Ciorita, S.C. Tripon, D. Nica, H. Al-Salami, L. Barbu-Tudoran, Applications of superparamagnetic iron oxide nanoparticles in drug and therapeutic delivery, and biotechnological advancements, Beilstein J. Nanotechnol. 11 (2020) 1092–1109.
[403] Y. Wu, Z. Lu, Y. Li, J. Yang, X. Zhang, Surface modification of iron oxide-based magnetic nanoparticles for cerebral theranostics: Application and prospection, Nanomaterials 10 (8) (2020) 1441.
[404] C. Liang, X. Zhang, Z. Cheng, M. Yang, W. Huang, X. Dong, Magnetic iron oxide nanomaterials: A key player in cancer nanomedicine, View 1 (3) (2020) 20200046.
[405] F. Soetaert, P. Korangath, D. Serantes, S. Fiering, R. Ivkov, Cancer therapy with iron oxide nanoparticles: Agents of thermal and immune therapies, Adv. Drug Delivery Rev. 163–164 (2020) 65–83.
[406] L. Jingchao, W. Shige, S. Xiangyang, S. Mingwu, Aqueous-phase synthesis of iron oxide nanoparticles and composites for cancer diagnosis and therapy, Adv. Colloid Interface Sci. 249 (2017) 374–385.
[407] S. Zhao, X. Yu, Y. Qian, W. Chen, J. Shen, Multifunctional magnetic iron oxide nanoparticles: An advanced platform for cancer theranostics, Theranostics 10 (14) (2020) 6278–6309.
[408] A.A. Hernández-Hernández, G. Aguirre-Álvarez, R. Cariño-Cortés, L.H. Mendoza-Huizar, R. Jiménez-Alvarado, Iron oxide nanoparticles: Synthesis, functionalization, and applications in diagnosis and treatment of cancer, Chem. Pap. 74 (11) (2020) 3809–3824.
[409] S. Pillarisetti, S. Uthaman, K.M. Huh, Y.S. Koh, S. Lee, I.-K. Park, Multimodal composite iron oxide nanoparticles for biomedical applications, Tissue Eng. Regen. Med. 16 (5) (2019) 451–465.
[410] P. Martinkova, M. Brtnicky, J. Kynicky, M. Pohanka, Iron oxide nanoparticles: Innovative tool in cancer diagnosis and therapy, Adv. Healthc. Mater. 7 (5) (2018) 1700932.
[411] S. Palanisamy, Y.-M. Wang, Superparamagnetic iron oxide nanoparticulate system: Synthesis, targeting, drug delivery and therapy in cancer, Dalton Trans. 48 (26) (2019) 9490–9515.
[412] K. Li, H. Nejadnik, H.E. Daldrup-Link, Next-generation superparamagnetic iron oxide nanoparticles for cancer theranostics, Drug Discov. Today 22 (9) (2017) 1421–1429.
[413] M. Saeed, W. Ren, A. Wu, Therapeutic applications of iron oxide based nanoparticles in cancer: Basic concepts and recent advances, Biomater. Sci. 6 (4) (2018) 708–725.
[414] X. Ren, H. Chen, V. Yang, D. Sun, Iron oxide nanoparticle-based theranostics for cancer imaging and therapy, Front. Chem. Sci. Eng. 8 (3) (2014) 253–264.
[415] S. Natarajan, K. Harini, G.P. Gajula, B. Sarmento, M.T. Neves-Petersen, V. Thiagarajan, Multifunctional magnetic iron oxide nanoparticles: Diverse synthetic approaches, surface modifications, cytotoxicity towards biomedical and industrial applications, BMC Mater. 1 (2019) 2.
[416] V. Mulens-Arias, J.M. Rojas, D.F. Barber, The intrinsic biological identities of iron oxide nanoparticles and their coatings: Unexplored territory for combinatorial therapies, Nanomaterials 10 (5) (2020) 837.

[417] M. Nabavinia, J. Beltran-Huarac, Recent progress in iron oxide nanoparticles as therapeutic magnetic agents for cancer treatment and tissue engineering, ACS Appl. Bio Mater. (2020) 3 (12) (2020) 8172–8187.
[418] D. Shi, M.E. Sadat, A.W. Dunn, D.B. Mast, Photo-fluorescent and magnetic properties of iron oxide nanoparticles for biomedical applications, Nanoscale 7 (18) (2015) 8209–8232.
[419] L.S. Ganapathe, M.A. Mohamed, R.M. Yunus, D.D. Berhanuddin, Magnetite (Fe_3O_4) nanoparticles in biomedical application: FromSynthesis to surface functionalisation, Magnetochemistry 6 (4) (2020) 68.
[420] Y. Li, H. Zhang, Fe_3O_4-based nanotheranostics for magnetic resonance imaging-synergized multifunctional cancer management, Nanomedicine (London) 14 (11) (2019) 1493–1512.
[421] N. Lamichhane, S. Sharma, Parul, A.K. Verma, I. Roy, T. Sen, Iron oxide-based magneto-optical nanocomposites for in Vivo biomedical applications, Biomedicines 9 (3) (2021) 288.
[422] Y. Zhang, X. Li, Y. Zhang, J. Wei, W. Wang, C. Dong, Y. Xue, M. Liu, R. Pei, Engineered Fe_3O_4-based nanomaterials for diagnosis and therapy of cancer, New J. Chem. 45 (18) (2021) 7918–7941.
[423] S. Laurent, D. Forge, M. Port, A. Roch, C. Robic, L.V. Elst, R.N. Muller, Magnetic iron oxide nanoparticles: Synthesis, stabilization, vectorization, physicochemical characterizations, and biological applications, Chem. Rev. 108 (6) (2008) 2064–2110.
[424] D. Ling, T. Hyeon, Chemical design of biocompatible iron oxide nanoparticles for medical applications, Small 9 (9–10) (2013) 1450–1466.
[425] J. Volatron, F. Carn, J. Kolosnjaj-Tabi, Y. Javed, Q.L. Vuong, Y. Gossuin, C. Ménager, N. Luciani, G. Charron, M. Hémadi, D. Alloyeau, F. Gazeau, Ferritin protein regulates the degradation of iron oxide nanoparticles, Small 13 (2) (2017) 1602030.
[426] V. Trujillo-Alonso, E.C. Pratt, H. Zong, A. Lara-Martinez, C. Kaittanis, M.O. Rabie, V. Longo, M.W. Becker, G.J. Roboz, J. Grimm, M.L. Guzman, FDA-approved ferumoxytol displays anti-leukaemia efficacy against cells with low ferroportin levels, Nat. Nanotechnol. 14 (6) (2019) 616–622.
[427] J. Wallyn, N. Anton, S. Akram, T.F. Vandamme, Biomedical imaging: Principles, technologies, clinical aspects, contrast agents, limitations and future trends in nanomedicines, Pharm. Res. 36 (6) (2019) 78.
[428] Y. Chu, X.-Q. Xu, Y. Wang, Ultradeep photothermal therapy strategies, J. Phys. Chem. Lett. 2022 13 (41) (2022) 9564–9572.
[429] Y. Cao, J.-H. Dou, N.-j. Zhao, S. Zhang, Y.-Q. Zheng, J.-P. Zhang, J.-Y. Wang, J. Pei, Y. Wang, Highly efficient NIR-II photothermal conversion based on an organic conjugated polymer, Chem. Mater. 29 (2) (2017) 718–725.
[430] S.L. Jacques, Optical properties of biological tissues: A review, Phys. Med. Biol. 58 (11) (2013) R37–R61.
[431] A.N. Bashkatov, K.V. Berezin, K.N. Dvoretskiy, M.L. Chernavina, E.A. Genina, V.D. Genin, V.I. Kochubey, E.N. Lazareva, A.B. Pravdin, M.E. Shvachkina, P.A. Timoshina, D.K. Tuchina, D.D. Yakovlev, D.A. Yakovlev, I.Y. Yanina, O.S. Zhernovaya, V.V. Tuchin, Measurement of tissue optical properties in the context of tissue optical clearing, J. Biomed. Opt. 23 (9) (2018) 091416.
[432] A.N. Bashkatov, E.A. Genina, V.I. Kochubey, V.V. Tuchin, Optical properties of human skin, subcutaneous and mucous tissues in the wavelength range from 400 to 2000 nm, J. Phys. D Appl. Phys. 38 (15) (2005) 2543–2555.
[433] R.R. Anderson, J.A. Parrish, The optics of human skin, J. Investig. Dermatol. 77 (1) (1981) 13–19.
[434] A. Alex, B. Považay, B. Hofer, S. Popov, C. Glittenberg, S. Binder, W. Drexler, Multispectral in Vivo three-dimensional optical coherence tomography of human skin, J. Biomed. Opt. 15 (2) (2010) 026025.
[435] E. Salomatina, B. Jiang, J. Novak, A.N. Yaroslavsky, Optical properties of normal and cancerous human skin in the visible and near-infrared spectral range, J. Biomed. Opt. 11 (6) (2006) 064026.
[436] M. Clement, G. Daniel, M. Trelles, Optimising the design of a broad-band light source for the treatment of skin, J. Cosmet. Laser Ther. 7 (3–4) (2015) 177–189.
[437] American National Standard for Safe Use of Lasers (ANSI Z136.1-2007), Laser Institute of America, Orlando, USA, 2007.
[438] M.H. Smith, R.L. Fork, S.T. Cole, Safe delivery of optical power from space, Opt. Express 8 (10) (2001) 537–546.
[439] R.M. Cornell, U. Schwertmann, The Iron Oxides: Structure, Properties, Reactions, Occurrences and Uses, second ed., Wiley-VCH Verlag GmbH & Co, Weinheim, Germany, 2003.
[440] M.R. Querry, Optical Constants, Contractor Report CRDC-CR-85034, 1985.
[441] J. Tang, M. Myers, K.A. Bosnick, L.E. Brus, Magnetite Fe_3O_4 nanocrystals: Spectroscopic observation of aqueous oxidation kinetics, J. Phys. Chem. B 107 (30) (2003) 7501–7506.
[442] Y.P. He, Y.M. Miao, C.R. Li, S.Q. Wang, L. Cao, S.S. Xie, G.Z. Yang, B.S. Zou, C. Burda, Size and structure effect on optical transitions of iron oxide nanocrystals, Phys. Rev. B 71 (12) (2005) 125411.
[443] A.M. Mansour, R.S. Ibrahim, A.A.y Azab, Structure, morphology, optical and magnetic studies of Fe_3O_4-doped CdS nanocomposite, J. Mater. Sci., Mater. Electron. 33 (13) (2022) 10251–10258.
[444] E.A. Dolgopolova, D. Li, S.T. Hartman, J. Watt, C. Ríos, J. Hu, R. Kukkadapu, J. Casson, R. Bose, A.V. Malko, A.V. Blake, S. Ivanov, O. Roslyak, A. Piryatinski, H. Htoon, H.-T. Chen, G. Pilania, J.A. Hollingsworth, Strong Purcell enhancement at telecom wavelengths afforded by spinel Fe_3O_4 nanocrystals with size-tunable plasmonic properties, Nanoscale Horiz. 7 (3) (2022) 267–275.
[445] M. Barrow, A. Taylor, A.M. Fuentes-Caparrós, J. Sharkey, L.M. Daniels, P. Mandal, B.K. Park, P. Murray, M.J. Rosseinsky, D.J. Adams, SPIONs for cell labelling and tracking using MRI: magnetite or maghemite? Biomater. Sci. 6 (1) (2018) 101–106.
[446] S. Bhagwat, H. Singh, A. Athawale, B. Hannoyer, S. Jouen, B. Lefez, D. Kundaliya, R. Pasricha, S. Kulkarni, S. Ogale, Low temperature synthesis of magnetite and maghemite nanoparticles, J. Nanosci. Nanotechnol. 7 (12) (2007) 4294–4302.
[447] H. Jung, A.M. Schimpf, Photochemical reduction of nanocrystalline maghemite to magnetite, Nanoscale 13 (41) (2021) 17465–17472.
[448] A. Schlegel, S.F. Alvarado, P. Wachter, Optical properties of magnetite (Fe_3O_4), J. Phys. C Solid State Phys. 12 (6) (1979) 1157–1164.
[449] P.B. Johnson, R.W. Christy, Optical constants of the noble metals, Phys. Rev. B 6 (12) (1972) 4370–4379.
[450] H. Rodríguez-Rodríguez, G. Salas, J.R. Arias-Gonzalez, Heat generation in single magnetic nanoparticles under near-infrared irradiation, J. Phys. Chem. Lett. 11 (6) (2020) 2182–2187.
[451] D.K. Roper, W. Ahn, M. Hoepfner, Microscale heat transfer transduced by surface plasmon resonant gold nanoparticles, J. Phys. Chem. C 111 (9) (2007) 3636–3641.
[452] H. Chen, L. Shao, T. Ming, Z. Sun, C. Zhao, B. Yang, J. Wang, Understanding the photothermal conversion efficiency of gold nanocrystals, Small 6 (20) (2010) 2272–2280.
[453] K. Jiang, D.A. Smith, A size-dependent photothermal conversion efficiencies of plasmonically heated gold nanoparticles, J. Phys. Chem. C 117 (51) (2013) 27073–27080.
[454] G. Guan, B. Li, W. Zhang, Z. Cui, S.A. He, R. Zou, X. Lu, J. Hu, High-efficiency and safe sulfur-doped iron oxides for magnetic resonance imaging-guided photothermal/magnetic hyperthermia therapy, Dalton Trans. 49 (17) (2020) 5493–5502.
[455] H. Sun, B. Chen, X. Jiao, Z. Jiang, Z. Qin, D. Chen, Solvothermal synthesis of tunable electroactive magnetite nanorods by controlling the side reaction, J. Phys. Chem. C 116 (9) (2012) 5476–5481.
[456] J. Yang, L. Fan, Y. Xu, J. Xia, Iron oxide nanoparticles with different polymer coatings for photothermal therapy, J. Nanopart. Res. 19 (10) (2017) 333.
[457] A. Lak, J. Dieckhoff, F. Ludwig, J.M. Scholtyssek, O. Goldmann, H. Lünsdorf, D. Eberbeck, A. Kornowski, M. Kraken, F.J. Litterst, K. Fiege, P. Mischnick, M. Schilling, Highly stable monodisperse PEGylated iron oxide nanoparticle aqueous suspensions: A nontoxic tracer for homogeneous magnetic bioassays, Nanoscale 5 (23) (2013) 11447–11455.

[458] H. Khurshid, J. Alonso, Z. Nemati, M.H. Phan, P. Mukherjee, M.L. Fdez-Gubieda, J.M. Barandiarán, H. Srikanth, Anisotropy effects in magnetic hyperthermia: A comparison between spherical and cubic exchange-coupled FeO/Fe_3O_4 nanoparticles, J. Appl. Phys. 109 (8) (2011) 083921.
[459] I. Castellanos-Rubio, I. Rodrigo, R. Munshi, O. Arriortua, J.S. Garitaonandia, A. Martinez-Amesti, F. Plazaola, I. Orue, A. Pralle, M. Insausti, Outstanding heat loss via nano-octahedra above 20 nm in size: From wustite-rich nanoparticles to magnetite single-crystals, Nanoscale 11 (35) (2019) 16635–16649.
[460] Z. Wang, Y. Ju, Z. Ali, H. Yin, F. Sheng, J. Lin, B. Wang, Y. Hou, Near-infrared light and tumor microenvironment dual responsive size-switchable nanocapsules for multimodal tumor theranostics, Nature Commun. 10 (2019) 4418.
[461] L. Zhang, S. Tong, J. Zhou, G. Bao, Accurate quantification of disease markers in human serum using iron oxide nanoparticle-linked immunosorbent assay, Theranostics 6 (9) (2016) 1353–1361.
[462] R. Chen, M.G. Christiansen, A. Sourakov, A. Mohr, Y. Matsumoto, S. Okada, A. Jasanoff, P. Anikeeva, High-performance ferrite nanoparticles through nonaqueous redox phase tuning, Nano Lett. 16 (2) (2016) 1345–1351.
[463] A.G. Malyutin, H. Cheng, O.R. Sanchez-Felix, K. Carlson, B.D. Stein, P.V. Konarev, D.I. Svergun, B. Dragnea, L.M. Bronstein, Coat protein-dependent behavior of poly(ethylene glycol) tails in iron oxide core virus-like nanoparticles, ACS Appl. Mater. Interfaces 7 (22) (2015) 12089–12098.
[464] A. Lak, D. Niculaes, G.C. Anyfantis, G. Bertoni, M.J. Barthel, S. Marras, M. Cassani, S. Nitti, A. Athanassiou, C. Giannini, T. Pellegrino, Facile transformation of FeO/Fe_3O_4 core–shell nanocubes to Fe_3O_4 via magnetic stimulation, Sci. Rep. 6 (2016) 33295.
[465] J.-W. Park, S. Kim, S.-H. Choi, H. Lee, Optical properties of transition-metal oxides of MnO and $Fe_{0.925}O$ crystals studied with spectroscopic ellipsometry and Raman spectroscopy, New Phys. Sae Mulli 63 (7) (2013) 818–825.
[466] R.U. Ichikawa, A.G. Roca, A. López-Ortega, M. Estrader, I. Peral, X. Turrillas, J. Nogués, Combining X-ray whole powder pattern modeling, rietveld and pair distribution function analyses as a novel bulk approach to study interfaces in heteronanostructures: Oxidation front in FeO/Fe_3O_4 core/shell nanoparticles as a case study, Small 14 (30) (2018) 1800804.
[467] J. Park, K. An, Y. Hwang, J.-G. Park, H.-J. Noh, J.-Y. Kim, J.-H. Park, N.-M. Hwang, T. Hyeon, Ultra-large-scale syntheses of monodisperse nanocrystals, Nature Mater. 3 (12) (2004) 891–895.
[468] M. Estrader, A. López-Ortega, I.V. Golosovsky, S. Estradé, A.G. Roca, G. Salazar-Alvarez, L. López-Conesa, D. Tobia, E. Winkler, J.D. Ardisson, W.A.A. Macedo, A. Morphis, M. Vasilakaki, K.N. Trohidou, A. Gukasov, I. Mirebeau, O.L. Makarova, R.D. Zysler, F. Peiró, M.D. Baró, L. Bergström, J. Nogués, Origin of the large dispersion of magnetic properties in nanostructured oxides: Fe_XO /Fe_3O_4 nanoparticles as a case study, Nanoscale 7 (7) (2015) 3002–3015.
[469] E. Wetterskog, C. Tai, J. Grins, L. Bergström, G. Salazar-Alvarez, Anomalous magnetic properties of nanoparticles arising from defect structures: Topotaxial oxidation of $Fe_{1-x}O|Fe_{3-\delta}O4$ core|shell nanocubes to single-phase particles, ACS Nano 7 (8) (2013) 7132–7144.
[470] D. del Pozo-Bueno, M. Varela, M. Estrader, A. López-Ortega, A.G. Roca, J. Nogués, F. Peiró, S. Estradé, Direct evidence of a graded magnetic interface in bimagnetic core/shell nanoparticles using electron magnetic circular dichroism (EMCD), Nano Lett. 21 (16) (2021) 6923–6930.
[471] D.W. Kavich, J.H. Dickerson, S.V. Mahajan, S.A. Hasan, J.-H. Park, Exchange bias of singly inverted FeO/Fe_3O_4 core–shell nanocrystals, Phys. Rev. B 78 (17) (2008) 174414.
[472] A. Fluksman, A. Lafuente, Z. Li, J. Sort, S. Lope-Piedrafita, M.J. Esplandiu, J. Nogues, A.G. Roca, O. Benny, B. Sepulveda, Efficient tumor eradication at ultralow drug concentration via externally controlled and boosted metallic iron magnetoplasmonic nanocapsules, ACS Nano 17 (3) (2023) 1946–1958.
[473] Y.M. Yang, H.J. Wang, Recent progress in nanophotosensitizers for advanced photodynamic therapy of cancer, J. Phys. Mater. 4 (1) (2021) 014003.
[474] C. Zhang, X. Wang, J. Du, Z. Gu, Y. Zhao, Reactive oxygen species-regulating strategies based on nanomaterials for disease treatment, Adv. Sci. 8 (3) (2021) 2002797.
[475] H. Hou, X. Huang, G. Wei, F. Xu, Y. Wang, S. Zhou, Fenton reaction-assisted photodynamic therapy for cancer with multifunctional magnetic nanoparticles, ACS Appl. Mater. Interfaces 11 (33) (2019) 29579–29592.
[476] H. Wu, K. Cheng, Y. He, Z. Li, H. Su, X. Zhang, Y. Sun, W. Shi, D. Ge, Fe_3O_4-based multifunctional nanospheres for amplified magnetic targeting photothermal therapy and fenton reaction, ACS Biomater. Sci. Eng. 5 (2) (2019) 1045–1056.
[477] R.J. Wydra, C.E. Oliver, K.W. Anderson, T.D. Dziubla, J.Z. Hilt, Accelerated generation of free radicals by iron oxide nanoparticles in the presence of an alternating magnetic field, RSC Adv. 5 (24) (2015) 18888–18893.
[478] Z. Tang, P. Zhao, H. Wang, Y. Liu, W. Bu, Biomedicine meets fenton chemistry, Chem. Rev. 121 (4) (2021) 1981–2019.
[479] L. Shi, X. Wang, Y. Hu, Y. He, Investigation of photocatalytic activity through photo-thermal heating enabled by Fe_3O_4/TiO_2 composite under magnetic field, Sol. Energy 196 (2020) 505–512.
[480] B. Yan, Z. Shi, J. Lin, L. Zhang, L. Han, X. Shi, Q. Yang, Boosting heterogeneous fenton reactions for degrading organic dyes via the photothermal effect under neutral conditions, Environ. Sci. Nano 9 (2) (2022) 532–541.
[481] S.W. Yoo, G. Oh, J.C. Ahn, E. Chung, Non-oncologic applications of nanomedicine-based photo-therapy, Biomedicines 9 (2) (2021) 113.
[482] Q. Han, J.W. Lau, T.C. Do, Z. Zhang, B. Xing, Near-infrared light brightens bacterial disinfection: Recent progress and perspectives, ACS Appl. Bio Mater. 4 (5) (2021) 3937–3961.
[483] Z. Zhang, Q. Wang, L. Han, S. Du, H. Yu, H. Zhang, Rapid and sensitive detection of salmonella typhimurium based on the photothermal effect of magnetic nanomaterials, Sensors Actuators B 268 (2018) 188–194.
[484] A. Indoliya, M. Mohan, P. Kharey, S. Gupta, R. Poddar, Polymerically modified superparamagnetic iron oxide nanoparticles as a multi-model molecular probe for functionalized optical coherence tomography, Opt. Laser Technol. 141 (2021) 107108.
[485] P. Kharey, A. Indoliya, R. Gupta, R. Poddar, D. Sharma, S. Gupta, Near-infrared active superparamagnetic iron oxide nanoparticles for magnetomotive optical coherence tomography imaging and magnetic hyperthermia therapeutic applications, J. Magn. Magn. Mater. 549 (2022) 169038.
[486] L.K. Bogart, A. Taylor, Y. Cesbron, P. Murray, R. Lévy, Photothermal microscopy of the core of dextran-coated iron oxide nanoparticles during cell uptake, ACS Nano 6 (7) (2012) 5961–5971.
[487] L. Zhang, W. Li, R. Parvin, X. Wang, Q. Fan, F. Ye, Screening prostate cancer cell-derived exosomal MicroRNA expression with photothermal-driven digital PCR, Adv. Funct. Mater. 32 (48) (2022) 2207879.
[488] Z. Li, A. López-Ortega, A. Aranda-Ramos, J.L. Tajada, J. Sort, C. Nogués, P. Vavassori, J. Nogués, B. Sepúlveda, Simultaneous local heating/thermometry based on plasmonic magnetochromic nanoheaters, Small 14 (24) (2018) 1800868.
[489] A.G. Leonel, A.A.P. Mansur, H.S. Mansur, Advanced functional nanostructures based on magnetic iron oxide nanomaterials for water remediation: A review, Water Res. 190 (2021) 116693.
[490] B. Kumar, K. Smita, L. Cumbal, A. Debut, S. Galeas, V.H. Guerrero, Phytosynthesis and photocatalytic activity of magnetite (Fe_3O_4) nanoparticles using the andean blackberry leaf, Mater. Chem. Phys. 179 (2016) 310–315.
[491] Z. Xiu, Y. Cao, Z. Xing, T. Zhao, Z. Li, W. Zhou, Wide spectral response photothermal catalysis-fenton coupling systems with 3D hierarchical $Fe_3O_4/Ag/Bi_2MoO_6$ ternary hetero-superstructural magnetic microspheres for efficient high-toxic organic pollutants removal, J. Colloid Interface Sci. 533 (2019) 24–33.
[492] X. Xin, Q. Wei, J. Yang, L. Yan, R. Feng, G. Chen, B. Du, H. Li, Highly efficient removal of heavy metal ions by amine-functionalized mesoporous Fe_3O_4 nanoparticles, Chem. Eng. J. 184 (2012) 132–140.

[493] S.-H. Huang, D.-H. Chen, Rapid removal of heavy metal cations and anions from aqueous solutions by an amino-functionalized magnetic nano-adsorbent, J. Hazard. Mater. 163 (2009) 174–179.
[494] S. Lin, D. Lu, Z. Liu, Removal of arsenic contaminants with magnetic γ-Fe_2O_3 nanoparticles, Chem. Eng. J. 211–212 (2012) 46–52.
[495] P.G. Struchalin, H. Thon, D.M. Kuzmenkov, K.V. Kutsenko, P. Kosinski, B.V. Balakin, Solar steam generation enabled by iron oxide nanoparticles: Prototype experiments and theoretical model, Int. J. Heat Mass Transfer 158 (2020) 119987.
[496] Y. Zeng, J. Yao, B.A. Horri, K. Wang, Y. Wu, D. Li, H. Wang, Solar evaporation enhancement using floating light-absorbing magnetic particles, Energy Environ. Sci. 4 (10) (2011) 4074–4078.
[497] T. Jiang, Y. Wang, Z. Li, H. Asland, L. Sun, Y. Sun, W. Wang, M. Yu, Prussian blue-encapsulated Fe_3O_4 nanoparticles for reusable photothermal sterilization of water, J. Colloid Interface Sci. 540 (2019) 354–361.
[498] Y. Liu, J. Tian, L. Xu, Y. Wang, X. Fei, Y. Li, Multilayer graphite nano-sheet composite hydrogel for solar desalination systems with floatability and recyclability, New J. Chem. 44 (46) (2020) 20181–20191.
[499] B. Wu, X. Cui, H. Jiang, N. Wua, C. Peng, Z. Hub, X. Liang, Y. Yan, J. Huang, D. Li, A superhydrophobic coating harvesting mechanical robustness, passive anti-icing and active de-icing performances, J. Colloid Interface Sci. 590 (2012) 301–310.
[500] X. Yin, Y. Zhang, D. Wang, Z. Liu, Y. Liu, X. Pei, B. Yu, F. Zhou, Integration of self-lubrication and near-infrared photothermogenesis for excellent anti-icing/deicing performance, Adv. Funct. Mater. 25 (27) (2015) 4237–4245.
[501] D. Mateo, J.L. Cerrillo, S. Durini, J. Gascon, Fundamentals and applications of photo-thermal catalysis, Chem. Soc. Rev. 50 (3) (2021) 2173–2210.
[502] R.J.G. Johnson, K.M. Haas, B.J. Lear, Fe_3O_4 nanoparticles as robust photothermal agents for driving high barrier reactions under ambient conditions, Chem. Commun. 51 (2) (2015) 417–420.
[503] M. Chen, Z. Zhang, C. Zeng, J. Jiang, H. Gao, L. Ai, Synergistically boosting oxygen evolution performance of iron-tannic electrocatalyst via localized photothermal effect, Colloids Surf. A 638 (2022) 128248.
[504] N. Li, H. Jia, M. Guo, J. Zhang, W.Y. Zhang, Z.X. Guo, M.X. Li, Z.X. Jia, G.S. Qin, Broadband Fe_3O_4 nanoparticles saturable absorber for Q-switched fiber lasers, Opt. Fiber Technol., Mater. Devices Syst. 61 (2021) 102421.
[505] H. Zhang, J. Peng, J. Yao, X. Yang, D. Li, Y. Zheng, 1.3μm Passively Q-switched mode-locked laser with Fe_3O_4 nanoparticle saturable absorber, Laser Phys. 30 (12) (2020) 125801.
[506] D.H.G. Espinosa, C.L.P. Oliveia, A.M.F. Neto, Influence of an external magnetic field in the two-photon absorption coefficient of magnetite nanoparticles in colloids and thin films, J. Opt. Soc. Amer. 35 (2) (2018) 346–355.
[507] S. Perumbilavil, A. López-Ortega, G.K. Tiwari, J. Nogués, T. Endo, R. Philip, Enhanced ultrafast nonlinear optical response in ferrite core/shell nanostructures with excellent optical limiting performance, Small 14 (6) (2018) 1701001.
[508] Y. Zhao, M.E. Sadat, A. Dunn, H. Xu, C.-H. Chen, W. Nakasuga, R.C. Ewing, D. Shi, Photothermal effect on Fe_3O_4 nanoparticles irradiated by white-light for energy-efficient window applications, Sol. Energy Mater. Sol. Cells 161 (2017) 247–254.
[509] M. Lyu, J. Lin, J. Krupczak, D. Shi, Light angle dependence of photothermal properties in oxide and porphyrin thin films for energy-efficient window applications, MRS Commun. 10 (3) (2020) 439–448.
[510] Y. Chen, X. Zhao, Y. Li, Z.-Y. Jin, Y. Yang, M.-B. Yang, B. Yin, Light- and magnetic-responsive synergy controlled reconfiguration of polymer nanocomposites with shape memory assisted self-healing performance for soft robotics, J. Mater. Chem. C 9 (16) (2021) 5515–5527.
[511] H. Yang, W. Chao, X. Di, Z. Yang, T. Yang, Q. Yu, F. Liu, J. Li, G. Li, C. Wang, Multifunctional wood based composite phase change materials for magnetic-thermal and solar-thermal energy conversion and storage, Energy Convers. Manage. 200 (2019) 112029.
[512] F. Pujol-Vila, P. Güell-Grau, J. Nogués, M. Alvarez, B. Sepúlveda, Soft optomechanical systems for sensing, modulation, and actuation, Adv. Funct. Mater. 33 (14) (2023) 2213109.